

Cold collisions of alkali atoms in a laser field

Citation for published version (APA):

Boesten, H. M. J. M. (1996). *Cold collisions of alkali atoms in a laser field*. [Phd Thesis 1 (Research TU/e / Graduation TU/e), Applied Physics and Science Education]. Technische Universiteit Eindhoven.
<https://doi.org/10.6100/IR468537>

DOI:

[10.6100/IR468537](https://doi.org/10.6100/IR468537)

Document status and date:

Published: 01/01/1996

Document Version:

Publisher's PDF, also known as Version of Record (includes final page, issue and volume numbers)

Please check the document version of this publication:

- A submitted manuscript is the version of the article upon submission and before peer-review. There can be important differences between the submitted version and the official published version of record. People interested in the research are advised to contact the author for the final version of the publication, or visit the DOI to the publisher's website.
- The final author version and the galley proof are versions of the publication after peer review.
- The final published version features the final layout of the paper including the volume, issue and page numbers.

[Link to publication](#)

General rights

Copyright and moral rights for the publications made accessible in the public portal are retained by the authors and/or other copyright owners and it is a condition of accessing publications that users recognise and abide by the legal requirements associated with these rights.

- Users may download and print one copy of any publication from the public portal for the purpose of private study or research.
- You may not further distribute the material or use it for any profit-making activity or commercial gain
- You may freely distribute the URL identifying the publication in the public portal.

If the publication is distributed under the terms of Article 25fa of the Dutch Copyright Act, indicated by the "Taverne" license above, please follow below link for the End User Agreement:

www.tue.nl/taverne

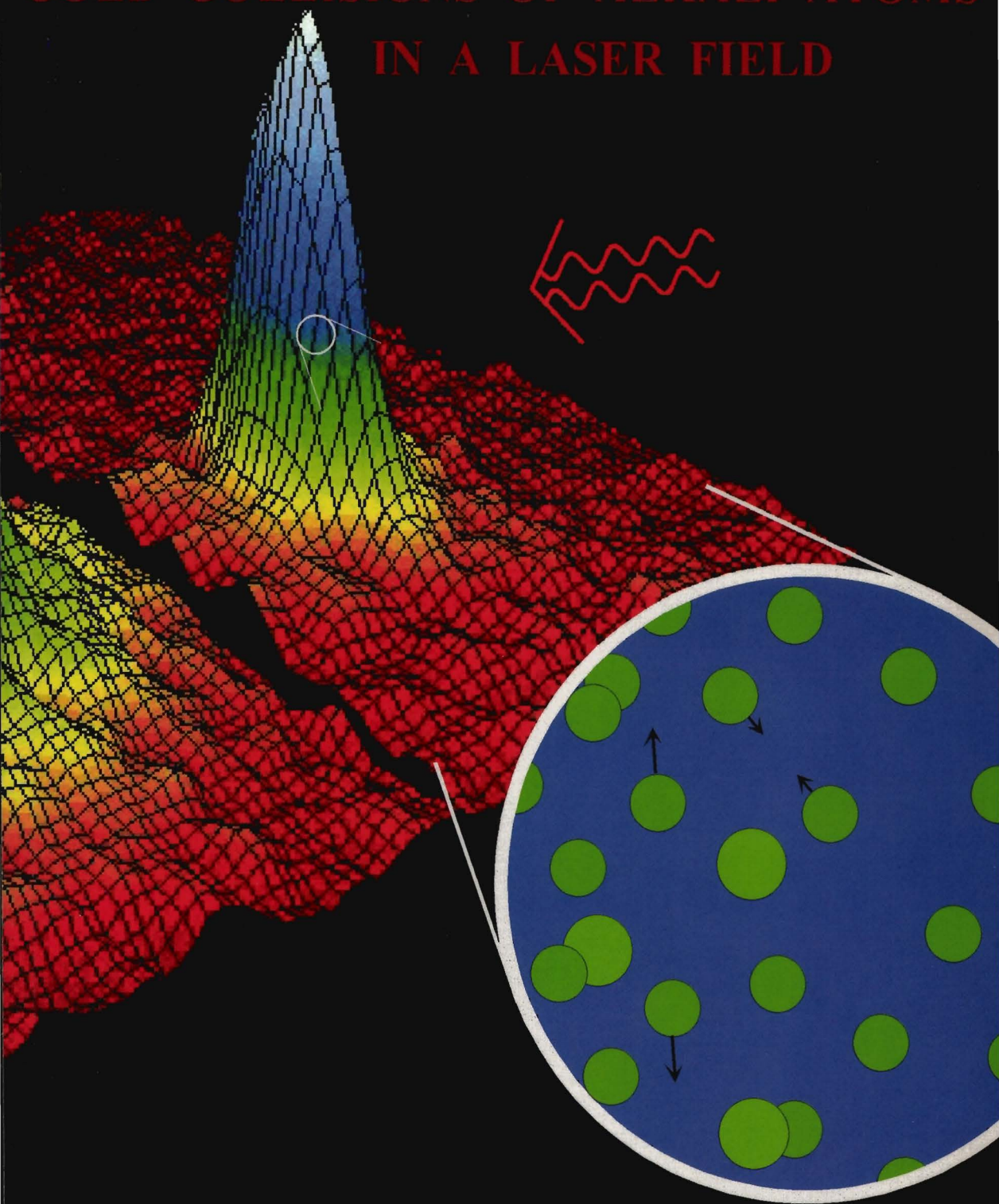
Take down policy

If you believe that this document breaches copyright please contact us at:

openaccess@tue.nl

providing details and we will investigate your claim.

COLD COLLISIONS OF ALKALI ATOMS IN A LASER FIELD



Hugo Boesten

Cold collisions of alkali atoms in a laser field

PROEFSCHRIFT

ter verkrijging van de graad van doctor aan de Technische Universiteit
Eindhoven, op gezag van de Rector Magnificus, prof.dr. M. Rem, voor
een commissie aangewezen door het College van Dekanen in het open-
baar te verdedigen op maandag 28 oktober 1996 om 16.00 uur

door

HUBERTUS MARIE JOZEF MATHEUS BOESTEN

Geboren te Melick

Dit proefschrift is goedgekeurd
door de promotoren:
prof.dr. B.J. Verhaar
en
prof.dr. H.C.W. Beijerinck

CIP-GEGEVENS KONINKLIJKE BIBLIOTHEEK, DEN HAAG

Boesten, Hubertus Marie Jozef Matheus

Cold collisions of alkali atoms in a laser field /
Hubertus Marie Jozef Matheus Boesten. - Eindhoven :
Technische Universiteit Eindhoven
Proefschrift Technische Universiteit Eindhoven. - Met lit.
opg. - Met samenvatting in het Nederlands.
ISBN 90-386-0019-4

Contents

1	Introduction	3
1.1	Contents of this thesis	4
2	Time-independent and time-dependent photoassociation of spin-polarized rubidium	9
2.1	Introduction	9
2.2	Shape resonances	15
2.3	Determination of excited-state parameters	17
2.4	Decay mechanisms of the ^{85}Rb g -wave shape resonance	19
2.4.1	Introduction	19
2.4.2	Photoassociation rate constant including inelastic decay	20
2.4.3	Time-dependent photoassociation spectroscopy	27
3	Collisions of doubly spin-polarized, ultracold ^{85}Rb atoms	35
4	Observation of a shape resonance in the collision of two cold ^{87}Rb atoms	45
4.1	Introduction	45
4.2	Experiment and analysis	47
4.3	Discussion and conclusion	52
5	Observation of a shape resonance in cold-atom scattering by pulsed photoassociation	57
6	Dipolar decay in two recent Bose-Einstein condensation experiments	67
7	Properties of cold collisions of ^{39}K atoms and of ^{41}K atoms in relation to Bose-Einstein condensation	75
8	Introduction to optical collisions	87
8.1	Introduction	87
8.2	Schrödinger equation for optical collisions	90
8.3	Quantum-mechanical optical-Bloch equation	94

9	Quantum suppression of collisional loss rates in optical traps	105
9.1	Introduction	105
9.2	Method of calculation	106
9.3	Results and discussion	109
10	Simple quantum-mechanical picture of cold optical collisions	121
	Summary	129
	Samenvatting	131
	Dankwoord	134
	Curriculum Vitae	134

Cover: Observation of a Bose-Einstein condensate in a cold ^{87}Rb gas by the JILA research team led by prof.dr. E.A. Cornell and prof.dr. C.E. Wieman. False-color images display the velocity distribution of the cloud of rubidium atoms at (back) just before the appearance of the Bose-Einstein condensate, (spine) just after the appearance of the condensate and (front) after further evaporation leaving a sample of nearly pure condensate. The color corresponds to the number of atoms at each velocity, with red being the fewest and white being the most [see also M.H. Anderson, J.R. Enscher, M.R. Mathews, C.E. Wieman, and E.A. Cornell, Science 269, 198 (1995)]. Images courtesy of the JILA research team. An illustration of laser-induced collisions has been added to the front page.

Chapter 1

Introduction

The field of “cold atomic collisions” was initiated around 1980 in connection with the study of spin-polarized atomic hydrogen in a cryogenic environment [1]. One of the first achievements in this field was the observation of the “spontaneous polarization” of a cold gas sample of atomic hydrogen in a strong magnetic field [2,3], a phenomenon predicted shortly before by Statt and Berlinsky [4] to arise from preferential recombination of non-doubly spin-polarized hydrogen atoms in two-body collisions at the walls. Important landmarks in the further development were the theoretical contributions by Kagan and Shlyapnikov [1,5], van den Eijnde, Koelman and Stoof [1,6–8], leading to a rather complete overview of all possible transitions that can take place in cold ground-state collisions. Most of this work was carried out in connection with experiments trying to realize Bose-Einstein condensation (BEC), as well as in connection with the cryogenic hydrogen maser.

In the second half of the eighties a stimulus for a new development in the field came from the novel technique of laser cooling of alkali atomic gas samples and the associated interest in collisions between cold ground-state alkali atoms [9,10]. Most of this work was again associated with BEC and cold atomic clocks. In fact, the first theoretical papers in this subfield [11,12] were dedicated to these applications. Further theoretical work [13] led to rapidly growing insight in collisions between lithium atoms and between sodium atoms. Ground-state collisions play a key role in many cold-atom experiments. The accuracy of atomic clocks based on a fountain of laser-cooled atoms is limited by frequency shifts due to collisions of atoms during their fountain orbit [14,15,10]. The static and dynamic properties of the condensate in a BEC experiment can be described with a non-linear Schrödinger equation containing a single parameter only: the scattering length [16]. More generally, this characterizes completely the effective interaction between atoms in a cold gas. A positive sign corresponds to effective repulsion and a negative sign to effective attraction. In particular, the sign determines the stability (+) or instability (–) of the Bose condensate in a BEC experiment [17–19]. Such predictions have been of much interest in connection with the recent successful realizations of BEC [20–22]. The lifetime of the condensate is another quantity determined by collisions. Depending on the density of the gas sample either

two-body [23,24] or three-body [25] collisions are the dominant decay mechanism.

Partly parallel to this development came the rapidly growing interest in collisions of cold alkali atoms in laser fields [26]. A laser field can have a dramatic influence on a cold collision. This will be the main subject of the present thesis. Collisions between atoms in a laser field are of great interest for experiments dealing with (magneto-)optical traps, because they induce exothermal transitions between trapped states or between trapped and untrapped states, thus giving rise to heating of trapped gas samples and loss of atoms. Apart from such applications, these “optical collisions” are of interest also from a theoretical point of view. In various ways optical collisions are different from ground-state collisions in the absence of laser fields. First, interactions between atoms in cold optical collisions generally take place at much larger interatomic distances (20 to 5000 a_0) than in other cold collisions (20 to 200 a_0). Secondly, the collision dynamics is drastically changed in the presence of laser light, because the collisional time scale may become comparable to the spontaneous decay time of an atom excited by the laser during the collision. This implies that more than one subsequent laser excitation - spontaneous emission cycle can take place during the same collision, thus leading to a fascinating interplay of statistically pure and mixed states and the associated inevitable irreversibility.

Besides the above-mentioned interests, optical collisions can also be used to perform spectroscopic studies on cold gas samples. By tuning the laser in such a way that the atoms, approaching each other via a ground state potential, are promoted to a molecular bound excited state, one can extract information about the ground and excited state potentials and other collision properties from the excitation probability as a function of laser detuning. This process is called photoassociation and was proposed by Thorsheim, Weiner and Julienne [27] as a new free-bound spectroscopy for cold atoms with accuracies comparable to the usual bound-bound spectroscopy and first observed experimentally by Miller, Cline and Heinzen [28] and by the NIST (Gaithersburg) group [29]. Another pioneering experimental paper has been published by a group at Rice University [30]. One of the powerful possibilities offered by this technique is a more or less direct “mapping” of collisional radial wave functions along a frequency axis, provided the experimental circumstances are carefully chosen. This thesis will also deal with this choice.

1.1 Contents of this thesis

This thesis is based on a series of papers that have been or will be published in the literature, apart from Chapter 8, which is an introduction to the final two chapters. The thesis can be divided into two parts.

The first part of this thesis, which consists of Chapter 2 to 7, addresses collision phenomena related to BEC experiments. In order to describe the phenomena observed in these experiments, a detailed knowledge of long-range atom-atom interactions and long-range collisional wave functions is required. Due to the extreme sensitivity of cold collisions to these

interatomic interactions, current ab-initio calculations do not lead to sufficiently accurate results. For instance, the number of triplet $^{87}\text{Rb}_2$ bound states following from such calculations is 38 ± 3 [31]. Since the scattering length changes over the full range from $+\infty$ to $-\infty$ each time a new bound state enters the potential, this accuracy is far from sufficient. This indicates the need for experiments to extract the relevant collision properties. In the case of the ^{85}Rb and ^{87}Rb atoms we use data from photoassociation experiments using doubly-spin polarized atoms to determine cold collision properties. In the case of the potassium isotopes ^{39}K and ^{41}K we use experimental data obtained from two-photon spectroscopy. We also devote a chapter to derive decay properties for trapped gas samples from the collisional information deduced in the foregoing part.

In the second part of this thesis we study optical collisions, i.e., atomic collisions in an almost resonant laser field. These collisions take place at very large interatomic distances. Complications, however, are the large number of partial waves involved in the collision process and the hyperfine interaction which is relevant at large interatomic distances. Taking into account these effects in a theoretical description is straightforward. However, solving the corresponding equations goes beyond the present computational power. Therefore it is of interest to investigate partial aspects of the full problem in order to obtain so much insight that adequate approximative descriptions can eventually be developed. In this thesis we restrict ourselves to a two-channel model, to study some of these aspects.

Chapter 2 is an introduction to the photoassociation process and the basic principles of the analysis that we apply. Chapter 3 deals with the analysis of a photoassociation experiment on spin-polarized ^{85}Rb . This analysis enabled us to determine the sign and magnitude of the scattering lengths for ^{85}Rb and for ^{87}Rb atoms colliding via a triplet collisional channel, which turned out to be of direct interest experimentally. On the basis of the obtained positive scattering length for the case of ^{87}Rb atoms we predicted that a Bose condensate in a ^{87}Rb gas sample would be stable. Shortly after the publication of our paper, BEC was observed for the first time in a gas sample of spin-polarized ^{87}Rb atoms [20]. In Chapter 4 the observation of a d -wave shape resonance in the collision of two ^{87}Rb atoms is reported. From this experiment we have been able to extract the $^{87}\text{Rb} + ^{87}\text{Rb}$ triplet scattering length very accurately. In Chapter 5 a new time-dependent photoassociation experiment and its analysis are described, based on the observation of a g -wave shape resonance in the collision of two ^{85}Rb atoms. This experiment has enabled us to extract very accurately the $^{85}\text{Rb} + ^{85}\text{Rb}$ triplet scattering length and to observe for the first time the inelastic decay due to ground-state spin-spin interactions as an effect in a photoassociation process. In Chapter 6 we use the collisional information we obtained in the previous chapters to calculate dipolar decay rates associated with $^{87}\text{Rb} + ^{87}\text{Rb}$, $^{85}\text{Rb} + ^{85}\text{Rb}$ and $^{23}\text{Na} + ^{23}\text{Na}$ collisions, of direct relevance for ongoing BEC experiments. In Chapter 7 we have been able to extract a number of relevant collision properties of cold ^{39}K and ^{41}K gasses, applying a new multichannel inverted perturbation approach [32] to a set of ^{39}K spectroscopic bound-state data.

Chapter 8 is an introduction to optical collisions. In this chapter the quantum-mechanical

optical-Bloch equations are derived, necessary to describe optical collisions in the last two chapters. In Chapter 9 we present the first fully quantum-mechanical study of optical collisions. The limitation is that it describes loss rates to first order in the laser intensity. This is not a severe limitation in view of experimental evidence that loss rates behave linearly as a function of laser intensity for an unexpectedly large range of intensities. Our quantum-mechanical treatment shows that loss rates are suppressed at low temperatures relative to a semiclassical description that has usually been applied to describe experiments [33]. This low-temperature suppression has been observed experimentally [34]. In Chapter 10 we present an improved semiclassical description of optical collisions that agrees very well with our fully quantum-mechanical results. This new semiclassical description offers the great advantage of a more transparent and explicit interpretation of cold optical collisions than is possible by quantum-mechanical coupled-channel equations.

References

- [1] I.F. Silvera and J.T.M. Walraven, in *Progress in Low Temperature Physics*, edited by G. Grynberg and R. Stora (North-holland, Amsterdam, 1984), p. 1125.
- [2] R.W. Cline, T.J. Greytak, and D. Kleppner, *Phys. Rev. Lett.* **47**, 1195 (1981).
- [3] R. Sprik, J.T.M. Walraven, G.H. van Yperen, and I.F. Silvera, *Phys. Rev. Lett.* **49**, 153 (1982).
- [4] B.W. Statt and A.J. Berlinsky, *Phys. Rev. Lett.* **45**, 2105 (1980).
- [5] Yu. Kagan, I.A. Vartan'yants, and G.V. Shlyapnikov, *Zh. Eksp. Teor. Fiz.* **81**, 1113 (1981) [*Sov. Phys.-JETP* **54**, 590 (1981)]; Yu. Kagan, G.V. Shlyapnikov, and N.A. Glukhov, *Pis'ma Zh. Eksp. Teor. Fiz.* **41**, 197 (1985) [*JETP Lett.* **41**, 238 (1985)].
- [6] J.P.H.W. van den Eijnde, Thesis Eindhoven University, 1984; J.M.V.A. Koelman, Thesis Eindhoven University, 1988; H.T.C. Stoof, Thesis Eindhoven University, 1989.
- [7] A. Lagendijk, I.F. Silvera, and B.J. Verhaar, *Phys. Rev. A* **33**, 626 (1986).
- [8] H.T.C. Stoof, J.M.V.A. Koelman, and B.J. Verhaar, *Phys. Rev. B* **38**, 4688 (1987).
- [9] P.S. Julienne and F.H. Mies, *J. Opt. Soc. Am. B* **6**, 2257 (1989).
- [10] B.J. Verhaar, *Laser Phys.* **4**, 1054 (1994); B.J. Verhaar, in *Atomic Physics 14*, edited by D.J. Wineland, C.E. Wieman and S.J. Smith (American Institute of Physics Press, New York, 1995), p. 351.
- [11] E. Tiesinga, S.J.M. Kuppens, B.J. Verhaar, and H.T.C. Stoof, *Phys. Rev. A* **43**, R5188 (1991).

- [12] E. Tiesinga, B.J. Verhaar, H.T.C. Stoof, and D. van Bragt, *Phys. Rev. A* **45**, 2671 (1992).
- [13] A.J. Moerdijk, Thesis Eindhoven University, 1996.
- [14] K. Gibble and S. Chu, *Metrologia* **29**, 201 (1992).
- [15] K. Gibble and S. Chu, *Phys. Rev. Lett.* **70**, 1771 (1993).
- [16] J.R. Taylor, *Scattering Theory* (Wiley, New York, 1972).
- [17] K. Huang, *Statistical Mechanics* (Wiley, New York, 1963).
- [18] A.L. Fetter and J.D. Walecka, *Quantum Theory of Many-Particle Systems* (McGraw-Hill, New York, 1971), p. 222.
- [19] E. Tiesinga, A.J. Moerdijk, B.J. Verhaar, and H.T.C. Stoof, *Phys. Rev. A* **46**, R1167 (1992).
- [20] M.H. Anderson, J.R. Ensher, M.R. Matthews, C.E. Wieman, and E.A. Cornell, *Science* **269**, 198 (1995).
- [21] C.C. Bradley, C.A. Sacket, J.J. Tollet, and R.G. Hulet, *Phys. Rev. Lett.* **75**, 1687 (1995).
- [22] K.B. Davis, M-O Mewes, M.R. Anderson, N.J. van Druten, D.S. Durfee, D.M. Kurn, and W. Ketterle, *Phys. Rev. Lett.* **75**, 3969 (1995).
- [23] F.H. Mies, C.J. Williams, P.S. Julienne, and M. Krauss (unpublished).
- [24] A.J. Moerdijk and B.J. Verhaar, *Phys. Rev. A* **53**, R19 (1996); H.M.J.M. Boesten, A.J. Moerdijk, and B.J. Verhaar, *Phys. Rev. A* **54**, R29 (1995).
- [25] A.J. Moerdijk, H.M.J.M. Boesten, and B.J. Verhaar, *Phys. Rev. A* **53**, 916 (1996).
- [26] P.S. Julienne, A.M. Smith, and K. Burnett, *Adv. At. Mol. Phys.* **30**, 141 (1992).
- [27] H.R. Thorsheim, J. Weiner, and P.S. Julienne, *Phys. Rev. Lett.* **58**, 2420 (1987).
- [28] J.D. Miller, R.A. Cline, and D.J. Heinzen, *Phys. Rev. Lett.* **71**, 2204 (1993).
- [29] P.D. Lett, K. Helmerson, W.D. Phillips, L.P. Ratliff, S.L. Rolston, and M.E. Wagshul, *Phys. Rev. Lett.* **71**, 2200 (1993).
- [30] W.I. McAlexander, E.R.I. Abraham, N.W.M. Ritchie, C.J. Williams, H.T.C. Stoof, and R.G. Hulet, *Phys. Rev. A* **51**, R871 (1995).
- [31] M. Krauss and W.J. Stevens, *J. Chem. Phys.* **93**, 4236 (1993).
- [32] J.M. Vogels, H.M.J.M. Boesten, and B.J. Verhaar (to be published).

- [33] P.S. Julienne and J. Vigué, Phys. Rev. A **44**, 4464 (1991); Y.B. Band and P.S. Julienne, Phys. Rev. A **46**, 330 (1992).
- [34] C.D. Wallace, V. Sanchez-Villicana, T.P. Dinneen, and P.L. Gould, Phys. Rev. Lett. **74**, 1087 (1995).

Chapter 2

Time-independent and time-dependent photoassociation of spin-polarized rubidium

H.M.J.M. Boesten, A.J. Moonen, B.J. Verhaar, C.C. Tsai, and D.J. Heinzen

To be published in Physical Review A

Abstract

We describe the observation of a d-wave shape resonance in the scattering of two cold ground-state ^{87}Rb atoms and that of a g-wave shape resonance in the scattering of two cold ground-state ^{85}Rb atoms. Both arise from a quasi-bound state inside a centrifugal barrier. The g-wave shape resonance is sufficiently long-lived that it can be observed in a time-dependent experiment. We observe the build-up of the resonance state through the barrier after depleting it by a photoassociation laser pulse and measuring the rate of photoassociation by a second laser pulse with a variable delay time. We describe the information about collision properties that can be extracted from the combination of the time-independent and time-dependent experiments.

2.1 Introduction

Interactions between ground-state alkali atoms play a key role in many experiments in cold atom physics. The accuracy of atomic clocks based on an atomic fountain of laser cooled Cs atoms, for instance, is limited by frequency shifts due to binary collisions between the atoms during their fountain orbit [1]. Collisions also determine whether a Bose-condensate in a gas sample cooled below the critical transition temperature T_C is stable or unstable, and, if stable, how fast it will decay [2–4]. A number of methods are presently available to obtain information on such collision processes. A very powerful method developed only recently is based on the photoassociation process [5–9]. In this free-bound transition process two colliding ground-state atoms are excited by a photoassociation (PA) laser to a bound electronically excited state. Due to the Franck-Condon principle, the excitation occurs preferably near the outer turning point r_0 of the excited state, where the atoms have a velocity comparable to that in the ground-state channel. A direct consequence is that the excitation

probability is approximately proportional to the ground-state collisional radial wave function squared at this outer turning point [10], which enables one to map out the nodal structure of this wave function along a frequency axis. Figure 2.1 shows a presentation of radial wave functions of the ground state and the excited state, together with their above-mentioned Franck-Condon relationship.

The actual application of this simple idea still leads to a very complicated situation because of several facts:

1. The hyperfine structure of the excited electronic states, the so-called hyperfine “spaghetti” [11].
2. The difficulty of determining a large number of combined triplet and singlet parameters in the ground-state collision simultaneously.
3. The fact that several ground-state partial waves l , ranging from $J - 2$ (or 0) to $J + 2$, contribute to the excitation of a single rovibrational excited state v, J . This is due to two circumstances:
 - (a) The electronic spins contribute to the total molecular angular momentum,
 - (b) The laser photon inducing the transition introduces an angular momentum $l\hbar$ into the system with in principle various orientations relative to the initial angular momentum of the two-atom system.

As a consequence, by angular momentum conservation each J peak can be reached starting from non-negative l values ranging from $J - 2$ to $J + 2$.

By a careful choice of experimental circumstances we have been able to eliminate all three complications [9]. The first step is to doubly-polarize the ground-state atoms, i.e., to prepare them in the hyperfine state with fully stretched electronic and nuclear spins along a magnetic field \vec{B} with optical pumping lasers. In this way only the triplet spin state in the initial channel is involved, thus avoiding complication 2).

The second step is to concentrate on the excitation of a suitable excited electronic state: the 0_g^- state connected with the ${}^2S_{1/2} + {}^2P_{1/2}$ separated-atom limit (we will refer to this state as the lower 0_g^- state). The structure of this and all other excited states associated with the ${}^2S + {}^2P$ separated-atom limits has been studied by Movre and Pichler [12]. In the radial range of outer turning points of the highest $0_g^-({}^2S_{1/2} + {}^2P_{1/2})$ rovibrational states observed, ranging from $41a_0$ to $48a_0$, this electronic state has a very simple structure, determined by a 2×2 eigenvalue problem containing the fine-structure splitting of the excited atom and the interatomic $1/r^3$ resonant electric dipole interaction. Due to the fact that the fine-structure splitting dominates, the structure of the electronic state considered is simply given by the antisymmetrized product of the separated-atom states,

$$\left[\left({}^2S_{1/2}\{1A\} \ {}^2P_{1/2}\{2B\} \right)_{j=0} - \left({}^2S_{1/2}\{1B\} \ {}^2P_{1/2}\{2A\} \right)_{j=0} \right] / \sqrt{2}, \quad (2.1)$$

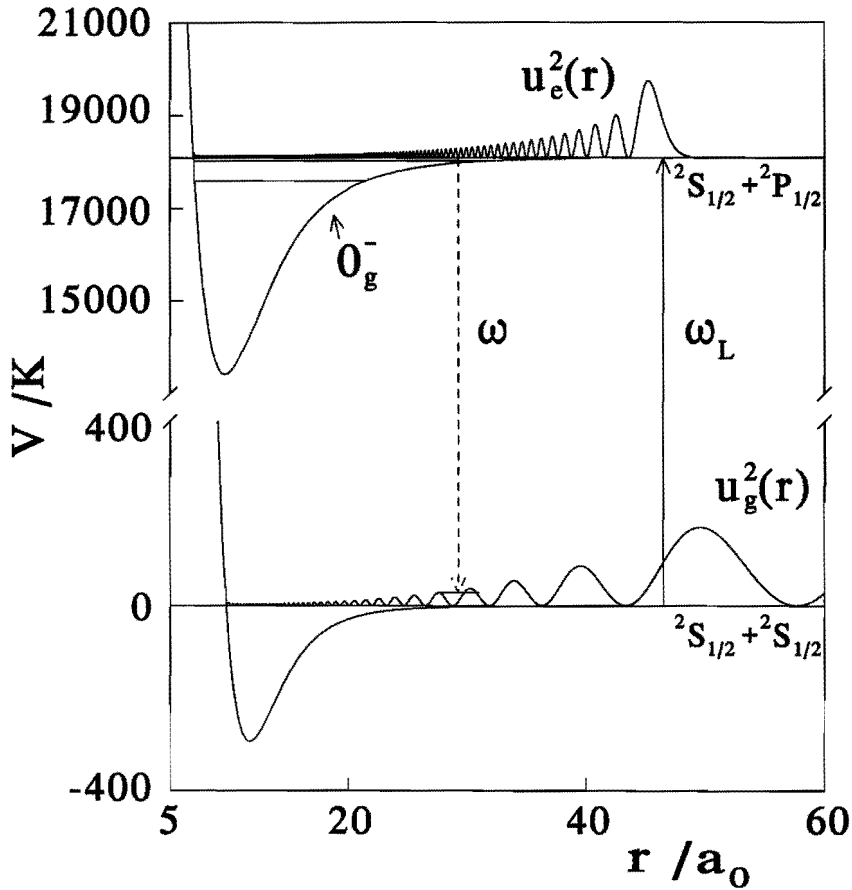


Figure 2.1: (a) Cold-atom photoassociation. Excitation of a colliding pair of Rb atoms by a photon (ω_L) leads to the formation of an excited Rb_2 molecule in the 0_g^- excited state potential and is followed by spontaneous decay (frequency ω). The square of the ground-state radial wave function $u_g^2(r)$ of the initial collisional state and of the excited-state radial wave function $u_e^2(r)$ are shown.

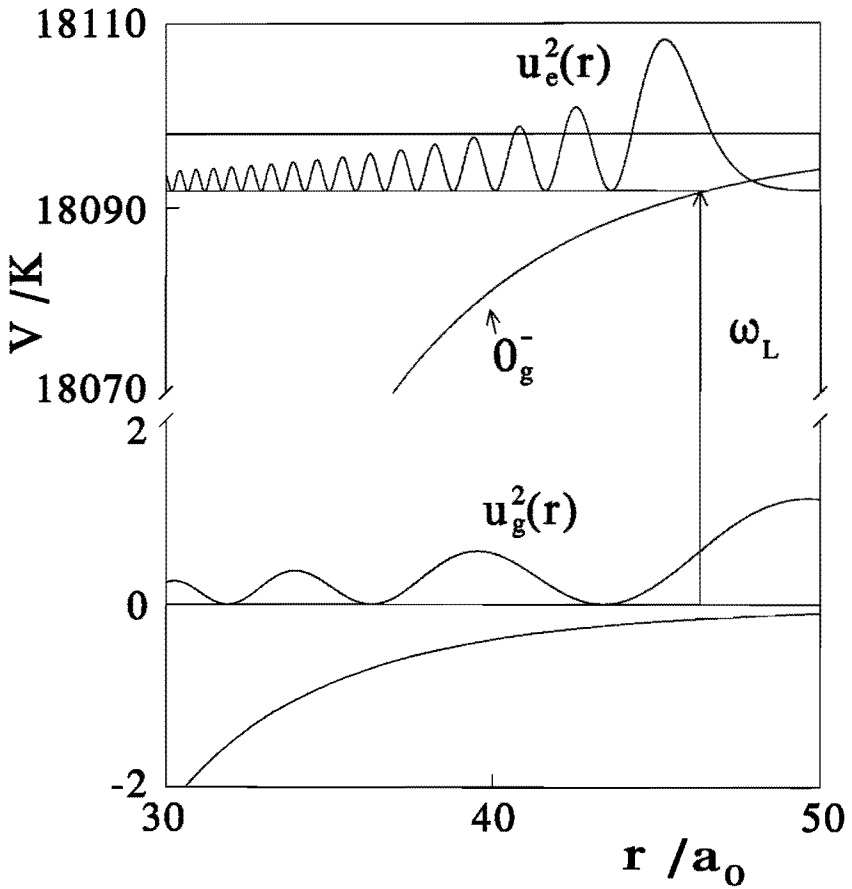


Figure 2.1: (b) Cold-atom photoassociation in the interatomic distance interval relevant for our analysis.

with the electronic angular momenta $1/2$ coupled to total $j = 0$. We use the notation $1A$, for instance, to denote that the set of electrons 1 occupies the state indicated around nucleus A . The angular-momentum coupling and the subtraction in the above expression together assure the correct symmetry properties corresponding to the quantum numbers 0_g^- . As pointed out in Ref. [13], to our knowledge this is the first observed example of a Hund's (e) case in the literature, i.e., both the total electronic angular momentum j and the rotational angular momentum have definite values. The latter is conserved in the PA excitation process, so that J equals the ground-state l value, thus avoiding complication 3): each photoassociation peak J is the direct probe of the ground-state radial wave function for a single l .

Another advantage of the above choice of excited state is that it is a pure triplet state, since $j = 0$ can only arise from a total electronic orbital angular momentum quantum number 1 , when this is coupled with $S = 1$. We conclude that the laser does not introduce a singlet admixture, which would spoil the above pure triplet situation in higher order in the laser intensity, a complication that would occur in the analysis of the time-dependent experiment in the following.

By the same choice of excited state complication 1) is avoided. The value $j = 0$ implies that in very good approximation the nuclear spins are decoupled from the remaining angular momenta. The hyperfine splitting is only second order and no complex hyperfine-coupled problem needs to be handled in the final state. By the unique initial nuclear spin state only the fully nuclear-spin polarized final state contributes.

Due to the vanishing j value, the total electronic angular momentum before the excitation, i.e., the vector sum of the electronic spins, is equal to minus the angular momentum of the dipole PA photon absorbed. Using a PA laser beam propagating in the direction of the static magnetic field \vec{B} and preparing the ground-state atoms in the hyperfine state with fully stretched electronic and nuclear spins along \vec{B} , we therefore find that a right-circularly polarized PA beam does not lead to excitation. This was observed experimentally [9]. On the other hand, a left-circular polarization does lead to excitation. Experimentally, indeed only even J rotationally resolved states are excited, in agreement with Bose symmetry in the (spin-symmetric) ground-state channel. We thus achieve our goal: we are able to study the nodal structure in a single ground-state channel by mapping it out as a function of the laser frequency.

In Ref. [9] we have been able, using the above approach, to make the first predictions for the triplet scattering length a_T for binary collisions of ^{85}Rb atoms, and making use of a mass-scaling rule, also for ^{87}Rb atoms. The PA excitation probability is measured by having the PA laser beam on intermittently with a trapping (FORT) laser and two optical pumping laser beams during a certain time period. The number of atoms remaining in the trap is reduced, because virtually all excited pairs of atoms decay spontaneously to free pairs with a kinetic energy that is too large to remain in the trap (frequency ω in Fig. 2.1(a)). Probing the atoms with laser-induced fluorescence, this results in a detectable change in the fluorescence level, i.e., in a measurement of the photoassociation loss rate. Figure 2.2 shows an experimental

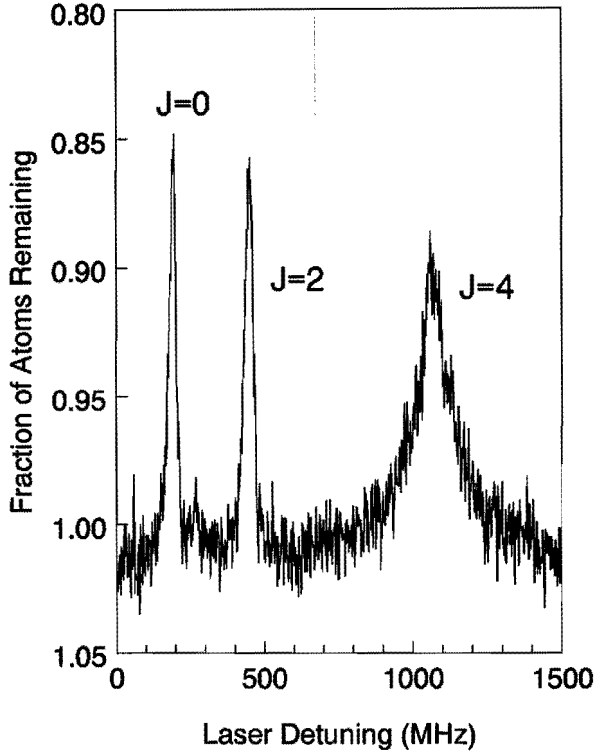


Figure 2.2: Photoassociation spectrum of the 0_g^- vibrational level at $12,573.05 \text{ cm}^{-1}$, relative to the $S_{1/2} + P_{1/2}$ separated-atom limit, for the collision of spin-polarized ^{85}Rb atoms. Notice the absence of odd rotational lines due to Bose statistics.

rotationally-resolved PA spectrum for a vibrational state of the lower 0_g^- state, measured using a linearly polarized PA laser beam. Contrary to the case without optical pumping only even J peaks occur.

The unique relation between J and l thus realized makes it possible to simplify the analysis considerably. In a dressed-state picture, represented schematically in Fig. 2.3, either the bound excited level is shifted downward by the laser photon energy $\hbar\omega_L$ or the ground-state potential is shifted upward by the same energy (the resonance level E_{res} within the centrifugal barrier will be discussed in the following section). It thus becomes clear that the bound excited state, which has already a finite width γ_0 for spontaneous emission, is embedded in the ground-state continuum and thus turns into a Feshbach resonance [15] with an additional width γ_L for laser-induced continuum decay.

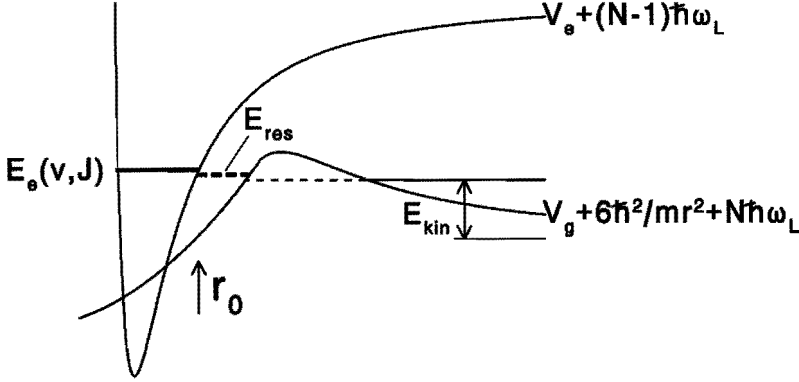


Figure 2.3: Dressed-states picture of photoassociation process, including schematic ground-state ($V_g + 6\hbar^2/mr^2$) and excited-state (V_e) potentials. Changing the laser frequency ω_L , the excited bound state energy $E_e(v, J)$ with vibrational quantum number v , rotational quantum number J , and outer turning point r_0 , shifts over the Maxwellian energy distribution in incoming channel. The bold dashed line indicates the position of the shape resonance E_{res} .

While the observed spectrum contained $J = 0, 2, 4$ rotational peaks, we used only the $J = 0, 2$ peaks in the analysis. The $J = 4$ peak in the ^{85}Rb PA spectrum showed anomalous features, which precluded an analysis along the same lines. In Ref. [14] we recognized this anomaly, as well as a similar anomalous $J = 2$ peak in the ^{87}Rb PA spectrum, as being due to a shape resonance in the ground-state channel. Very recently, making use of the long lifetime of the ^{85}Rb g -wave shape resonance, we have been able to observe for the first time the time-dependence of a collision of two cold atoms [13] via a pulsed photoassociation experiment. In this paper we will focus on this last experiment and its analysis.

2.2 Shape resonances

When two atoms collide via a partial wave $l \neq 0$ a long-lived state inside the centrifugal barrier may form during the collision process. Such a state is commonly referred to as a shape resonance. Figure 2.3 shows in addition a schematic picture of a shape resonance in the ground-state potential. It has a dramatic influence on all inelastic processes taking place within the barrier. Figure 2.4, for instance, shows the radial wave function squared for d -wave $^{87}\text{Rb} + ^{87}\text{Rb}$ scattering in the presence of a shape resonance (the actual situation)

and without. The wave function without shape resonance is calculated by modifying the inner part of the potential slightly so that the shape resonance shifts downward to negative energies. Clearly visible in Fig. 2.4 is the phase shift between the wave function with and without shape resonance. If, in a photoassociation experiment, the laser is tuned in such a

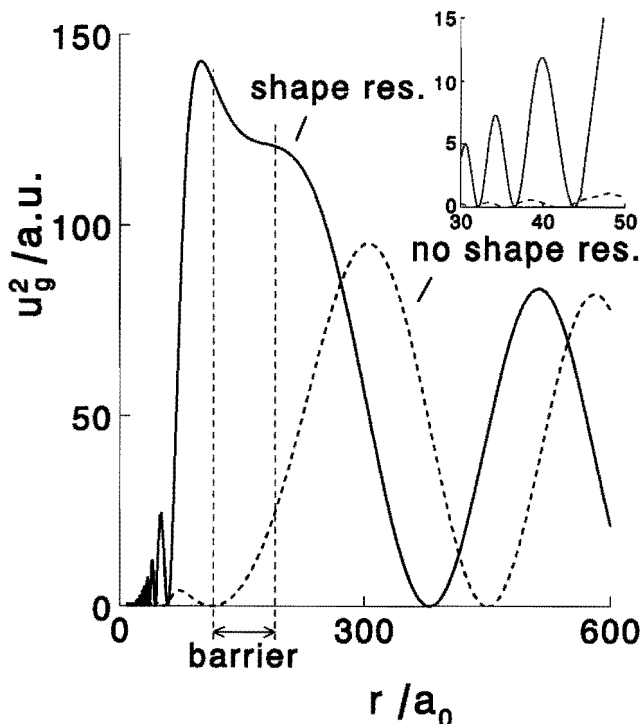


Figure 2.4: Square of $l = 2$ partial wave ground-state wave functions (^{87}Rb) $u_g^2(r)$ in the presence of a shape resonance and in the absence of a shape resonance at a collision energy $E = 0.3$ mK. The interatomic distances for which the collision energy is smaller than the potential energy, i.e., for which in a semiclassical picture the atoms tunnel through the barrier, are indicated. Inset: $u_g^2(r)$ in relevant interatomic distance interval for photoassociation. Note the enhancement if a shape resonance is present.

way that the outer turning points of excited states are at suitable radii, atoms within the barrier are excited and one sees a tremendous increase in the PA loss rate relative to that without a shape resonance. The actual place where this enhancement enters the expressions for the PA

loss rate is in the partial width γ_L : this partial width for decay of the PA Feshbach resonance in its turn then shows a resonance dependence on the collision energy, as will be described explicitly in the following section.

The existence of a shape resonance in a partial wave channel has great influence on the information that can be extracted from a photoassociation experiment. Without it, as explained above, the Franck-Condon oscillations lead to information on the nodes in the radial wave function in the excitation region. Translating this to the nodal structure at infinity requires sufficiently accurate knowledge of the long-range interaction. For this reason, in the analysis of the usual type of photoassociation experiment one generally needs to use theoretical information on dispersion coefficients, in particular the C_6 coefficient [9]. The existence of a shape resonance below the top of the barrier yields precisely the independent information, that makes it possible to discard this theoretical input, essentially because its energy depends also on the long-range potential outside the barrier. In Ref. [14] we have demonstrated this more explicitly (see in particular Fig. 4 in that paper).

2.3 Determination of excited-state parameters

The expression for the partial width γ_L used in our analysis of PA experiments contains a radial transition matrix element with a product of excited and ground-state radial wave functions. To calculate the former we need a sufficiently accurate excited-state potential V_e . The determination of this potential is not only of interest for this purpose. Investigations of the excited-state potential have led to a very accurate prediction of the excited state lifetime of optically excited atoms. The possibility of such a prediction arises from the fact that the lifetime contains the same electric-dipole matrix element as that occurring in the $1/r^3$ resonant electric-dipole part of V_e .

Existing methods to extract dipole matrix elements from photoassociation spectra are based on a semiclassical approximation [5] or limited by the uncertainty of the inner part of the potential [16]. The 0_g^- state asymptotically connecting with the $S_{1/2} + P_{3/2}$ fine-structure limit is an exception to this last statement, because this is a pure long range state which can entirely be described by a limited set of dispersion coefficients [17–20]. In this section we will present a new approach, based on the accumulated-phase method [9,21], not limited by any semiclassical approximation or inaccuracy of the inner part of the potential.

As pointed out above, the excited state we are using in our experiment is a 0_g^- state, asymptotically connecting with the $S_{1/2} + P_{1/2}$ state (the lower 0_g^- state). In the foregoing we have briefly referred to the 2×2 eigenvalue problem determining the electronic structure of the excited 0_g^- -states at large interatomic distances. It contains the fine-structure splitting of the excited atom and the interatomic $1/r^3$ resonant dipole interaction. In the fine-structure basis it is given by

$$V_{0_g^-} = \begin{pmatrix} E_{at}(S_{1/2}) + E_{at}(P_{3/2}) & 0 \\ 0 & E_{at}(S_{1/2}) + E_{at}(P_{1/2}) \end{pmatrix} + V_{dd}$$

$$= -\frac{1}{4\pi\epsilon_0 r^3} \begin{pmatrix} d(P_{3/2}) d(P_{3/2}) & \sqrt{2} d(P_{1/2}) d(P_{3/2}) \\ \sqrt{2} d(P_{1/2}) d(P_{3/2}) & 0 \end{pmatrix} + \begin{pmatrix} E_{fs} & 0 \\ 0 & 0 \end{pmatrix}, \quad (2.2)$$

with E_{at} the energies of the atomic states involved, V_{dd} the resonant electric dipole-dipole part, E_{fs} the fine-structure splitting and $d(P_{1/2}), d(P_{3/2})$ the atomic electric-dipole matrix elements, connecting the ground state with the $P_{1/2}, P_{3/2}$ excited states. Note that the ${}^2S_{1/2} + {}^2P_{1/2}$ diagonal matrix element of the $1/r^3$ interaction vanishes because an electronic $j = 0$ state is spherically symmetric, so that there is no preferential orientation of the atomic centers of mass relative to one another. In more formal terms this interaction has the angular momentum structure proportional to

$$\left[Y_2(\hat{r}), (\vec{d}(1), \vec{d}(2))_2 \right]_{00}, \quad (2.3)$$

and according to the Wigner-Eckart theorem the expectation value of a rank 2 tensor operator in an angular momentum 0 state is zero. As a consequence, since we are studying photoassociation at interatomic distances for which E_{fs} is much larger than the electric dipole-dipole interaction, the product $d(P_{1/2})d(P_{3/2})$ is the leading term in the strength of the $1/r^3$ coefficient of the lower 0_g^- potential. In the following we will use the shorthand notation

$$d^2 = d(P_{1/2}) d(P_{3/2}) \quad (2.4)$$

for this product. Notice that at smaller distances higher order dispersion coefficients C_{2ne} ($n = 3, 4, 5$) become important.

To justify some aspects of our method we construct a model 0_g^- potential. For the long range part we use the dispersion coefficients of Bussery [22] and Gardner *et al.* [9]. The inner part is based on a calculation of the eigenvalues of a potential matrix, consisting of the triplet potentials of Spiegelmann *et al.* [23] and an r -independent fine-structure splitting. The two parts are connected by an exponentially varying exchange term. Using this potential we calculate the phase ϕ_0 of the radial wave function at an interatomic distance $r_1 = 30a_0$ for the whole range of experimental excited bound-state energies. It turns out that to very good accuracy ϕ_0 varies linearly over the entire energy range. This implies that we can describe the radial wave functions in the range of experimental energies entirely with a very limited number of four parameters only: ϕ_0 , its derivative with respect to the bound-state energy ϕ_E , d^2 , and the C_{6e} dispersion coefficient. The higher order dispersion coefficients C_{2ne} ($n \geq 4$) turn out to be unimportant, provided that these are taken within the bounds of the present uncertainty [22].

In our analysis we use $J = 0$ levels for ${}^{85}\text{Rb}$ and $J = 2$ levels for ${}^{87}\text{Rb}$. In the combined analysis of these sets we have only five parameters, because the phase-derivatives for the two isotopes can directly be related to each other by a \sqrt{m} scaling rule

$${}^{87}\phi_E = \sqrt{\frac{m({}^{87}\text{Rb})}{m({}^{85}\text{Rb})}} {}^{85}\phi_E. \quad (2.5)$$

Note that $^{87}\phi_g$ and $^{85}\phi_0$ have a similar scaling relationship, but we vary these phases mod π independently, because we do not know their integer $\times \pi$ parts. We now calculate for each set of these parameters the corresponding bound-state energies and construct a χ^2 -function

$$\chi^2 = \sum_{i=1}^{24} \left(\frac{E_{exp,i} - E_{th,i}({}^{85}\phi_0, {}^{87}\phi_0, {}^{85}\phi_E, C_{6e}, d^2)}{\sigma_{E_{exp,i}}} \right)^2, \quad (2.6)$$

with $E_{exp,i}$ the experimental bound-state energy levels, $E_{th,i}$ the theoretically calculated ones and $\sigma_{E_{exp,i}}$ the standard deviation in the experimental level i . In Fig. 2.5 the area in the C_{6e} , d^2 -plane is shown where χ^2 is minimal or at most equal to twice the minimum value, for the optimum values of the three phase parameters. This condition clearly defines a strip in the C_{6e} , d^2 -plane with a width of 0.2 a.u. in the d^2 -direction. Using the theoretical C_{6e} value from Ref. [22] we find $d^2 = 8.8 \pm 0.1$ a.u. in good agreement with a recent value [24], measured by a different method.

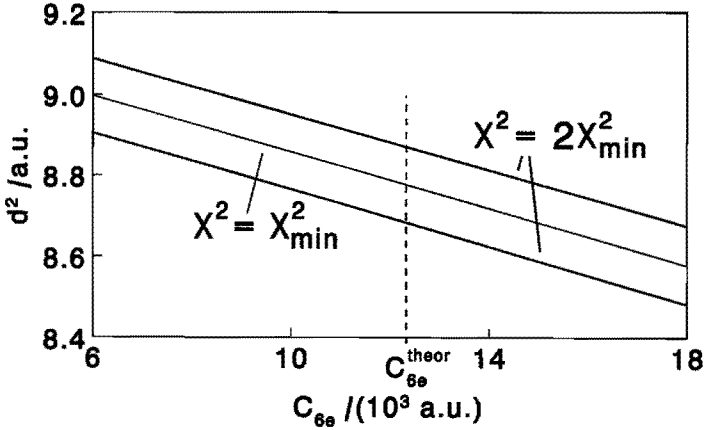


Figure 2.5: Contour plot of χ^2 as a function of C_{6e} and d^2 for the optimum values of the three phase parameters. The dashed vertical line indicates the theoretical value (C_{6e}^{theor}) of Ref. [22].

2.4 Decay mechanisms of the ^{85}Rb g -wave shape resonance

2.4.1 Introduction

In the foregoing we considered the decay of the shape resonance by the PA laser excitation. Also other decay processes become important if the lifetime of the shape resonance is

comparable to or longer than the time scale for these decay mechanisms. In this section we consider inelastic scattering mechanisms due to decay to other ground-state hyperfine channels. As pointed out in a brief first report on our work [13], long-lived shape resonances lend themselves to a new kind of sensitive study of such processes. In this connection special interest goes to the so-called second-order spin-orbit coupling $V_{so}^{(2)}$, or indirect spin-spin interaction, which arises from a mechanism very similar to the magnetic dipolar interaction V_{dip} between the valence electron spins, the only difference being that it does not mediate directly through a magnetic field but via the electric field from the charges in the system. Both the strength and radial dependence of the indirect spin-spin interaction are largely unknown. Recently, a theoretical estimate was presented [25] for the case of ^{87}Rb atoms. For low molecular states expectation values have been measured as well as calculated [26], but these give information on small internuclear distances only.

Three mechanisms compete in depleting the shape resonance: the inelastic decay with rate constant γ_{inel}/\hbar due to coherent contributions from dipolar decay and spin-orbit decay: $\gamma_{inel} = (\sqrt{\gamma_{dip}} + \sqrt{\gamma_{so}})^2$, the tunneling rate (γ_{out}/\hbar) and the excitation to the excited state via photoassociation (γ_L/\hbar). Note that scattering theory [15] shows that the partial wave amplitudes, denoted above as $\sqrt{\gamma_{dip}}$ and $\sqrt{\gamma_{so}}$, are (positive or negative) real quantities. All these quantities hinge critically on the exact energy E_{res} of the shape resonance, which is subject to large uncertainty even if we know that it exists below the top of the centrifugal barrier. Knowing the energy of this resonant state is comparable to knowing the last bound state energy of a potential [27] and thus is important in determining the scattering length, of great relevance for Bose-Einstein condensation experiments.

As pointed out above, not only E_{res} , but also γ_{inel} is largely unknown, due to its γ_{so} part. To determine both quantities we have performed a simultaneous analysis of time-dependent photoassociation data at high laser power, thus eliminating complicated cross-terms between γ_{inel} coupling and laser coupling during the photoassociation pulses, and time-independent photoassociation data at very low laser intensity, for which the laser excitation can be treated in first order. Combining these data enables us to determine E_{res} and γ_{inel} . To study the influence of γ_{inel} on the photoassociative losses at low laser intensities we have to include its influence in the PA loss rate. This will be done in the following part of this section. In the last part we will discuss the analysis of the time-dependent data and the determination of E_{res} and γ_{so} .

2.4.2 Photoassociation rate constant including inelastic decay

To first order in the laser intensity, the squared scattering S -matrix element describing the single-atom optical excitation for a pair of colliding ground-state atoms with collision energy ϵ and the subsequent spontaneous decay (decay rate γ_0/\hbar), using a photoassociation laser with frequency ω_L and field strength $\vec{E}_L = E_L \vec{\sigma}_L$, can be written as

$$|S_{PA}|^2 = \frac{\gamma_0 \gamma_L (SM_S l m_l, \epsilon \rightarrow \Omega J M)}{(\epsilon + E_g + \hbar \omega_L - E_e)^2 + \gamma_0^2/4}. \quad (2.7)$$

In this expression the previously mentioned partial width γ_L for excitation of an $|SM_S l m_l, \epsilon\rangle$ ground state to an $|\Omega J M\rangle$ excited state is equal to

$$\gamma_L = 2\pi \left| \langle \Omega J M | [\vec{d}(1) + \vec{d}(2)] \cdot \vec{E}_L | SM_S l m_l, \epsilon \rangle \right|^2. \quad (2.8)$$

In Eqs. (2.7) and (2.8) E_e is the excited rovibrational state energy, E_g the asymptotic internal energy in the ground-state channel, $\vec{d}(i)$ the dipole operator for atom i , Ω the total electronic magnetic quantum number along the internuclear axis z' , and J, M the total molecular angular momentum quantum numbers.

After thermally averaging the $v\sigma$ product corresponding to $|S_{PA}|^2$ we obtain the photoassociation rate constant $K(T, \omega_L)$ for a gas of cold atoms with temperature T :

$$K(T, \omega_L) = \langle v \frac{\pi}{k^2} |S_{PA}|^2 \rangle_{th}. \quad (2.9)$$

For our purposes the most important factor in this rate constant is the partial width γ_L , which will be worked out in more detail in the following paragraphs.

We expand the excited state $|\Omega J M\rangle$ in atomic fine-structure states with a well-defined electronic angular momentum j, m_j :

$$\begin{aligned} |\Omega J M\rangle &= \sum_j c_j(r) |j \Omega J M\rangle \\ &= \sum_j c_j(r) \sum_l (-1)^{j-\Omega} (J \Omega j - \Omega |l 0) |j l J M\rangle \\ &= \sum_{j m_j l m_l} c_j(r) (-1)^{j-\Omega} (J \Omega j - \Omega |l 0) (j m_j l m_l | J M) |j m_j l m_l\rangle. \end{aligned} \quad (2.10)$$

Substituting this in Eq. (2.8) leads to

$$\begin{aligned} \gamma_L &= \frac{2\pi I_L}{\epsilon_0 c} \left| \sum_{j m_j} (-1)^{j-\Omega} (J \Omega j - \Omega |l 0) (j m_j l m_l | J M) \times \int_0^\infty dr c_j(r) u_{\Omega J}(r) \times \right. \\ &\quad \left. \langle j m_j | [\vec{d}(1) + \vec{d}(2)] \cdot \vec{\sigma}_L | SM_S \rangle u_{SM_S l m_l, \epsilon}(r) \right|^2, \end{aligned} \quad (2.11)$$

i.e., the basic Franck-Condon overlap between the ground-state and excited-state radial wave functions $u_{SM_S l m_l, \epsilon}(r)$ and $u_{\Omega J}(r)$, respectively. A shape resonance in the ground-state channel causes the initial radial wave function and thus γ_L to show resonance behavior. We again refer to Fig. 4 demonstrating the strong enhancement.

Note that by the above substitution of Eq. (2.10) in Eq. (2.8) an additional independent summation over l, m_l quantum numbers of the final state would in principle appear. Since the quantum numbers of the initial state stand only for the asymptotic incoming spherical wave part, which may be different from the additional partial waves introduced into the initial state by inelastic interactions, one will in general have incoherent contributions for various final choices of these quantum numbers. This freedom should in principle be allowed for, once one is to include inelastic ground-state contributions that change the relative orbital angular

momentum, such as the direct and indirect spin-spin coupling. This is what we are now going to consider.

A straightforward but laborious method to include the influence of inelastic scattering on the shape resonance would be to replace the simple initial state in Eq. (2.11) by a coupled-channels wave function. This would automatically include combined effects from the shape resonance and the inelastic ground-state transitions. Concentrating on the g -wave shape resonance, a calculation of the coupled-channels state for the nine incoming m_l spherical waves, for a large set of collision energies, and for the large number of inelastic hyperfine channels would be very laborious. Fortunately, we were able to show that a much simpler approach is possible, by comparing a few representative coupled-channel wave functions inside the barrier (the only positions where they enter the Franck-Condon integral) for a ground-state model potential, with and without the inclusion of the inelastic spin-spin terms. Like the model potential for the 0_g^- state, this model potential is only introduced for the purpose of studying the general properties of the corresponding wave functions.

The Hamiltonian of the coupled-channel ground-state problem is of the form

$$H = T + V_c + V_{hf} + V_Z + V_{dip} + V_{so}^{(2)}, \quad (2.12)$$

a sum of a kinetic energy operator T , the central interaction V_c , a sum of single-atom hyperfine interactions V_{hf} , the Zeeman interaction V_Z , the magnetic dipolar interaction V_{dip} , and the second-order spin-orbit interaction $V_{so}^{(2)}$. Following Mies *et al.* [28] we assume a gaussian radial profile for $V_{so}^{(2)}$ centered around $12a_0$. The coupled-channel calculation shows that the exact location and shape is irrelevant. The only relevant quantity is the area $\bar{V}_{so}^{(2)}$ of the radial profile since in the radial transition integral the elastic wave functions are virtually identical and oscillate so rapidly at the interatomic distances where $V_{so}^{(2)}$ is effective, that only the above area multiplied by the elastic amplitude squared is of importance. The central interaction V_c is only partially known. The long range part of the triplet potential and associated partial-wave radial wave functions for $r > 35a_0$ follow from our previous analyses of photoassociation spectra [9,14,13]. At these distances they can be described by a C_6 -tail and an asymptotic behavior dictated by the triplet scattering length. For the inner part we use the theoretical potential of Krauss and Stevens [29]. We take the singlet potential from Amiot [30] and the above-mentioned C_6 value for the tail. Finally, to vary the unknown singlet scattering length we add a variable phase to the singlet radial wave functions at small interatomic distances.

Without the inelastic spin-spin terms the shape resonance can only decay via tunneling through the centrifugal barrier. This implies that the initial state $|SM_S l m_l, \epsilon\rangle$ in Eq. (2.8) contains only the single partial-wave radial wave function $u_{SM_S l m_l, \epsilon}(r)$. Calculating this at a fixed arbitrary radius r_1 inside the barrier, we find that its dependence on the collision energy can be very accurately described by a factor

$$\frac{\sqrt{E}^{l+1/2}}{E - E_{res} + i\gamma_{out}/2}, \quad (2.13)$$

with $l + 1/2 = 4.5$ for the g -wave considered [31]. For the energy range where the resonance energy E_{res} is expected to occur the tunneling width γ_{out} of the resonance agrees very well with the semiclassical value.

We now proceed by adding the direct and indirect spin-spin terms V_{dip} and $V_{so}^{(2)}$ to the Hamiltonian. We then find also inelastic hyperfine components of the initial state, which make it necessary to extend Eq. (2.8) for γ_L by adding nuclear spin quantum numbers I, M_I to the final state and an incoherent summation over the possible two-atom values. We stress again that the nuclear spins are decoupled in the final state. Also the asymptotic incoming quantum numbers of the initial state have to be supplemented with I, M_I values. To keep the discussion transparent we now add a superscript “0” to the quantum numbers of the elastic component of the initial state, to distinguish them from values for the inelastic components. Because of the choice of a fully spin-stretched initial spin state we have the restriction $S^0 = 1, M_S^0 = +1, I^0 = 5, M_I^0 = +5, l^0 = 4$. Note that for this doubly-polarized situation we have also $f_1^0 = 3, f_2^0 = 3, F^0 = 6, M_F^0 = +6$. The initial states differ only in the value of m_l^0 , which varies from -4 to $+4$. For each of these initial states the coupled-channels calculation leads to a superposition of components.

It turns out that the complicated coupled-channel superpositions can be calculated to very high accuracy by a simple approach, in which one calculates the influence of the inelastic interactions on the original shape resonance state by perturbation theory. This leads to a splitting into a set of shape resonance states with resonance energies and widths changed by ΔE_{res} and $\Delta\gamma$. A detailed study shows each ΔE_{res} to vary linearly with the unknown strength of $V_{so}^{(2)}$ for reasonable strengths, just as expected from first order time-independent perturbation theory. The total width of each of the splitted resonances turns out to be equal to the (incoherent) sum of the tunneling width γ_{out} and a contribution from coherent direct and indirect spin-spin terms:

$$\Delta\gamma = \left(\sqrt{\gamma_{dip}} + \sqrt{\gamma_{so}} \right)^2 \quad (2.14)$$

Figure 2.6 illustrates this result. In the $\bar{V}_{so}^{(2)}$ range considered, $\Delta\gamma$ varies quadratically with the strength of $V_{so}^{(2)}$, as expected from first-order time-dependent perturbation theory. It should be pointed out that the dipolar interaction already leads to similar changes by itself.

Our simple approach consists of calculating the shifts ΔE_{res} by including a limited number of inelastic hyperfine channels that are significantly coupled in. The appropriate basis to discuss this point is the hyperfine basis $|(f_1 f_2) F M_F\rangle$. It turns out that of all possible components allowed by the selection rules only a very limited number contribute significantly to γ_L : those that are enhanced by the existence of the shape resonance, are sufficiently close in energy and are coupled in via significant matrix elements. Since the hyperfine splitting is very large compared to the inelastic interaction strengths, the coupling between the three f_1, f_2 subspaces can be neglected. We restrict ourselves to the $f_1 = 3, f_2 = 3$ subspace, because it contains the incoming fully spin-stretched state. As a consequence, the operators V_{hf}, V_Z, V_{dip} , and $V_{so}^{(2)}$ are equivalent to simpler effective operators: V_{hf} becomes a constant,

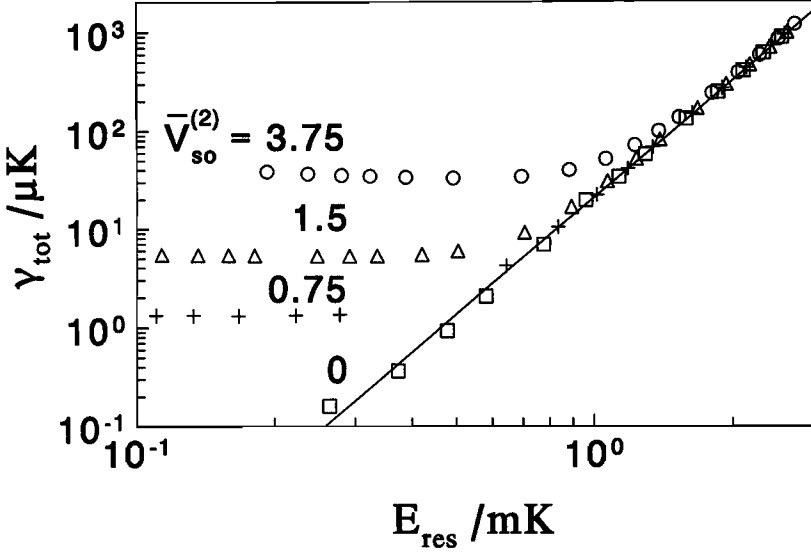


Figure 2.6: Total width $\gamma_{tot} = \gamma_{out} + (\sqrt{\gamma_{dip}} + \sqrt{\gamma_{so}})^2$ of the elastic wave function as a function of the resonance energy for various $\bar{V}_{so}^{(2)}$ values (in Ka_0) following from CC calculations. The straight line shows the tunneling width ($\gamma_{out} \sim E^{4.5}$).

V_Z couples the z -components f_{1z} and f_{2z} with effective gyromagnetic ratios

$$\gamma_f = (\gamma_e s - \gamma_n i) / f = \gamma_e / 6 - 5\gamma_n / 6 \quad (2.15)$$

to the field instead of the electronic and nuclear spins separately, V_{dip} as well as $V_{so}^{(2)}$ couple \vec{f}_1 and \vec{f}_2 , instead of \vec{s}_1 and \vec{s}_2 .

The picture thus arising is that of a new spectroscopy of long-lived states of two atoms inside a barrier, the structure of which follows from the competition between the mutual spin-spin interaction, coupling \vec{f}_1 with \vec{f}_2 , and the Zeeman precession. A fascinating aspect is the weakness of the effective spin-spin interaction: taking into account the available volume inside the barrier it is only of order 0.02 mK. The field strength needed to break it is only of order 0.2 G. With an actual field of only 7 G we are already in the strong-field limit. Although the radial dependences of $V_{so}^{(2)}$ and V_{dip} are highly different, they operate spatially only via the c-number expectation values of their radial parts. The problem is therefore completely equivalent to that of two magnetic dipoles with the orientation-dependent interaction

$$V_{spin-spin} = V_{dip} + V_{so}^{(2)} = (a_{dip} + a_{so}) [\vec{f}_1 \cdot \vec{f}_2 - 3(\hat{r} \cdot \vec{f}_1)(\hat{r} \cdot \vec{f}_2)], \quad (2.16)$$

confined to move inside a barrier. Including the angular degrees of freedom, the eigenstates are superpositions of basis states $\{|(f_1 f_2) F M_F l m_l\rangle$, subject to the selection rule $M_F + m_l = 6 + m_l^0$.

For the special case of the incident value $m_l^0 = +4$, for instance, the solution is very simple. In that case we have an elastic wave function component only, which differs, however, from that without inelastic interactions. It again shows a resonance behavior as a function of collision energy (see Fig. 2.7), but with the original Breit-Wigner resonance denominator of Eq. (2.13) replaced by a modified one. Apart from this replacement, there is to very good accuracy no change in the elastic wave function.

For $m_l^0 = +3$ the situation becomes more complicated. The number of coupled channels, including all interactions in (2.12), increases from 9 ($m_l^0 = +4$) to 16 and also the elastic-channel wave function becomes now strongly coupled to a nearby lying resonant state. The two significantly coupled states are the $f_1 = 3, f_2 = 3, F = 5, M_F = +5, l = 4, m_l = +3$ and the $f_1 = 3, f_2 = 3, F = 5, M_F = +4, l = 4, m_l = +4$ state, degenerate without Zeeman and inelastic interactions. This degeneracy is lifted by the Zeeman interaction. Considering V_{dip} and $V_{so}^{(2)}$ as first order perturbations we thus find the energy shifts for the splitted shape resonance states. Figure 2.8 shows a comparison between energy shifts following from coupled-channel calculations and values from the simple first order perturbation treatment in which only $\bar{V}_{so}^{(2)}$ occurs as a parameter. Clearly, the first order perturbation treatment describes the rigorous coupled-channel results very well. The same conclusion holds for lower m_l^0 values and other B -values ($\gg 0.2$ G).

The widths of the new shape resonance states can also be described with a perturbation treatment. In this case the lower f_1, f_2 hyperfine subspaces cannot be left out: the large final available phase space leads to large contributions to the total decay width. The total inelastic width of the resonant state is a sum of partial widths for decay to all possible hyperfine channels. Each width contains a radial transition matrix element of the sum of $V_{so}^{(2)}$ and V_{dip} between the wave functions before and after decay, to which the earlier remark about the area of the radial profile of $V_{so}^{(2)}$ applies. Making use of some Clebsch-Gordan algebra, we can express the total set of decay matrix elements and thus the total change of the width for all m_l^0 and B values in terms of the same unknown constant $\bar{V}_{so}^{(2)}$.

Only one aspect needs to be discussed before finishing the presentation of the simple approach. For $m_l^0 = 4$ there is only one channel involved. The replacement of the unperturbed Breit-Wigner denominator by a perturbed one is then equivalent to a simple multiplication of the total unperturbed state in Eqs. (2.8) and (2.11) by the ratio

$$\frac{E - E_{res} + i\gamma_{out}/2}{E - (E_{res} + \Delta E_{res}) + i(\gamma_{out} + \Delta\gamma)/2}. \quad (2.17)$$

For lower m_l^0 values the situation is more complicated. In that case the perturbed shape resonance states i are superpositions of unperturbed states with coefficients α_{i,m_l} , distinguishing the latter states by the quantum number m_l . We then need to multiply the unperturbed elastic

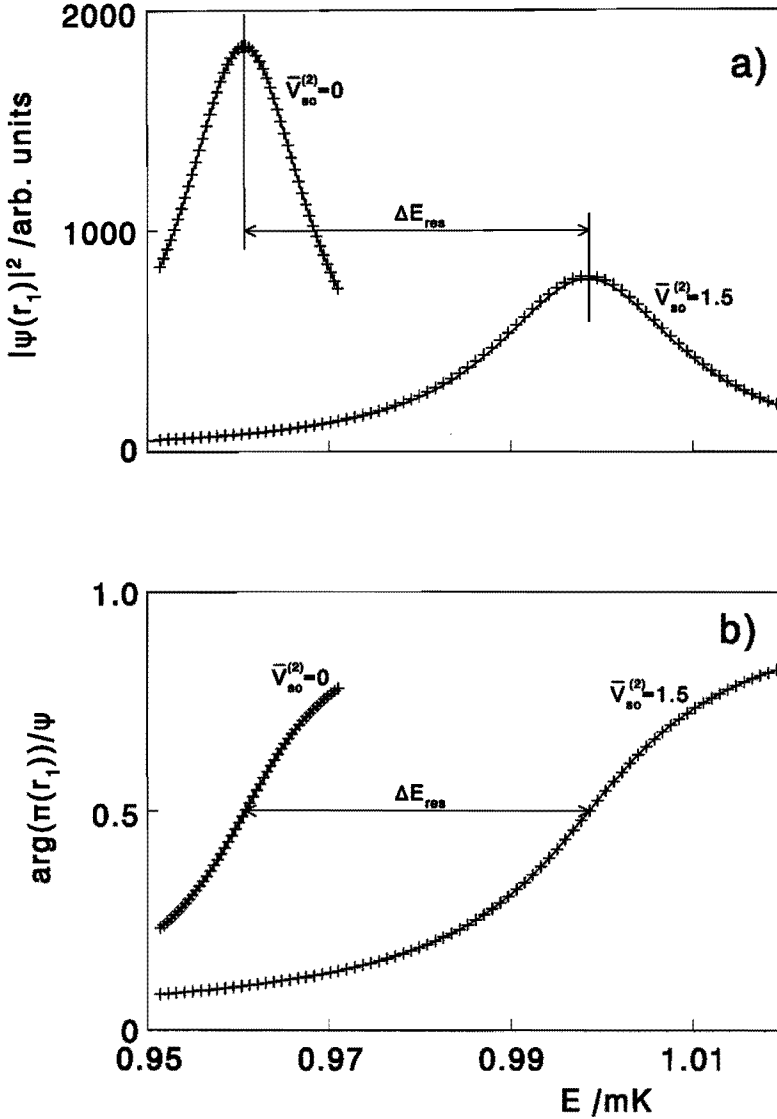


Figure 2.7: Square (a) and argument (b) of the elastic ground-state wave function at $r_1 = 45 a_0$ as a function of collision energy for $\bar{V}_{so}^{(2)} = 0$ and $\bar{V}_{so}^{(2)} = 1.5 \text{ Ka}_0$. The wave functions are corrected for the background behaviour $E^{4.5}$. The crosses are CC results, the lines show the result of the resonance formula, in the case $\bar{V}_{so}^{(2)} = 1.5 \text{ Ka}_0$ with $E_{res} = 1.00 \text{ mK}$ and $\gamma_{tot} = \Delta\gamma + \gamma_{out} = 25.4 \mu\text{K}$. The energy shift due to $V_{so}^{(2)}$ is indicated by ΔE_{res} .

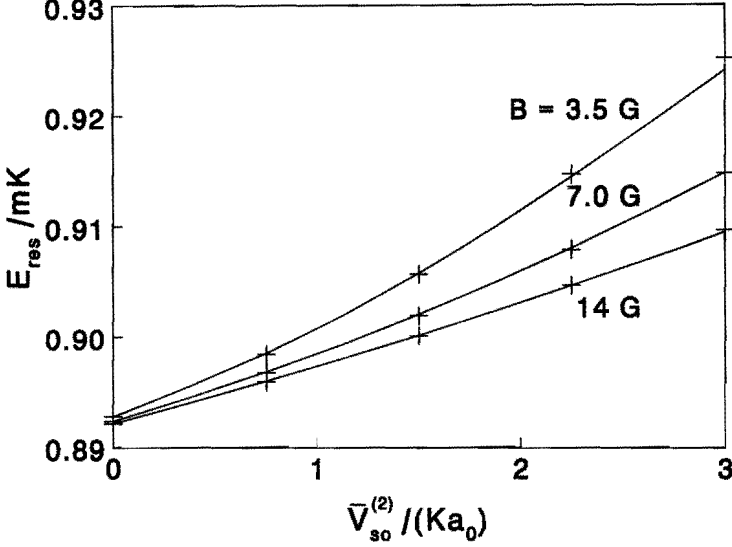


Figure 2.8: Position of a resonant level as a function of $\bar{V}_{so}^{(2)}$ for the $m_l = 3$ entrance channel for various magnetic fields. In the absence of $\bar{V}_{so}^{(2)}$ and V_{dip} the resonance occurs at $E_{res} = 0.889$ mK. The plusses are CC-results, the lines are based on a first order perturbation model. The energy shift of the resonant level due to V_{dip} alone is $3\mu\text{K}$.

scattering wave function by

$$\sum_i \alpha_{i,m_l} \frac{E - E_{res} + i\gamma_{out}/2}{E - (E_{res} + \Delta E_{res}^i) + i(\gamma_{out} + \Delta\gamma^i)/2}. \quad (2.18)$$

In other words, the coefficients α also play the role of determining the amplitudes by which an incoming channel excites the various perturbed shape resonances.

Comparing the ratio of theoretical $J = 4$ and $J = 0$ or $J = 2$ peak areas to the corresponding experimental values *without inelastic decay*, we find the theoretical ratio to be too large. This is the $J = 4$ anomaly that we pointed out previously. The theoretical $J = 4$ peak area is suppressed by the above replacement of Breit-Wigner denominators. This point is further discussed in Chapter 5.

2.4.3 Time-dependent photoassociation spectroscopy

In the previous sections we have studied a limiting situation of very low laser intensities for which the analysis of the $J = 4$ peak became feasible. Our analysis showed that it is

impossible to determine the energy location E_{res} of the g -wave shape resonance and γ_{inel} separately from low-intensity data alone. A completely new, time-dependent photoassociation experiment, however, does give complementary information about E_{res} and γ_{inel} and also shows direct evidence for the existence of a shape resonance within the $l = 4$ ground state barrier.

The time-dependent photoassociation experiment is an extension of the time-independent one as described in the introduction. A more extensive description of the time-dependent experiment can be found in Ref. [13]. The basic idea (see Fig. 2.9) is that the time period, during which the (FORT) trapping and the optical pumping lasers are switched off, is used for a pulse sequence consisting of either a single photoassociation pulse (experiment a) or a set of two pulses separated by a delay time T (experiment b). The PA laser is tuned in such a way that only atoms within the barrier are excited. If the PA laser intensity is chosen to be so high that the first pulse in experiment b excites all atoms within the barrier, the loss rate due to the second pulse is a measure for the build-up of the resonance state through the barrier during the delay time T and thus also a measure for the lifetime τ of the resonance in the absence of laser light. Comparing losses in experiments a and b enables us to determine τ . If $T \gg \tau$ the loss in experiment b will be twice as high as in experiment a, while if $T \ll \tau$ the two loss rates will be equal. This time-dependent effect is directly visible in the experimental spectra in Fig. 2.9 and in Fig. 2.11. Figure 2.11 shows the time-dependent signal A_2/A_1 : the total loss A_2 due to the set of second pulses only (area of $J = 4$ peak in the difference spectrum), divided by the total loss A_1 due to the set of single laser pulses per cycle (area of $J = 4$ peak in case a), as a function of the delay time.

In the model we construct to analyze the time-dependent photoassociation data we divide the trapped atoms in two classes: N_{in} , the number of atoms within the $l = 4$ ground state centrifugal barrier, and N_{out} , the number of atoms outside the barrier. The rate equations governing the evolution of these numbers are

$$\frac{dN_{in}}{dt} = - \{ \gamma_L/\hbar + \gamma_{out}/\hbar + \gamma_{inel}/\hbar \} N_{in} + (\gamma_{in}/\hbar) N_{out}, \quad (2.19)$$

$$\frac{dN_{out}}{dt} = -(\gamma_{in}/\hbar) N_{out} + (\gamma_{out}/\hbar) N_{in}, \quad (2.20)$$

with γ_L/\hbar the rate constant for laser excitation to a bound excited state, γ_{out}/\hbar the rate constant for tunneling outward through the barrier, γ_{in}/\hbar the rate constant for tunneling inward and γ_{inel}/\hbar the rate constant for inelastic decay to lower ground-state hyperfine levels, related to γ_{dip}/\hbar and γ_{so}/\hbar as previously indicated.

A complication in solving these equations is that saturation effects need to be taken into account in γ_{in} and γ_{out} , due to E_{res} , and in γ_L . To study these effects we constructed a two-state coupled-channels program with a triplet ground state ($|g\rangle$) and a 0_g^- excited state ($|e\rangle$), including an imaginary potential term to describe flux loss due to spontaneous emission. Using this program we calculate the probability $1 - |S_{el}|^2$ for escape from the elastic channel, with S_{el} the elastic S-matrix element, as a function of the collision energy. For low laser

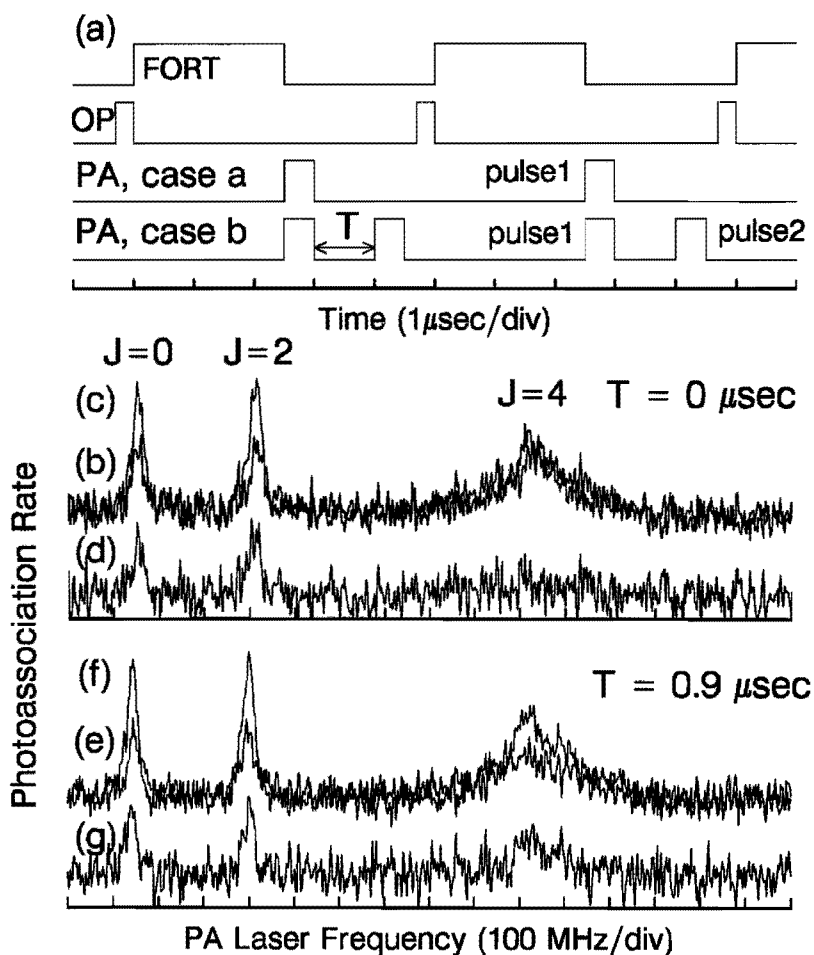


Figure 2.9: (a) Timing of laser pulses in the time-dependent photoassociation experiment. (b) to (g) Spectra of 0_g^- vibrational level at $12,573.04 \text{ cm}^{-1}$ for $T = 0$ ((b) to (d)) and $T = 0.9 \text{ μs}$ ((e) to (f)). (b) and (e) Spectrum with one photoassociation pulse only; (c) and (f) Spectrum with two photoassociation pulses. (d) and (g) Difference spectra showing the effect of pulse 2 alone, for $T = 0$ and $= 0.9 \text{ μs}$, respectively.

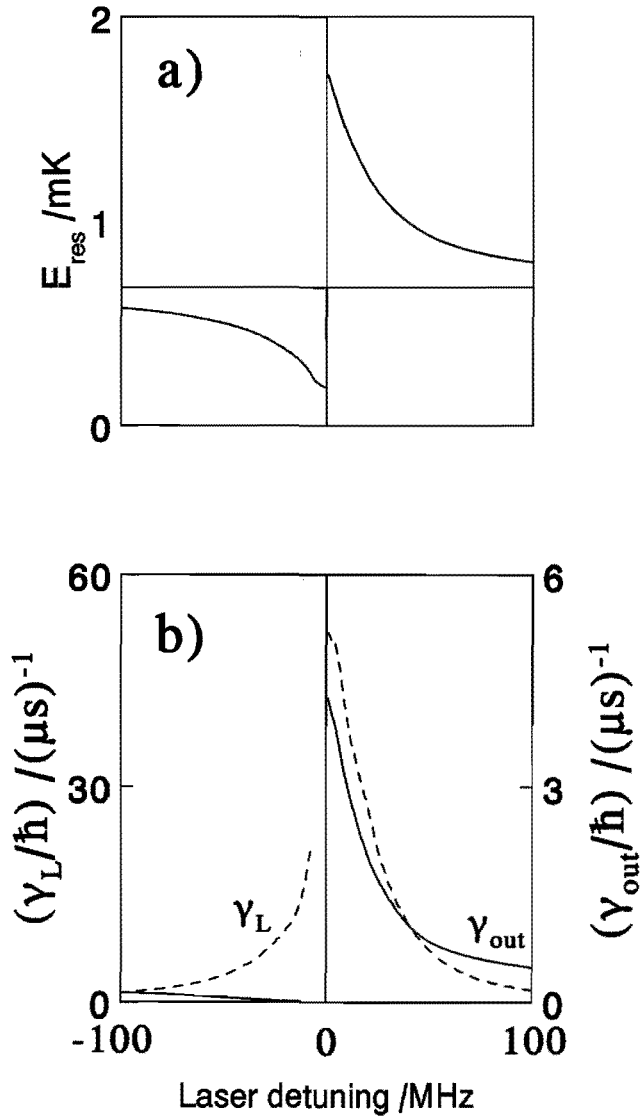


Figure 2.10: a) g -wave resonance energy; b) γ_{out} (full line) and γ_L (dashed line) as a function of laser detuning for $I = 48 \text{ W/cm}^2$.

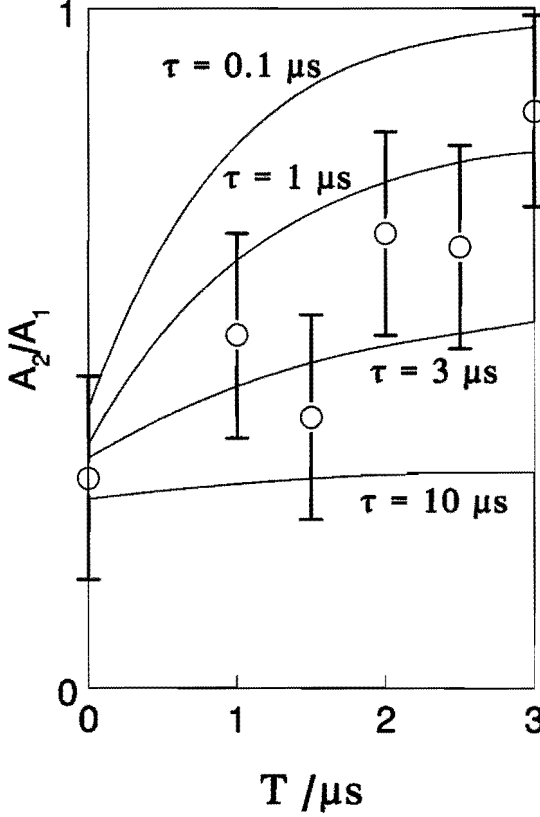


Figure 2.11: Time-dependent signal A_2/A_1 as a function of delay time T for $I = 50$ W/cm^2 , $T = 0.35$ mK and $\gamma_{out}/\gamma_{so} = 2$. Experimental data with error bars are indicated as well as theoretical curves for various lifetimes of the shape resonance τ .

intensities we reproduce Eq. (2.7), making use of the unitarity relation

$$|S_{el}|^2 + |S_{PA}|^2 = 1. \quad (2.21)$$

For high laser intensities we can directly determine γ_L , γ_{out} , and E_{res} from the escape probability [15]. In Fig. 2.10 these quantities are shown as a function of laser detuning. In this figure the laser detuning is given with respect to the laser frequency for which the bound excited level and the shape resonance overlap exactly. For vanishing laser detuning relative to the molecular transition frequency, we find γ_{out} to be reduced by a factor of 2 with respect to the corresponding semiclassical value. This is due to the fact that the laser coupling is so strong that the tunneling process cannot be discussed in terms of the bare states $|g\rangle$ and $|e\rangle$.

Instead, the dressed states [32] $|1N\rangle = (|g\rangle + |e\rangle)/\sqrt{2}$ and $|2N\rangle = (|g\rangle - |e\rangle)/\sqrt{2}$ have to be used.

The rate constants γ_L , γ_m , and γ_{out} , obtained in this way, can be used for solving Eqs. (2.19) and (2.20). The calculated loss rates, integrated over the laser detuning can directly be compared with the corresponding experimental quantities. In Fig. 2.11 the ratio of the loss A_2 due to the second pulse in experiment b alone and the loss A_1 due to the pulse in experiment a is compared with the corresponding theoretical ratio for $\gamma_{out}/\gamma_{inel} = 2$. For a discussion of the consequences of this result for γ_{so} and the indirect spin-spin relaxation of a ^{87}Rb condensate, we refer to Ref. [13].

In connection with the present work we have to address the question whether the above-mentioned conclusions concerning the role of $V_{so}^{(2)}$ in the photoassociation process affect the results of Ref. [14]. An analysis along the lines of the present work for ^{87}Rb shows that the tunneling lifetime of the d -wave shape resonance in this case is much shorter than γ_{inel} , justifying the earlier analysis in which we neglected the spin-orbit (and dipolar) relaxation of the shape resonance.

References

- [1] K. Gibble and S. Chu, *Metrologia* **29**, 201 (1992).
- [2] M.H. Anderson, J.R. Ensher, M.R. Matthews, C.E. Wieman, and E.A. Cornell, *Science* **269**, 198 (1995).
- [3] C.C. Bradley, C.A. Sacket, J.J. Tollet, and R.G. Hulet, *Phys. Rev. Lett.* **75**, 1687 (1995).
- [4] K.B. Davis, M-O Mewes, M.R. Anderson, N.J. van Druten, D.M. Kurn, and W. Ketterle, *Phys. Rev. Lett.* **75**, 3969 (1995).
- [5] J.D. Miller, R.A. Cline, and D.J. Heinzen, *Phys. Rev. Lett.* **71**, 2204 (1994); R.A. Cline, J.D. Miller, and D.J. Heinzen, *Phys. Rev. Lett.* **73**, 632 (1994).
- [6] L.P. Ratliff, M.E. Wagshull, P.D. Lett, S.L. Rolston, and W.D. Phillips, *J. Chem. Phys.* **101**, 2638 (1994).
- [7] W.I. McAlexander, E.R.I. Abraham, N.W.M. Ritchie, C.J. Williams, H.T.C. Stoof, and R.G. Hulet, *Phys. Rev. A* **51**, 871 (1995).
- [8] R. Napolitano, J. Weiner, C.J. Williams, and P.S. Julienne, *Phys. Rev. Lett.* **73**, 1352 (1994).
- [9] J.R. Gardner, R.A. Cline, J.D. Miller, D.J. Heinzen, H.M.J.M. Boesten, and B.J. Verhaar, *Phys. Rev. Lett.* **74**, 3764 (1995).

- [10] This approximation can easily be improved by calculating a radial transition integral. This is done in the actual analysis.
- [11] P.D. Lett, P.S. Julienne, and W.D. Phillips, *Ann. Rev. Phys. Chem.* **46**, 423 (1995); E.R.I. Abraham, W.I. McAlexander, H.T.C. Stoof, and R.G. Hulet, *Phys. Rev. A* **53**, 3092 (1996); C.J. Williams, E. Tiesinga, and P. Julienne (unpublished).
- [12] M. Movre and G. Pichler, *J. Phys. B* **10**, 2631 (1977).
- [13] H.M.J.M. Boesten, C.C. Tsai, B.J. Verhaar, and D.J. Heinzen (unpublished).
- [14] H.M.J.M. Boesten, C.C. Tsai, J.R. Gardner, D.J. Heinzen, and B.J. Verhaar (unpublished).
- [15] H. Feshbach, *Theoretical Nuclear Physics, Part I: Nuclear Reactions* (Wiley, New York, 1992).
- [16] W.I. McAlexander, E.R.I. Abraham, and R.G. Hulet, *Phys. Rev. A* **54**, R5 (1996); W.I. McAlexander, E.R.I. Abraham, and R.G. Hulet, *Phys. Rev. A* **51**, R871 (1995).
- [17] W.I. McAlexander, E.R.I. Abraham, and R.G. Hulet, *Bul. Am. Phys. Soc.* **41**, 1065 (1996).
- [18] H. Wang, J. Li, P.L. Gould, and W.C. Stwalley, *Bul. Am. Phys. Soc.* **41**, 1083 (1996).
- [19] M. Marinescu, A. Dalgarno, C.C. Tsai, J.D. Miller, R.A. Cline, and D.J. Heinzen, *Bul. Am. Phys. Soc.* **41**, 1083 (1996).
- [20] K.M. Jones, P.S. Julienne, P.D. Lett, W.D. Phillips, E. Tiesinga, and C.J. Williams, *Bul. Am. Phys. Soc.* **41**, 1083 (1996).
- [21] A.J. Moerdijk, W.C. Stwalley, R.G. Hulet, and B.J. Verhaar, *Phys. Rev. Lett.* **72**, 40 (1994); A.J. Moerdijk and B.J. Verhaar, *Phys. Rev. Lett.* **73**, 518 (1994).
- [22] B. Bussery and M. Aubert-Frécon, *J. Chem. Phys.* **82**, 3224 (1985).
- [23] F. Spiegelmann, D. Pavolini, and J.-P. Daudley, *J. Phys. B* **22**, 2465 (1989).
- [24] U. Volz and H. Schmoranzler (private communication).
- [25] C.J. Williams, F.H. Mies, P.S. Julienne, and M. Krauss (unpublished).
- [26] A.M. Mizushima, *The Theory of Rotating Diatomic Molecules* (Wiley & Sons, New York, 1975).
- [27] E.R.I. Abraham, W.I. McAlexander, C.A. Sacket, and R.G. Hulet, *Phys. Rev. Lett.* **74**, 1315 (1995).

- [28] F.H. Mies, P.S. Julienne, and C.J. Williams (private communication).
- [29] M. Krauss and W.J. Stevens, *J. Chem. Phys.* **93**, 4236 (1990).
- [30] C. Amiot, *J. Chem. Phys.* **93**, 8591 (1990).
- [31] J.R. Taylor, *Scattering Theory* (Wiley, New York, 1972).
- [32] C. Cohen-Tannoudji, J. Dupont-Roc, G. Grynberg, *Atom-Photon Interactions* (Wiley, New York, 1992).

Chapter 3

Collisions of doubly spin-polarized, ultracold ^{85}Rb atoms

J. R. Gardner, R. A. Cline, J. D. Miller, D. J. Heinzen, H. M. J. M. Boesten, and B. J. Verhaar

Published in Physical Review Letters **74**, 3764 (1995)

Abstract

We study the collisions of doubly spin-polarized ^{85}Rb atoms at millikelvin temperatures using photoassociation spectroscopy. Because the atoms are spin polarized, only triplet collisional states are formed. This leads to photoassociation spectra of a particularly simple form, which provide a very direct probe of the ground state collision. These spectra are analyzed to yield the ground state triplet scattering length $-1000a_0 < a_T < -60a_0$ for ^{85}Rb , $+85a_0 < a_T < +140a_0$ for ^{87}Rb , and the product of the D-line dipole matrix elements $d(P_{1/2})d(P_{3/2}) = 8.75 \pm 0.25$ a.u.

Rapidly developing techniques for trapping and cooling neutral atoms using laser fields are opening up a wide array of new applications. These include the construction of very precise atomic clocks [1–3], sensitive electric dipole moment searches [4], and possible studies of quantum collective phenomena such as Bose-Einstein condensation. Success in each of these applications hinges critically on understanding the long-range interactions between cold atoms. Cold collision cross sections are very sensitive to long-range atomic interactions and play a dominant role in many experiments. For example, collisional frequency shifts may limit the accuracy of cold atomic fountain clocks [2,3]. Moreover, efforts to achieve Bose-Einstein condensation in a dilute laser-cooled gas depend critically on the ground state scattering length, which must be positive and preferably large [5–8].

Despite their importance, long-range interactions between atoms have been determined by conventional molecular spectroscopy in only a limited number of cases. The lack of extensive data is due in part to the difficulty of populating long-range states starting from the molecular ground state. On the other hand, these states are readily populated in collisions between ultracold atoms, in particular, by photoassociation spectroscopy [9]. Photoassociation spectra

of Na [10,11], Rb [12,13], and Li [14] have already been obtained directly yielding detailed information on their long-range excited state interactions. In this paper, we present new ^{85}Rb photoassociation data and analysis, and show for the first time that atomic ground state interaction parameters can be determined from photoassociation spectra.

A crucial aspect of our experiment is that we doubly spin polarize the colliding atoms. This is important, since the ground state collision is thereby restricted to the triplet channel, and the analysis becomes relatively straightforward. An experiment using unpolarized atoms would need to determine both singlet and triplet parameters simultaneously. As a result of the spin polarization, we are able to observe clear, quantum-statistical features of the collisions. By doubly polarizing the atoms, and choosing a suitable excited state, we obtain spectra which provide a very simple and direct probe of the ground state collision: Each peak effectively measures the amplitude of a particular partial wave of the collision, thus yielding detailed information about the ground state interatomic potential in a narrow radial range that may be varied by the choice of excited state energy. This is, to our knowledge, the first report of doubly spin-polarized ultracold collisions of alkali atoms.

In our experiment, we load approximately 10^4 ^{85}Rb atoms into a far off-resonance optical dipole force trap (FORT) [15]. The FORT laser beam is a linearly polarized, Gaussian beam containing about 1.5 W of optical power and focused to a waist of about 10 μm . The FORT laser is tuned to $12,289\text{ cm}^{-1}$, which lies between two well-resolved photoassociation peaks. To define a quantization axis, a magnetic field of 7 G is applied along the FORT laser beam propagation (\hat{z}) direction.

Once the atoms are loaded into the FORT, they are exposed to a combination of laser fields for 200 ms. Each 200 ms period is broken into a series of 5 μs cycles in which the atoms are irradiated by four laser fields in sequence. During the first 2.5 μs of each cycle, only the FORT laser is applied. During the next 0.6 μs , only two optical pumping (OP) beams interact with the atoms. One of these is tuned to the $^{85}\text{Rb } 5^2S_{1/2}(F=3) \rightarrow 5^2P_{3/2}(F=3)$ transition and is circularly polarized. It has an intensity of $100\ \mu\text{W}/\text{cm}^2$ and propagates along the z direction. The other optical pumping beam is tuned to the $^{85}\text{Rb } 5^2S_{1/2}(F=2) \rightarrow 5^2P_{3/2}(F=3)$ transition. During the last 1.9 μs of each cycle, only the photoassociation (PA) laser field is applied, which is linearly polarized, propagates in the z direction, and has an intensity in the range from 20 to 80 W/cm^2 . The combined effect of these fields is to trap the atoms, to keep them optically pumped into the $^{85}\text{Rb } 5^2S_{1/2}(F=3, M_F=3)$ state, and to induce photoassociation transitions. Alternation of the fields in time prevents the light shift of the FORT beam from disrupting the optical pumping or from shifting and broadening the photoassociation resonances. At least 95% of the atoms are in the doubly spin-polarized state.

Photoassociation transitions induced by the PA laser promote colliding pairs of Rb atoms into specific excited bound Rb_2^* states. In order to obtain a spectrum of these states, we repeat the loading and 200 ms irradiation period for a succession of PA laser frequencies [12,13]. At the end of each cycle we detect the number of atoms remaining in the trap with laser-induced

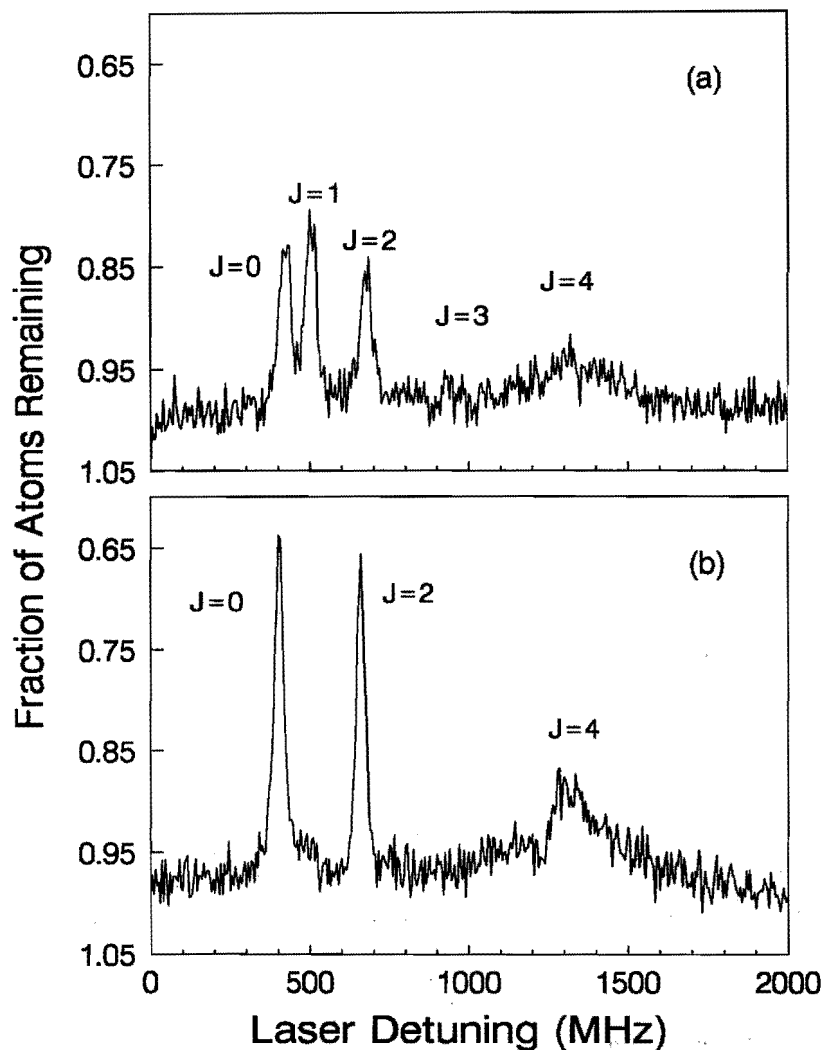


Figure 3.1: Photoassociation spectrum of the 0_g^- vibrational level at $12,573.05\text{ cm}^{-1}$. (a) Full rotational spectrum from $J = 0$ to 4 observed for atoms in $5^2S_{1/2}$, $F = 3$ level but otherwise unpolarized. (b) Spectrum recorded with doubly spin-polarized atoms. Odd rotational lines disappear as a consequence of spin statistics.

fluorescence. Because the excited Rb_2^* states decay predominantly to free pairs of atoms with kinetic energy sufficient to leave the trap, the photoassociation resonances are detectable as a reduction in the fluorescence.

A photoassociation spectrum of a single 0_g^- vibrational level at $12,573.05 \text{ cm}^{-1}$ is shown in Fig. 3.1. In Fig. 3.1(a), we show the spectrum observed when the atoms are maintained in the $5^2S_{1/2}$, $F = 3$ level but are otherwise unpolarized. A pure rotational spectrum spanning the range from $J = 0$ to 4 is observed. In Fig. 3.1(b), we show a spectrum recorded with doubly spin-polarized atoms. The odd rotational lines disappear as a consequence of spin statistics.

In order to realize a determination of the $^{85}\text{Rb}_2$ ground state parameters, we recorded data similar to that shown in Fig. 3.1 for a series of vibrational levels of the 0_g^- state that asymptotically connects to the $5^2S_{1/2} + 5^2P_{1/2}$ separated atom limit [16,17]. Five vibrational levels were used in the analysis, with $J = 0$ level energies of -3.365 , -4.088 , -4.901 , -5.812 and, -6.827 cm^{-1} with respect to the barycenter of the $5^2S_{1/2} + 5^2P_{1/2}$ dissociation limit, which corresponds to an energy of $12,578.864 \text{ cm}^{-1}$ in our spectrum. The outer turning points of these states range from $41.6 a_0$ to $46.7 a_0$.

The photoassociation spectrum is conveniently described in the dressed-state picture. In that framework each of the $\text{Rb} + \text{Rb}^*$ rovibrational states $|\Omega JM\rangle$ is a discrete state embedded in the ground state continuum [18]. As a result of the interaction with the PA laser field, it acquires a finite partial width γ_L for decay into each of the ground state channels in addition to its spontaneous linewidth γ_0 . This partial width γ_L is proportional to the PA laser intensity I_L and is given by Fermi's golden rule,

$$\gamma_L = 2\pi \left| \langle \Omega JM | [\vec{d}(1) + \vec{d}(2)] \cdot \vec{E}_L | SM_S l m_l, \epsilon \rangle \right|^2, \quad (3.1)$$

where $\vec{E}_L = E_L \vec{\sigma}_L$ is the PA laser field and $|SM_S l m_l, \epsilon\rangle$ is the energy-normalized continuum ground state. Accordingly, the squared S-matrix element for photoassociation followed by spontaneous emission is given by a Breit-Wigner expression. To first order in I_L

$$|S_{\Omega JM, SM_S l m_l}|^2 = \frac{\gamma_0 \gamma_L (\Omega JM \rightarrow SM_S l m_l)}{(\epsilon + E_g + \hbar\omega_L - E_e)^2 + \frac{1}{4}\gamma_0^2}. \quad (3.2)$$

Here E_g is the asymptotic $\text{Rb} + \text{Rb}$ internal energy, E_e is the energy of the $|\Omega JM\rangle$ state, and ϵ is the collision energy. Equation (3.2) is thermally averaged and summed over J, M, l, m_l to obtain the rate coefficient. The above expressions, without the directional dependences, were first used to analyze photoassociation spectra by Napolitano *et al.* [19]. Expanding $|\Omega JM\rangle$ in atomic fine-structure states [16,17] coupled to total electronic angular momentum $j m_j$,

$$\begin{aligned} \gamma_L &= \frac{2\pi I_L}{\epsilon_0 c} \left| \sum_j (J\Omega j - \Omega|l0)(j m_j l m_l | JM) \right. \\ &\quad \times \int_0^\infty dr c_j(r) u_{\Omega J}(r) (j m_j | [\vec{d}(1) + \vec{d}(2)] \cdot \vec{\sigma}_L | SM_S) u_i(r) \left. \right|^2. \end{aligned} \quad (3.3)$$

The above-mentioned $0_g^-(S + P_{1/2})$ electronic state has a number of simplifying features that facilitate the analysis considerably. First, it is a pure triplet state [16], so that no singlet amplitude is coupled in by the excitation. Second, as with any of the $\Omega = 0$ states, it has negligible second-order hyperfine energy shifts. Third, at the relevant interatomic distances near the outer turning point, this 0_g^- state is, to very good approximation, a product of independent atomic states $S_{1/2}$ and $P_{1/2}$, coupled to form $j = 0$. As a consequence, only states for which $J = l = \text{even}$ are excited. Thus our data display directly the quantum statistics of the atoms: Because they are bosons, they may only collide in even ground state partial waves. Note that the magnetic field has negligible influence on the spectrum.

We find γ_L for the 0_g^- state to be a product of a geometrical coefficient and a squared radial integral $\int dr u_{\Omega J}(r) d_{eg}(r) u_l(r)$, in abbreviated notation. Notice that a $j = 0$ component of the upper state cannot be excited by σ^+ laser light starting with doubly polarized ground state atoms with $S = M_S = +1$. Indeed, a full calculation of the excitation rate, taking into account all components of the 0_g^- state, shows this photoassociation rate to be smaller than that for σ^- light by 2 orders of magnitude. This prediction is confirmed by experiment.

Because of the small ranges of ϵ and l involved, cold collisions have the unique property of being insensitive to the detailed behavior of the badly known inner parts of the interatomic potential. The variation of the radial wave function with E and l is a very small first-order perturbation up to a rather large radius r_0 . The only relevant information is the accumulated information contained in the phase $\phi(E, l)$ of the rapidly oscillating wave function at r_0 and its first derivatives for $E = l = 0$ [20]. Model calculations show that for $l \leq 2$ and $r_0 = 30a_0$, the calculated photoassociation rates are sufficiently insensitive to the precise values of the first derivatives that they can be taken reliably from an *ab initio* calculation [21]. This insensitivity was used and explained previously in Refs. [22,23]. A similar accumulated-phase method was adopted for the excited state. At large distances where excitation of the above-mentioned five vibrational levels occurs, our calculated results are almost independent of the dispersion parameters C_{ne} ($n \geq 6$) for the excited state and C_{ng} ($n \geq 8$) for the ground state, provided that these are taken within the bounds of the present uncertainty [17,24–26].

From the energies of the five measured $J = 0$ levels we derive a value 8.75 ± 0.25 a.u. for the product $d(P_{1/2})d(P_{3/2})$ of D -line dipole matrix elements [27], which determines the strength of the resonant-dipole $1/r^3$ potential in the present r range. This value is in agreement with the most accurate previous measurements $d^2(P_{1/2}) = 8.43 \pm 0.20$ a.u. [28], $d^2(P_{3/2}) = 9.19 \pm 0.18$ a.u. [28], $d^2(P_{3/2}) = 9.08 \pm 0.28$ a.u. [29], and $d^2(P_{3/2}) = 8.68 \pm 0.16$ a.u. [30].

The analysis of the data is carried out as follows. As a first step, we use the strongest $J = 0$ and 2 rotational lineshapes to determine an optimum temperature for each point of a grid of C_{6g} - ϕ_g values by a least-squares fit to the measured data points. For this purpose, C_{6g} is taken to lie between between 3500 and 6000 a.u. and ϕ_g is allowed to span a full π range. Using these temperatures, we apply a least-squares fit to the ratios of the $J = 0$ peak areas over the C_{6g} and ϕ_g plane (least-squares function χ_1^2), which constrains these

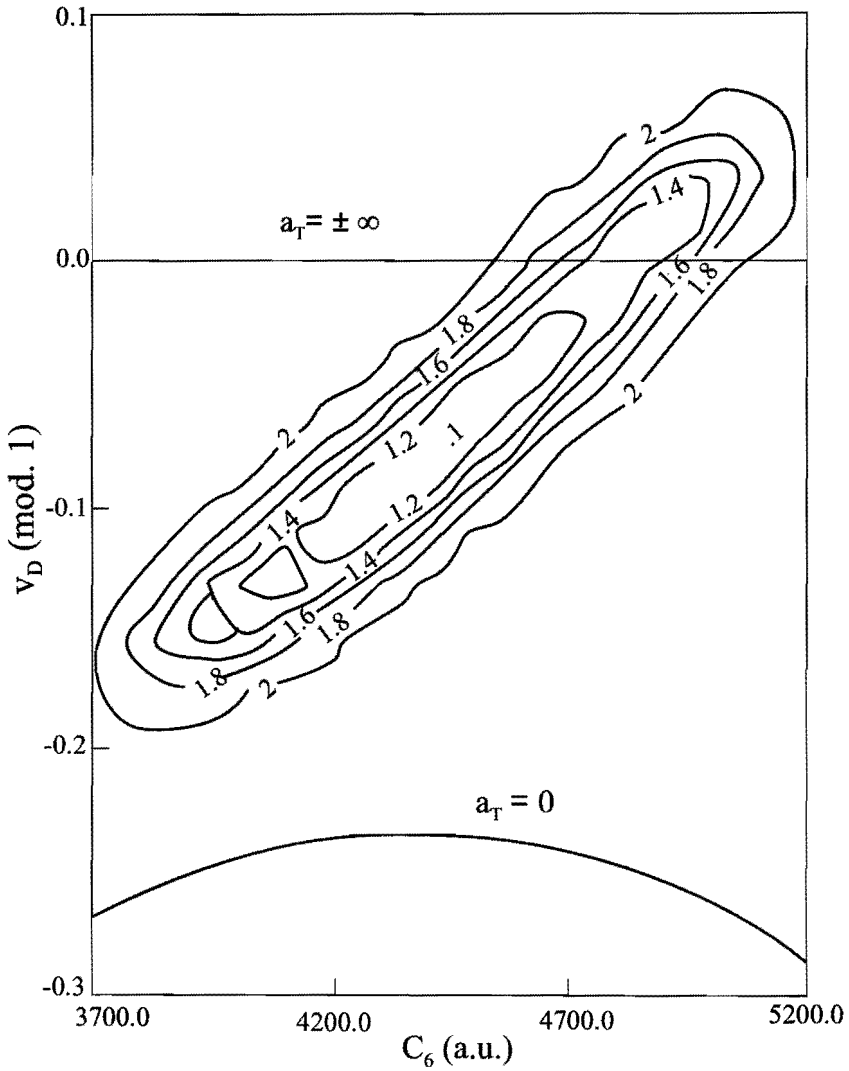


Figure 3.2: Contour plot of total χ^2 surface for ratios of $J = 0$ and 2 photoassociation peak areas, as a function of C_{6g} and s -wave vibrational quantum number v_D at dissociation. Lines where a_T changes sign are indicated.

parameters to lie in a narrow strip and determines the temperature to be $500 \pm 100 \mu\text{K}$. We then calculate the χ_2^2 and χ_3^2 functions associated with the four $J = 2$ and one $J = 2$ to $J = 0$ ratios of peak areas, respectively, over the limited ranges of C_{6g} and ϕ_g found previously. We find that χ_2^2 sets about the same limits on C_{6g} and ϕ_g as χ_1^2 . However, χ_3^2 sets a limit that corresponds to a different strip in the C_{6g} - ϕ_g plane. The intersection of these strips gives the estimated values and uncertainties of C_{6g} and ϕ_g . Figure 3.2 shows a contour plot of the total χ^2 surface combining the above three sets of ratios of peak areas. Instead of ϕ_g , we use the more transparent (fractional) s -wave vibrational quantum number v_D at dissociation as a parameter. The lines where the triplet scattering length a_T changes sign are indicated. While C_{6g} is experimentally constrained to about the full range of theoretically predicted values [17,24,31], $v_D(\text{mod } 1)$ is found to be in the interval between $+0.07$ and -0.19 . Including the uncertainty in d^2 , C_{6e} , and C_{8g} , we find a_T to be negative with at least 80% probability. For the recently predicted value $C_{6g} = 4426$ a.u. from Ref. [24], which is believed to be correct within a few percent [26], we find $v_D(^{85}\text{Rb}, \text{mod } 1) = -0.09 \pm 0.07$ and $-1000a_0 < a_T(^{85}\text{Rb}) < -60a_0$. Figure 3.3 shows a comparison of theoretical and

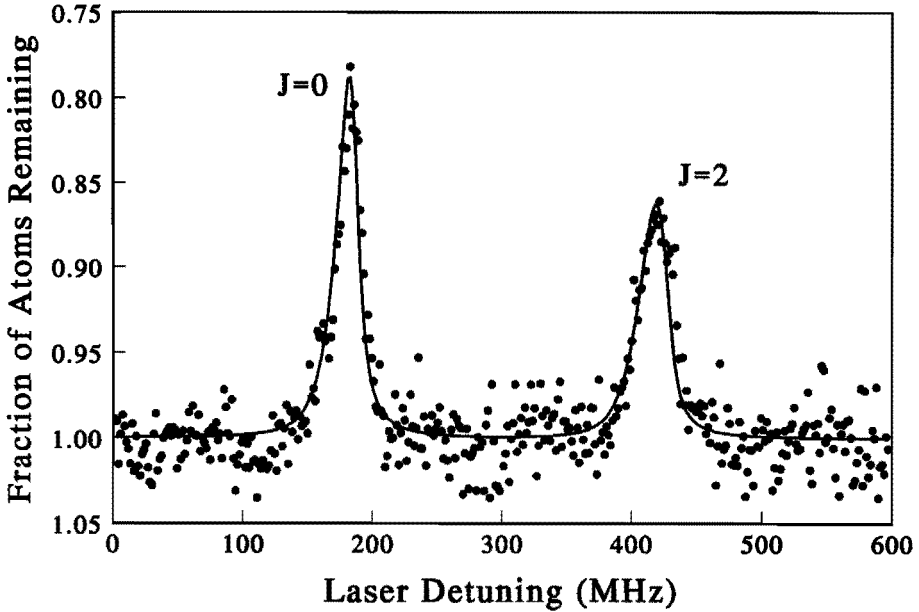


Figure 3.3: Comparison of theoretical and experimental line shapes for rotational levels at $12,573.96 \text{ cm}^{-1}$. Each J peak arises only from the partial wave $l = J$.

experimental line shapes of the $J = 0$ and 2 rotational levels at $12,573.96 \text{ cm}^{-1}$ for this value

of C_{6g} and $v_D(\text{mod } 1) = -0.09$.

A simple \sqrt{m} scaling procedure enables us to find the corresponding results for the ^{87}Rb isotope. On the basis of the triplet potential of Krauss and Stevens [21] we take the number of s -wave radial nodes within r_0 to be 34 ± 3 . We then derive ϕ_g for ^{87}Rb and by radial integration to larger distances, introducing five additional nodes, find $v_D(^{87}\text{Rb}, \text{mod } 1) = +0.37 \pm 0.10$ and $+85a_0 < a_T(^{87}\text{Rb}) < +140a_0$. Also for the total theoretical C_{6g} range a_T is found to be positive.

To summarize, we have used high-resolution photoassociation spectroscopy to study the collisions of ultracold ^{85}Rb atoms. By doubly spin polarizing the atoms, and choosing the particular excited state $0_g^-(5^2S_{1/2} + 5^2P_{1/2})$, we obtain spectra which provide a very simple and direct probe of the ground state collision: Each peak effectively measures the amplitude of a particular partial wave of the ground state collision, in a narrow radial range that may be varied by the choice of excited state energy. Because of this, we obtain detailed information about the ground state interatomic potential. Analysis of these spectra reveals that the ground state triplet scattering length of ^{85}Rb is large and negative, so that no stable Bose condensate is possible for this state of this isotope. Using mass scaling arguments, we are led to the opposite conclusion for the ^{87}Rb isotope. Apparently, its triplet scattering length is positive so that it remains a viable candidate for observation of a stable Bose-Einstein condensate.

References

- [1] A. Clairon, C. Salomon, S. Guellati, and W. D. Phillips, *Europhys. Lett.* **12**, 683 (1991).
- [2] K. Gibble and S. Chu, *Phys. Rev. Lett.* **70**, 1771 (1993).
- [3] E. Tiesinga, B. J. Verhaar, H. T. C. Stoof, and D. van Bragt, *Phys. Rev. A* **45**, R2671 (1992).
- [4] M. Bijlsma, B. J. Verhaar, and D. J. Heinzen, *Phys. Rev. A* **49**, R4285 (1994).
- [5] A. L. Fetter and J. D. Walecka, *Quantum Theory of Many-Particle Systems* (McGraw-Hill, New York, 1971), p. 218.
- [6] E. Tiesinga, A. J. Moerdijk, B. J. Verhaar, and H. T. C. Stoof, *Phys. Rev. A* **46**, R1167 (1992).
- [7] H. T. C. Stoof, *Phys. Rev. A* **49**, 3824 (1994).
- [8] C. Monroe, E.A. Cornell, C.A. Sacket, C.J. Myatt, and C.E. Wieman, *Phys. Rev. Lett.* **70**, 414 (1993).
- [9] H. R. Thorsheim, J. Weiner, and P. S. Julienne, *Phys. Rev. Lett.* **58**, 2420 (1987).

- [10] P. D. Lett, K. Helmerson, W. D. Phillips, L. P. Ratliff, S. L. Rolston, and M. E. Wagshul, *Phys. Rev. Lett.* **71**, 2200 (1993).
- [11] L. P. Ratliff, M. E. Wagshul, P. D. Lett, S. L. Rolston, and W. D. Phillips, *J. Chem. Phys.* **101**, 2638 (1994).
- [12] J. D. Miller, R. A. Cline, and D. J. Heinzen, *Phys. Rev. Lett.* **71**, 2204 (1993).
- [13] R. A. Cline, J. D. Miller, and D. J. Heinzen, *Phys. Rev. Lett.* **73**, 632 (1994).
- [14] W. I. McAlexander, E. R. I. Abraham, N. W. M. Ritchie, C. J. Williams, H. T. C. Stoof, and R. G. Hulet, *Phys. Rev. A* **51**, 871 (1995).
- [15] J. D. Miller, R. A. Cline, and D. J. Heinzen, *Phys. Rev. A* **47**, 4567 (1993).
- [16] M. Movre and G. Pichler, *J. Phys. B* **10**, 2631 (1977).
- [17] B. Bussery and M. Aubert-Frecon, *J. Chem. Phys.* **82**, 3224 (1985).
- [18] H. Feshbach, *Theoretical Nuclear Physics, Part 1: Nuclear Reactions* (Wiley, New York, 1992).
- [19] R. Napolitano, J. Weiner, C.J. Williams, and P.S. Julienne, *Phys. Rev. Lett.* **73**, 1352 (1994).
- [20] B.J. Verhaar, K. Gibble, and S. Chu, *Phys. Rev. A* **48**, R3429 (1993).
- [21] M. Krauss and W.J. Stevens, *J. Chem. Phys.* **93**, 4236 (1993).
- [22] A.J. Moerdijk, W.C. Stwalley, R.G. Hulet, and B.J. Verhaar, *Phys. Rev. Lett.* **72**, 40 (1994).
- [23] A.J. Moerdijk and B.J. Verhaar, *Phys. Rev. Lett.* **73**, 518 (1994).
- [24] M. Marinescu, H.R. Sadeghpour, and A. Dalgarno, *Phys. Rev. A* **49**, 982 (1994).
- [25] M. Marinescu and A. Dalgarno (private communication).
- [26] W.C. Stwalley (private communication).
- [27] H.M.J.M. Boesten *et al.* (to be published).
- [28] A. Gallagher and E. L. Lewis, *Phys. Rev. A* **10**, 231 (1974).
- [29] R. W. Schmeider *et al.*, *Phys. Rev. A* **2**, 1216 (1970).
- [30] J. K. Link, *J. Opt. Soc. Am.* **56**, 1195 (1966).

- [31] M.L. Manokov and V.O. Ovsianikov, *J. Phys. B* **10**, 659 (1985); A. Dalgarno, *Adv. Chem. Phys.* **12**, 143 (1967); F. Maeder and W. Knutznigg, *Chem. Phys.* **42**, 195 (1979).

Chapter 4

Observation of a shape resonance in the collision of two cold ^{87}Rb atoms

H. M. J. M. Boesten, C. C. Tsai, J. R. Gardner, D. J. Heinzen, and B. J. Verhaar

To be published in Physical Review A

Abstract

We observe a shape resonance in the scattering of two ultracold ^{87}Rb atoms, causing the colliding atoms to form a long-living compound system inside an $l = 2$ centrifugal barrier. Its existence follows from a photoassociation experiment in a gas sample of doubly polarized ^{87}Rb atoms. Using it we are able to carry out the first direct determinations of the triplet scattering length for ^{87}Rb , relevant to Bose-Einstein condensation experiments, and of the $\text{Rb} + \text{Rb } C_6$ dispersion coefficient. Consequences for the ^{85}Rb scattering length are discussed.

4.1 Introduction

A fascinating aspect of the recent successful Bose-Einstein condensation (BEC) experiments in cold gas samples of ^{87}Rb , ^7Li and ^{23}Na atoms [1] is its close resemblance to the ideal gas BEC paradigm as it was originally predicted by Bose and Einstein [2]. In fact, instead of the complicated particle interactions involved in other laboratory BEC phenomena, the atom-atom interaction enters the description of the phase transition in an ultracold dilute gas only in the form of a single parameter, the scattering length a . On the time scale of the two-body collisions any atomic gas behaves like a hypothetical gas with the same value of a but without bound two-body states. The (in)stability of the Bose condensate is one of the properties that are fully determined by a . It is believed that in a homogeneous gas a Bose condensate is stable only for positive a [3,4]. In a trap it is possible to form a condensate with a long lifetime also for $a < 0$ if the total number of atoms is below a certain maximum [5,6], but in this case too a is a crucial quantity governing the equilibrium and non-equilibrium condensate properties.

The significance of the two-body collision parameters in atomic gases is not restricted to BEC experiments. For instance, the accuracy of recent improved versions of the cesium atomic frequency standard based on a fountain of laser-cooled atoms depends critically on elastic collisions among the atoms during their fountain orbit [7].

Several methods have been developed to obtain reliable information on such cold collision properties. One is based on measuring the density-dependent frequency shift of a fountain clock [8]. A second method consists of extrapolation from the highest part of the bound-state spectrum through $E = 0$, i.e., by inferring triplet and singlet scattering lengths a_T and a_S from (differences of) energies of the highest bound triplet and singlet states [9–11]. A third method that has recently proven to be very powerful is based on photoassociation spectroscopy [12–16], which can directly measure the oscillations of the continuum wave function for low positive E [12,16,17].

In this paper, we consider a combination of the latter two methods. Using photoassociation spectroscopy we observe a strong d -wave shape resonance in the scattering of two doubly-spin polarized ^{87}Rb atoms. Such a quasi-bound state inside a centrifugal barrier is as restrictive for the description of cold collisions as finding a high-lying bound state of the $^{87}\text{Rb}_2$ triplet dimer: the usual Franck-Condon oscillations observed in photoassociation experiments only dictate the node structure of the ground-state radial wave function in the excitation region and this fixes the node structure at infinity, i.e., a_T , only when the long-range potential depending on C_6 is accurately known. The existence of a (quasi-)bound state close to threshold is precisely the additional piece of information needed to eliminate the remaining freedom. In the following we will demonstrate this more explicitly (see Fig. 4.4 and accompanying discussion). This allows us to carry out the first direct determination of the $^{87}\text{Rb} + ^{87}\text{Rb}$ triplet scattering length, i.e., not via ^{85}Rb , and of the $\text{Rb} + \text{Rb}$ C_6 dispersion coefficient. While the previous determination [16] of $a_T(^{87}\text{Rb})$ rested on a theoretical C_6 value [18] and on mass-scaling a result for ^{85}Rb to ^{87}Rb using a theoretical number of bound triplet s -wave states, we are now able to dispense with these and still obtain a much narrower a_T range. The mass-scaling estimate uses the relation

$$v_D(^{87}\text{Rb}) = v_D(^{85}\text{Rb}) \sqrt{\frac{m(^{87}\text{Rb})}{m(^{85}\text{Rb})}}, \quad (4.1)$$

based on the WKB-approximation, with v_D the (fractional) vibrational quantum number for $l = 0$ at dissociation [19]. The analysis of a photoassociation experiment does not give information on the integer part of v_D , i.e., on the number of bound states n_b minus 1. Making use of a theoretical C_6 value, this yielded a range $+85a_0 < a_T(^{87}\text{Rb}) < +200a_0$ [16]. In view of a possible deviation of C_6 an explicit exclusion of the “adjacent” large negative values is highly desirable. In the present paper we also derive an improved value for the Rb 5S-5P dipole matrix element, and obtain an indirect measurement of the number of $^{87}\text{Rb}_2$ triplet bound states.

4.2 Experiment and analysis

The experiment is similar to that of Ref. [16]. About 10^4 ^{87}Rb atoms are loaded into a far-off resonance optical dipole force trap (FORT) [20]. These atoms are exposed to a combination of laser fields for 200 ms. This period is divided into repeated $5\ \mu\text{s}$ cycles. During the first $2.5\ \mu\text{s}$ of each cycle only the trapping (FORT) laser is on. During the next $0.6\ \mu\text{s}$ of each cycle only two optical pumping laser beams are on, which maintain the atoms in their doubly spin polarized $5^2S_{1/2}(F=2, M_F=2)$ sublevel. During the last $1.9\ \mu\text{s}$ of each cycle, only the photoassociation (PA) laser beam is on, which is linearly polarized perpendicular to the quantization axis, and has an intensity in the range from 20 to $1000\ \text{W cm}^{-2}$.

At the end of each 200 ms period, we probe the atoms remaining in the trap with laser-induced fluorescence. If the PA laser is tuned to a photoassociation resonance, the number of atoms is reduced, because most of the pairs of atoms which are excited by the PA laser decay to free pairs with a kinetic energy that is too large to remain in the trap. This results in a detectable change in the fluorescence level. We build up a spectrum by repeating the loading, 200 ms irradiation period, and fluorescence probe cycle for a succession of laser frequencies.

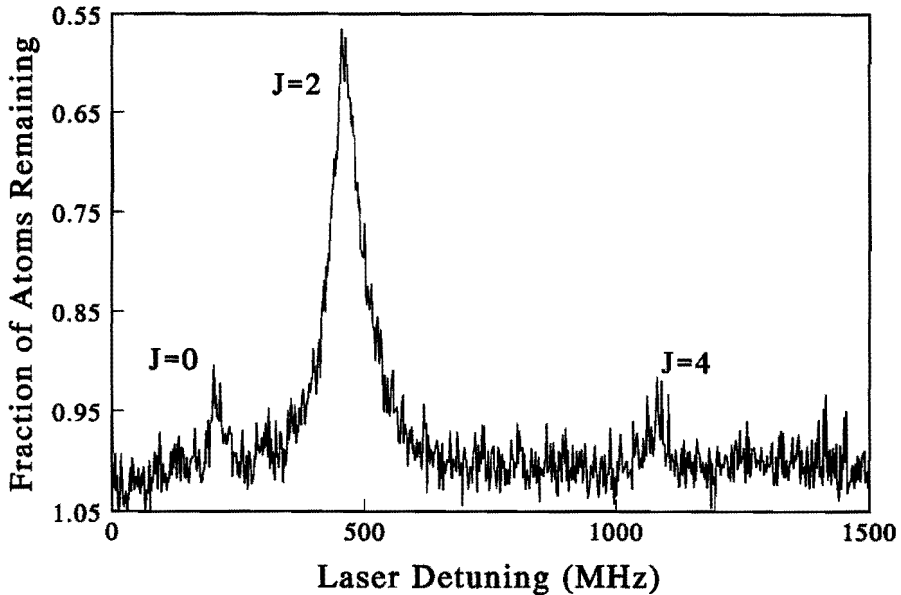


Figure 4.1: Measured rotationally resolved photoassociation spectrum of a single 0_g^- vibrational level $5.9\ \text{cm}^{-1}$ below the $5^2S_{1/2} + 5^2P_{1/2}$ limit, showing strong $J = 2$ excitation.

A typical photoassociation spectrum of a single vibrational level belonging to the 0_g^- state asymptotic to the $5^2S_{1/2} + 5^2P_{1/2}$ limit is shown in Fig. 4.1. A simple rotational spectrum is observed, with $J = 0, 2,$ and 4 lines visible. The most obvious feature of the data is the large size of the $J = 2$ peak, which is about 50 times larger than the $J = 0$ peak when saturation effects are accounted for. As discussed below, this large $J = 2$ peak arises due to a d -wave shape resonance in the ground state collision.

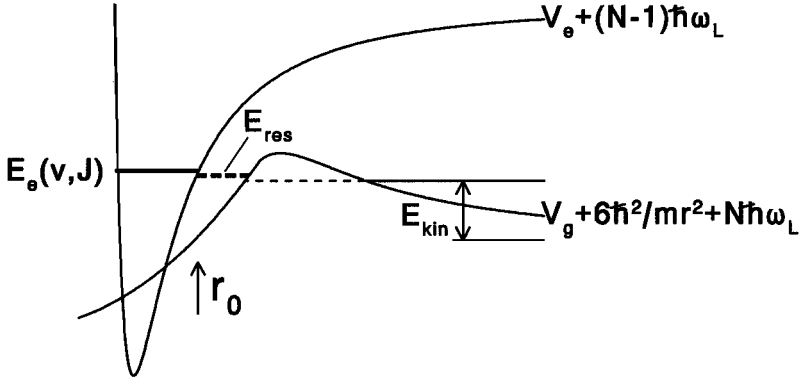


Figure 4.2: Dressed-states picture of photoassociation process, including schematic ground-state and excited-state potentials. Changing the laser frequency ω_L , the excited bound state energy $E_e(v, J)$ shifts over the Maxwellian energy distribution in incoming channel, causing a peak in photoassociation spectrum. The shape resonance E_{res} within the $l = 2$ centrifugal barrier enhances photo-excitation of the $E_e, J = 2$ state.

In a photoassociation collision two Rb ground-state atoms move along a potential V_g , absorb a photon from the PA laser and thereby undergo a transition to a bound Rb + Rb* state in an excited state potential V_e . In a dressed-state picture schematically represented in Fig. 4.2 the bound state, which has already a width γ_0 for spontaneous emission, is embedded in the ground-state continuum and thus turns into a Feshbach resonance with an additional width γ_L for laser-induced continuum decay. Changing ω_L shifts the Maxwellian distribution in the ground-state channel over the resonance, thereby giving rise to a peak in the photoassociation spectrum.

The large $J = 2$ peak may be easily understood from this picture. As has been discussed previously [16], for this spectrum the selection rule $J = l$ is obeyed, where l is the orbital angular momentum of the colliding atoms. The $l = 2$ centrifugal barrier, at $140 a_0$, is 0.42 mK high, as a summation of dispersion parts and centrifugal term shows. On the other hand, the optical excitation occurs at $r_0 \approx 40\text{-}48 a_0$, the range of the outer turning points of the

excited states involved. Both for the estimate of height and position of the barrier and for that of the range of outer turning points ab-initio calculated potentials suffice [21–23]. Therefore, the $J = 2$ peak measures the d -wave amplitude inside the centrifugal barrier. Its large size is due to the resonant buildup of this amplitude behind the barrier.

Information on the ground-state radial wave function $u_g(r)$ is contained in the peak heights and shapes, in particular in the partial width γ_L for decay of the shape resonance by laser excitation [16]:

$$\gamma_L = I_L |c \int u_e(r) d_{eg}(r) u_g(r) dr|^2, \quad (4.2)$$

with I_L the laser intensity, c a geometrical coefficient containing the full spin-angle structure, $u_g(r)$ the ground state radial wave function, $u_e(r)$ the excited state radial wave function, and $d_{eg}(r)$ the transition electric-dipole moment. The width γ_L occurs in the Breit-Wigner expression [24] for the squared S -matrix element for photoassociation:

$$|S_{PA}|^2 = \frac{\gamma_0 \gamma_L}{(\epsilon + E_g + \hbar\omega_L - E_e)^2 + \frac{1}{4}\gamma_0^2}, \quad (4.3)$$

in the notation of Ref. [16]. Both u_e and d_{eg} follow from the solution of a 2-level problem in which a sum of 2×2 matrices for the asymptotic fine-structure splitting, a resonant electric dipole interaction V_{dip} , and a dispersion part is diagonalized in the separated-atom basis [22]. This determines both $V_e(r)$ and the structure of the 0_g^- electronic state. It turns out that the electric-dipole matrix-elements $d(P_{1/2})$ and $d(P_{3/2})$ of the atomic D-lines entering V_{dip} are the most uncertain part of the analysis. A set of measured 0_g^- excited state level positions allows us to reduce this uncertainty sufficiently. We select a radius r_1 within but as close as possible to the outer turning point r_0 such that the local phase of the radial wave function is a linear function of energy over the small energy range involved. Calculations using an ab-initio potential indicate that V_e is deep enough to choose r_1 equal to $30a_0$ for $r_0 = 40 - 48a_0$. This implies that the entire inner part of the potential can be described by two phase parameters only. We calculate bound-state energies assuming phase values at a fixed energy for ^{87}Rb and ^{85}Rb , as well as energy derivatives connected by mass-scaling, and values for $d(P_{1/2})$ and $d(P_{3/2})$. Since the $S_{1/2} + P_{1/2}$ expectation value of V_{dip} vanishes and the interatomic distances involved are close to the separated-atom limit, only the product $d(P_{1/2})d(P_{3/2})$ comes in. Due to the long distances the dependence of the analysis on the $n \geq 8$ ground-state and $n \geq 6$ excited-state dispersion coefficients is weak. We take them from Ref. [18] and [21] and include their uncertainty in the final error limits. Comparing theoretical levels with sets of $J = 0$ levels for ^{85}Rb [16] and $J = 2$ levels for ^{87}Rb (this experiment), we find optimal values for the three phase parameters and a value $d(P_{1/2})d(P_{3/2}) = 8.8 \pm 0.1$ a.u., thus improving the accuracy of our previous determination of this product [16].

Since $u_e(r)$ and $d_{eg}(r)$ can thus be derived from an analysis of frequencies of photoassociation peaks, γ_L is a “finger-print” of the nodes of $u_g(r)$. At the large distances contributing to the integral in Eq. (4.2) the required information on $u_g(r)$ can be summarized in a single unknown phase at r_1 , while a C_6 dispersion coefficient governs the development of $u_g(r)$

outside r_1 . Alternatively [16], one may take C_6 and v_D , the (fractional) vibrational quantum number for $l = 0$ at dissociation [19], or C_6 and a_T as equivalent pairs of parameters.

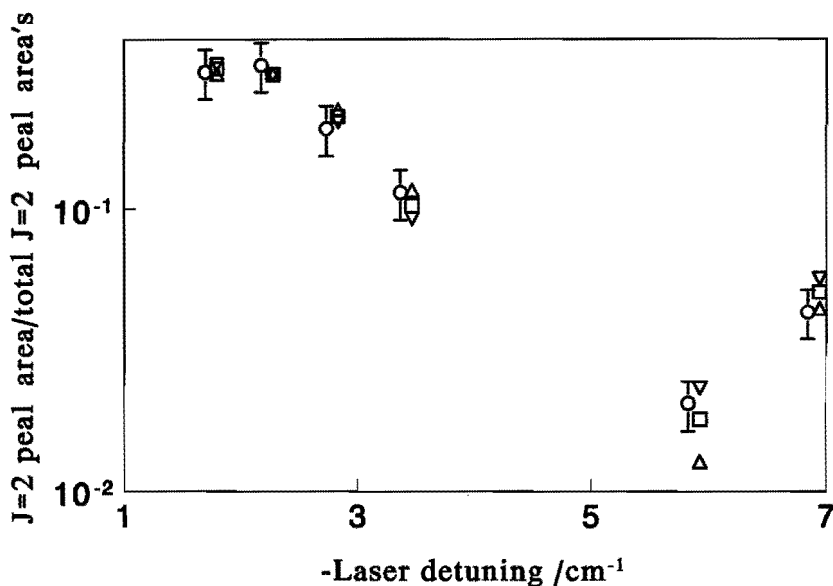


Figure 4.3: ^{87}Rb $J = 2$ peak areas measured for a number of 0_g^- vibrational states, showing Franck-Condon oscillation (circles), together with theoretical values for optimal χ_2^2 (squares, $C_6 = 4650$ a.u. and $v_D(\text{mod } 1) = 0.377$) and for two points on edges of χ_2^2 strip (triangles): downward pointing triangles, $C_6 = 4450$ a.u. and $v_D(\text{mod } 1) = 0.363$, upward pointing triangles, $C_6 = 4850$ a.u. and $v_D(\text{mod } 1) = 0.408$. For the sake of clarity, the theoretical points have been shifted slightly in the horizontal direction with respect to the experimental points.

Figure 4.3 shows the measured relative $J = 2$ peak areas (proportional to γ_L) for a number of 0_g^- vibrational states. A well-developed oscillation is visible of the kind one would expect from the simple Franck-Condon picture where the radial integral in Eq. (4.2) is dominated by its contribution from the region near the outer turning point r_0 of $u_e(r)$ [12]. In Fig. 4.4a we present the strip in the v_D - C_6 plane, resulting from the requirement that $u_g(r)$ has a node at the Franck-Condon radius corresponding to the node position following from Fig. 4.3. We also indicate in Fig. 4.4(a) the strip where a shape resonance occurs below the top of the $l = 2$ centrifugal barrier and that for the smaller energy range between 50 and 90% of the total barrier height following from the analysis below, taking the actual $J = 2$ enhancement into account. This illustrates clearly the important role of the shape resonance in our analysis: in

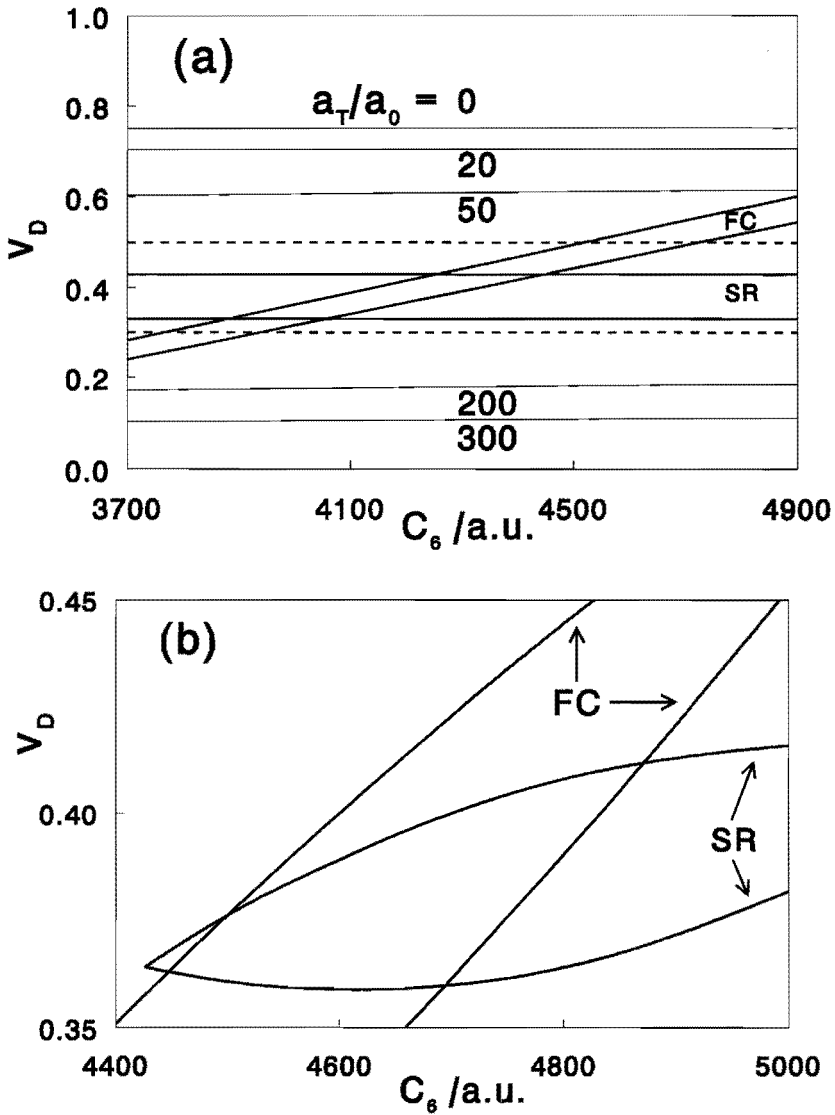


Figure 4.4: Franck-Condon (FC) and shape-resonance strips (SR) in v_D - C_6 plane. (a) Strips following from simple picture. Dashed lines: strip for shape resonance below top of $l = 2$ barrier. Thin lines: contour lines for a_T in units a_0 . (b) Strips following from ^{87}Rb analysis.

contrast to Ref. [16] we do not need a theoretical C_6 -value as a second ingredient besides the Franck-Condon oscillations to determine the two unknown parameters.

The actual analysis starts with the determination of a temperature from the $J = 2$ lineshapes for a grid of v_D and C_6 values. This temperature is used to calculate theoretical $J = 0$ and $J = 2$ peak areas. Two χ^2 functions then define the extent of agreement with experiment: a “shape-resonance”-type χ_1^2 corresponds to the ratio of the $J = 2$ and $J = 0$ peak areas for the peaks at detunings of 5.931 and 6.944 cm^{-1} , a “Franck-Condon”-type χ_2^2 is associated with the ratios of the areas of all ten measured $J = 2$ peaks. The resulting strips in the v_D - C_6 plane, presented in Fig. 4.4(b), are in qualitative agreement with the schematic picture of Fig. 4.4(a). Clearly, the more rigorous analysis on the basis of the radial integral of Eq. (4.2) effectively shifts the outer nodes in $u_g(r)$ over a small distance inward, which tends to decrease the local wavelength and increase C_6 . We find the two criteria to set independent strips in the parameter plane with an intersection leading to

$$0.35 < v_D(\text{mod } 1) < 0.42 \quad (4.4)$$

and

$$4400 < C_6 < 4900 \text{ a.u.} \quad (4.5)$$

The temperature turns out to be 0.25 ± 0.05 mK. Temperatures derived from our lineshape analyses are generally in agreement with those determined by direct measurement [20]. The values for v_D and C_6 together determine the scattering length. We find the limits

$$+99a_0 < a_T < +119a_0, \quad (4.6)$$

narrower than the range $+85a_0 < a_T < +140a_0$ in Ref. [16], and obtained with less input of information from theory.

4.3 Discussion and conclusion

Let us now discuss the consequences for the ^{85}Rb scattering length. If we use mass-scaling, assigning an upper limit ± 3 for the error bar on the number 38 of s -wave triplet bound $^{87}\text{Rb}_2$ states (n_b) derived from the Krauss-Stevens ab-initio triplet potential [23], we find a_T to be negative (see table 4.1) for the entire C_6 range of Eq. (4.5). This is consistent with an analysis based on direct ^{85}Rb measurements and the same C_6 -range (table 4.1), extending the ^{85}Rb data analyzed in Ref. [16] with an additional set of data obtained more recently, also leading to negative a_T values only. The new direct ^{85}Rb results are also consistent with Ref. [16], leading however to a narrower range of v_D -values: $-0.23 < v_D(\text{mod } 1) < -0.03$.

Our measured C_6 -value is consistent with a recent theoretical value of 4426 a.u. [18]. This calculation should have an accuracy which is comparable to or better than our measurement, since it is derived from a model which reproduces accurately known atomic properties of Rb including its polarizability. Allowing for a maximum deviation of C_6 from 4426 a.u. by 4% restricts $a_T(^{85}\text{Rb})$ to the least negative values and hardly changes $a_T(^{87}\text{Rb})$.

Results from analysis of	$a_T(^{87}\text{Rb}+^{87}\text{Rb})$	$a_T(^{85}\text{Rb}+^{85}\text{Rb})$
^{87}Rb	$+99 < a_T < +119$	$-\infty < a_T < -80$
^{85}Rb	$+85 < a_T < +200$	$-1200 < a_T < -10$

Table 4.1: Scattering lengths in a_0 , determined from ^{85}Rb and ^{87}Rb analyses for $4400 < C_6 < 4900$ a.u.

Finally, we can directly compare the ^{85}Rb and ^{87}Rb photoassociation spectra. Intensities of $J = 0$ lines in the ^{85}Rb spectrum are generally much larger than for ^{87}Rb with comparable PA laser intensity. This behavior may be understood from the limiting form of the scattering wave function at low energy [17]. For all parameters in table 4.1 ratios between theoretical ^{85}Rb and ^{87}Rb peak areas are consistent with experimental ratios.

We may also use the condition that mass-scaled results of the separate ^{85}Rb and ^{87}Rb analyses are consistent to derive the number of bound states in the $^{87}\text{Rb}_2$ triplet ground state. We determine $n_b = 42 \pm 4$, in good agreement with the theoretical value 38 derived from Ref. [23]. To our knowledge, there is no experimental information on this quantity.

From these parameter values the tunneling lifetime \hbar/γ_t of the $l = 2$ shape resonance is calculated to be in the range 20 - 100 ns, not very different from the spontaneous emission lifetime \hbar/γ_0 and from the time scale of the photoassociation process \hbar/γ_L for easily attainable laser intensities. It should therefore be possible to obtain direct information on the time it takes the atoms to tunnel through the barrier and form the shape resonance by suitable time-dependent photoassociation measurements.

In conclusion, we have observed a shape resonance in the collision of two cold ^{87}Rb atoms. Its existence has made it possible to carry out the first direct determination of the ^{87}Rb triplet scattering length without relying on a mass-scaling argument and a theoretical C_6 value. Nevertheless we find a much narrower positive interval. Likewise, we have obtained a more reliable and negative a_T range for ^{85}Rb . This information is relevant for present BEC experiments in rubidium gas samples. Finally, we have extracted a ground-state C_6 value with a 5% error limit and the number of bound states supported by the ^{87}Rb triplet potential with a 10% error limit.

References

- [1] M.H. Anderson, J.R. Ensher, M.R. Matthews, C.E. Wieman, and E.A. Cornell, *Science* **269**, 198 (1995); C.C. Bradley, C.A. Sacket, J.J. Tollet, and R.G. Hulet, *Phys. Rev. Lett.* **75**, 1687 (1995); K.B. Davis, M-O Mewes, M.R. Anderson, N.J. van Druten, D.S. Durfee, D.M. Kurn, and W. Ketterle, *Phys. Rev. Lett.* **75**, 3969 (1995).

- [2] S.N. Bose, *Z. Phys.* **26**, 178 (1924); A. Einstein, *Sitzungsber. Kgl. Preuss. Akad. Wiss.* **1924**, 261 (1924).
- [3] A.L. Fetter and J.D. Walecka, *Quantum Theory of Many-Particle Systems* (McGraw-Hill, New York, 1971), p. 218.
- [4] E. Tiesinga, A.J. Moerdijk, B.J. Verhaar, and H.T.C. Stoof, *Phys. Rev. A* **46**, R1167 (1992).
- [5] P.A. Ruprecht, M.J. Holland, K. Burnett, and M. Edwards, *Phys. Rev. A* **51**, 4704 (1995).
- [6] Yu. Kagan, G.V. Shlyapnikov, and J.T.M. Walraven, *Phys. Rev. Lett.* **76**, 2670 (1996).
- [7] K. Gibble and S. Chu, *Metrologia* **29**, 201 (1992).
- [8] B.J. Verhaar, K. Gibble, and S. Chu, *Phys. Rev. A* **48**, R3429 (1993).
- [9] A.J. Moerdijk, W.C. Stwalley, R.G. Hulet, and B.J. Verhaar, *Phys. Rev. Lett.* **72**, 40 (1994).
- [10] A.J. Moerdijk and B.J. Verhaar, *Phys. Rev. Lett.* **73**, 518 (1994).
- [11] E.R.I. Abraham, W.I. McAlexander, C.A. Sackett, and R.G. Hulet, *Phys. Rev. Lett.* **34**, 1315 (1995).
- [12] J.D. Miller, R.A. Cline, and D.J. Heinzen, *Phys. Rev. Lett.* **71**, 2204 (1994); R.A. Cline, J.D. Miller, and D.J. Heinzen, *Phys. Rev. Lett.* **73**, 632 (1994).
- [13] L.P. Ratliff, M.E. Wagshull, P.D. Lett, S.L. Rolston, and W.D. Phillips, *J. Chem. Phys.* **101**, 2638 (1994);
- [14] W.I. McAlexander, E.R.I. Abraham, N.W.M. Ritchie, C.J. Williams, H.T.C. Stoof, and R.G. Hulet, *Phys. Rev. A* **51**, 871 (1995).
- [15] R. Napolitano, J. Weiner, C. J. Williams, and P. S. Julienne, *Phys. Rev. Lett.* **73**, 1352 (1994).
- [16] J.R. Gardner, R.A. Cline, J.D. Miller, D.J. Heinzen, H.M.J.M. Boesten, and B.J. Verhaar, *Phys. Rev. Lett.* **74**, 3764 (1995).
- [17] R.C.Côté, A. Dalgarno, Y. Sun, and R.G. Hulet, *Phys. Rev. Lett.* **74**, 3581 (1995).
- [18] M. Marinescu, H.R. Sadeghpour, and A. Dalgarno, *Phys. Rev. A* **49**, 982 (1994).
- [19] The actual analysis makes use of a more rigorous scaling relation: that between the phases ϕ of the oscillating radial wave functions [16].

- [20] J.D. Miller, R.A. Cline, and D.J. Heinzen, *Phys. Rev. A* **47**, R4567 (1993).
- [21] M. Marinescu and A. Dalgarno, *Phys. Rev. A* **52**, 311 (1995).
- [22] M. Movre and G. Pichler, *J. Phys. B* **10**, 2631 (1977).
- [23] M. Krauss and W.J. Stevens, *J. Chem. Phys.* **93**, 4236 (1993).
- [24] H. Feshbach, *Theoretical Nuclear Physics, Part 1: Nuclear Reactions* (Wiley, New York, 1992).

Chapter 5

Observation of a shape resonance in cold-atom scattering by pulsed photoassociation

H.M.J.M. Boesten, C.C. Tsai, B.J. Verhaar, and D.J. Heinzen

Submitted to Physical Review Letters

Abstract

*We observe the time-dependence of a cold atom collision in a pulsed photoassociation experiment. For a g -wave shape resonance in the $^{85}\text{Rb} + ^{85}\text{Rb}$ system we measure the time needed to build up the resonant state by tunneling through the centrifugal barrier. Combining this with time-independent ^{85}Rb and ^{87}Rb photoassociation we determine the resonance energy and find evidence for the decay of the shape resonance into inelastic channels. We also determine the $^{85}\text{Rb} + ^{85}\text{Rb}$ and $^{87}\text{Rb} + ^{87}\text{Rb}$ C_6 coefficient and triplet scattering lengths without relying on *ab-initio* calculations.*

Recent developments in laser cooling and evaporative cooling techniques, especially for alkali gas samples, have led to the rapidly expanding field of cold collision physics. Collisions between cold atoms are exceptional in a number of aspects. One of these is the frequent occurrence of shape resonances, which are elastic scattering resonances associated with quasibound diatomic levels trapped behind a centrifugal barrier. These are important to the collision physics because the collision energies are typically lower than the centrifugal barrier even for the lowest non-vanishing l partial waves. Considering the vibrational and rotational energy spacings of the alkali dimers, the probability for any of these to have at least one quasi-bound state with $l \leq 6$ is more than 50%. Knowing the energy of a shape resonance leads very directly to an accurate scattering length for the corresponding potential and is nearly equivalent to finding the last bound state of that potential. Shape resonances may be expected to create possibilities for many exciting new experiments. In particular, they will shed new light on the elastic and inelastic interactions of cold atoms, which are of crucial importance for understanding Bose-Einstein condensation phenomena [1–3], laser-cooled atomic clocks [4] and other cold atom applications. They may also lead to a new kind

of spectroscopy of states inside the centrifugal barrier with a tunneling lifetime long enough for inelastic interactions to occur due to weak interaction terms that are difficult to study otherwise.

In this Letter, we present the first detailed study of a shape resonance in cold atomic scattering, focusing our attention on a g -wave resonance in the scattering of two ^{85}Rb atoms. We observe this resonance with cold atom photoassociation [5–10]. Photoassociation is particularly useful for the present study, since it allows us to excite atomic pairs in a narrow radial range around $40 a_0$ that is inside the centrifugal barrier at about $100 a_0$, and also because it allows us to probe individual partial wave components of the collision [10]. That is, we can selectively photoexcite the collision resonance.

The $^{85}\text{Rb} + ^{85}\text{Rb}$ g -wave shape resonance is sufficiently long-lived that we are also able, for the first time, to directly observe time-dependence in cold atomic collisions. With a pulsed photoassociation experiment, we measure the build-up of the resonance state by tunneling through the barrier in competition with various decay processes. The lifetime of the shape resonance is also long enough to be comparable to the time scale for inelastic interaction processes in the scattering of Rb ground state atoms. In agreement with this the time-independent photoassociation spectrum associated with the excitation of the $J = 4$ excited rotational state shows anomalous features that cannot be reproduced in terms of elastic scattering alone. The anomalous features can be explained in terms of an additional broadening of the resonance due to inelastic decay channels.

As in our previous experiments [5,6,10], we illuminate trapped, laser-cooled, doubly spin-polarized Rb atoms with light from a tunable photoassociation (PA) probe laser, and detect the absorption of this light by colliding pairs of atoms with a trap-loss method. To begin each measurement, we load about 10^4 ^{85}Rb atoms from a vapor-cell magneto-optical trap into a far-off resonance optical trap (FORT) with a waist of about $10 \mu\text{m}$ and depth 10 mK. Subsequently, for 200 ms the atoms are illuminated by a combination of laser fields. Each 200 ms period consists of repeated $5 \mu\text{s}$ cycles, as shown in Fig. 5.1(a). For the first $2.5 \mu\text{s}$, only the FORT laser beam is on. For the next $2.2 \mu\text{s}$, the atoms are illuminated by light from the tunable PA laser, and for the last $0.3 \mu\text{s}$, the atoms are illuminated by a pair of optical pumping (OP) beams. (We also sometimes use repeated $10 \mu\text{s}$ cycles, for which the PA laser period is $4.7 \mu\text{s}$.) The combination of the FORT and optical pumping light keeps the atoms trapped and in their doubly-spin polarized $|F = 3, M_F = 3\rangle$ state, in a manner exactly analogous to that described in Ref. [10]. At the end of each 200 ms period, the atoms are probed with laser-induced fluorescence (LIF), the intensity of which is proportional to the number of atoms remaining in the trap. If the PA laser induces free-bound optical transitions, the LIF signal is reduced, because any atoms which are excited decay predominantly to free atomic states which are too energetic to remain in the FORT. These steps are repeated for a succession of PA laser frequencies.

In order to directly probe the time-dependence of these collisions, we further subdivided the $2.2 \mu\text{s}$ (or $4.7 \mu\text{s}$) periods into a pulse sequence (Fig. 5.1(a)) consisting of either a

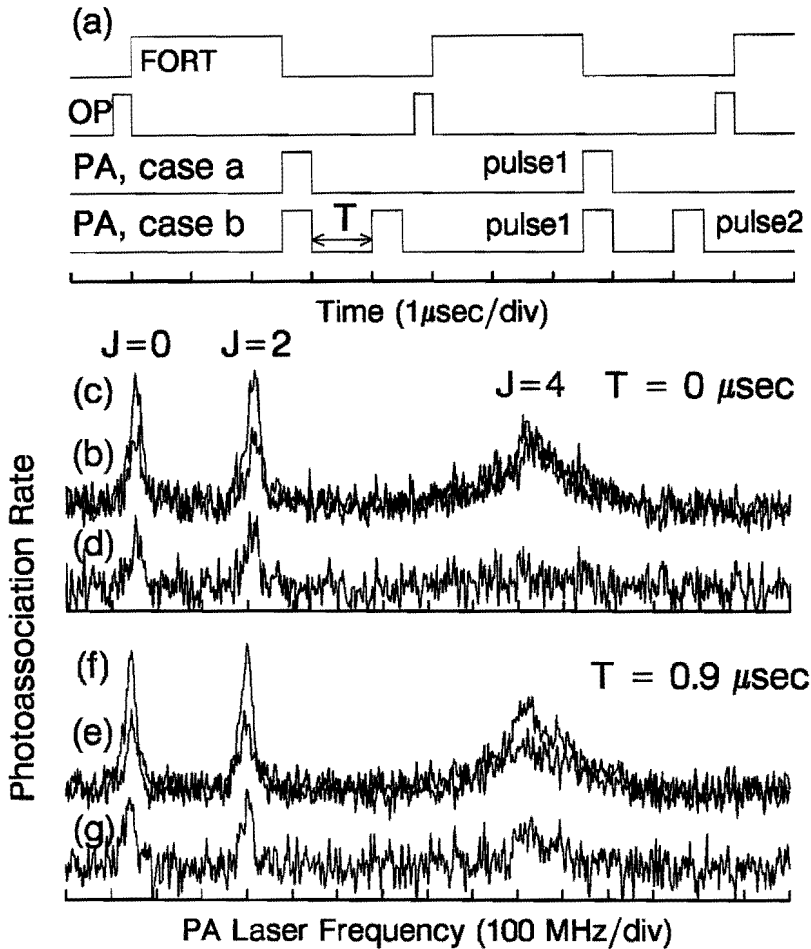


Figure 5.1: (a) Timing of laser pulses in the experiment. (b) to (g) Time-dependent photoassociation spectra of 0_g^- vibrational level at $12,573.04 \text{ cm}^{-1}$. (b) and (e) Spectrum with one photoassociation pulse only, (c) and (f) Spectrum with two photoassociation pulses. (d) and (g) Difference spectra showing the effect of pulse 2 alone. (b) to (d) $T=0$. (e) to (g) $T=0.9 \mu\text{s}$. Notice that, for $T=0$, in contrast to the $J = 0$ and $J = 2$ lines, the $J = 4$ peak is not twice as high in spectrum (b) in comparison with spectrum (a). But, when pulse 2 is delayed as in trace (f), additional signal appears in the $J = 4$ peak.

single $0.45 \mu\text{s}$ duration pulse (pulse 1) (case a), or a $0.45 \mu\text{s}$ duration pulse (pulse 1) followed by a variable time T , and then followed by a second $0.45 \mu\text{s}$ duration pulse (pulse 2) (case b). We tuned the PA laser over the ^{85}Rb ($5^2S_{1/2}F = 3, M_F = 3$) \rightarrow ^{85}Rb ($5^2S_{1/2}F = 3, M_F = 3$); $\epsilon, l, m_l, \rangle \rightarrow |^{85}\text{Rb}_2(0_g^- \sim 5^2S_{1/2} + 5^2P_{1/2})v, J\rangle$ transitions, where ϵ, l , and m_l denote the energy and orbital angular momentum quantum numbers of the initially free state. We probed all the rotational levels J belonging to the vibrational level v which lies at an energy of -3.365 cm^{-1} with respect to the barycenter of the $5^2S_{1/2} + 5^2P_{1/2}$ dissociation limit. A typical result, recorded at a PA laser intensity of 57 W/cm^2 , is shown in Fig. 5.1. Figures 5.1(b)- 5.1(d) show the result when the delay time T was set to zero, and Figs. 5.1(e)- 5.1(g) show the result when the delay time was set to $0.9 \mu\text{s}$. Figures 5.1(b) and 5.1(e) show the result for case a (pulse 1 only), Figs. 5.1(c) and 5.1(f) show the result for case b (pulse 1 and pulse 2), and Figs. 5.1(d) and 5.1(g) show the difference between case b and case a. The difference shown in Figs. 5.1(d) and 5.1(g) represents the signal due to pulse 2 alone.

Each spectrum consists of three lines, which correspond to the $J=0, 2$, and 4 rotational levels. As has been discussed previously [10], for the particular transition we have chosen to an electronically excited state with a Hund's case (e) structure [15], the selection rule $J=l$ is obeyed. Thus, the $J=0$ peak arises from the s -wave part of the scattering wave function, the $J=2$ peak from the d -wave part, and the $J=4$ feature from the g -wave part. The odd rotational peaks are suppressed because the spin-polarized Rb atoms are identical bosons and therefore cannot exist in odd partial wave states. The $J=4$ peak saturates at an intensity of 0.5 W/cm^2 , which is much less than the intensity of 15 W/cm^2 at which the $J=0$ and $J=2$ peaks saturate. This causes the $J=4$ peak to be power broadened when the $J=0$ and $J=2$ peaks are visible (Fig. 5.1). The greatly reduced saturation intensity of the $J=4$ peak occurs because the g -wave shape resonance increases the g -wave vibrational wave function amplitude and therefore increases its optical transition strength.

The lifetime of this resonance is long enough that we are able to see it directly in the data of Fig. 5.1. For a very rapid collision time scale, the signal should be proportional to the total time the PA laser is on. This occurs for the $J=0$ and 2 peaks, where the height of the peaks for case b (total PA on time/cycle = $0.9 \mu\text{s}$) is about twice that for case a (total PA on time/cycle = $0.45 \mu\text{s}$). However a completely different behavior is observed for the $J=4$ peak. For no delay time (Figs. 5.1(b)-(d)) pulse 2 induces much less signal than pulse 1. This occurs because pulse 1 is sufficiently intense to remove all pairs of atoms in the g -wave resonant state from the trap. Since it takes time for new atoms to tunnel through the g -wave centrifugal barrier, pulse 2 finds very few pairs of g -wave atoms at $\sim 40a_0$ separation. On the other hand, when the delay time is increased, as in Fig. 5.1(e)- 5.1(g), pulse 2 induces a significant additional signal. This occurs because the delay time is comparable to the tunneling time, so that new g -wave resonant states are formed and optically excited by the second pulse.

Three mechanisms compete in depleting the resonant amplitude built up by inward tunneling (rate γ_{in}): tunneling outward through the barrier (γ_{out}), photoassociation to a bound excited state (γ_L), and inelastic decay to lower ground-state hyperfine levels (γ_{inel}).

We find that if the theoretical model does not include the inelastic decay of the resonance, in line with all analyses of our cold-atom photoassociation experiments thus far, then the observed area of the $J = 4$ peak in the time-independent spectrum is too small with respect to the $J = 0$ and $J = 2$ peaks to be consistent with the theory. The theoretical $J = 4$ peak area is suppressed when the inelastic decay is included. Including it greatly complicates the analysis. The original $l = 4$ shape resonance, involving the external atomic degrees of freedom only, splits into a non-degenerate set of shape resonances arising from the spin-spin and Zeeman interactions of two atoms with $f_1 = f_2 = 3$, confined to move inside a barrier. Their partial width for inelastic decay to channels outside the $F = 6, l = 4$ subspace can be readily calculated if we assume that shape resonances do not occur for $(F, l) \neq (6, 4)$. We then find that the model and the data are consistent only if $\gamma_{out}/\gamma_{inel} = 2 \pm 1$.

In order to simplify the time-dependent analysis, we chose to take the time-dependent data at a sufficiently high laser intensity so that γ_L dominates over the inelastic decay rates during the PA laser pulses. The number of pairs of trapped atoms N_{in} which are in the resonant state evolves according to

$$\frac{dN_{in}}{dt} = -\{\gamma_L + \gamma_{out} + \gamma_{inel}\}N_{in} + \gamma_{in}N_{out}, \quad (5.1)$$

$$\frac{dN_{out}}{dt} = -\gamma_{in}N_{out} + \gamma_{out}N_{in}, \quad (5.2)$$

where N_{out} is the number of trapped atoms not in the resonant state, and the γ_L term is only included during the photoassociation laser pulses and the γ_{inel} term only in between.

Because of the high laser intensity saturation effects need to be taken into account in γ_L and in the resonance energy E_{res} determining γ_{in} and γ_{out} . We therefore calculated these quantities by means of a two states coupled-channels program with a triplet ground-state channel and a 0_g^- excited state channel including an absorptive potential accounting for spontaneous emission. Solving the above equations we then calculated the total atom loss during the 200 ms period with either one laser pulse or two laser pulses per cycle. An interesting aspect of the theoretical prediction for the difference signal is its asymmetry relative to the $J = 4$ peak itself, which is due to the variation of the tunneling rate over the width of the power-broadened shape resonance. The asymmetry is also visible in the experimental difference signals. Integrated over the laser detuning, the calculated losses can directly be compared with the corresponding experimental peak areas for a set of delay times and laser intensities. From this we determine the lifetime $\tau = (\gamma_{out} + \gamma_{inel})^{-1}$ of the g -wave shape resonance for a number of $\gamma_{inel}/\gamma_{out}$ ratios. Combining this result with those from the time-independent experiment [10], we find a value $0.6 < E_{res} < 0.8$ mK for the resonance energy, well below the barrier height 2.6 mK, a tunneling time $1 < 1/\gamma_{out} < 4\mu s$, and an inelastic decay time $2 < 1/\gamma_{inel} < 8\mu s$. Figure 5.2 shows a typical experimental signal as a function of delay time: A_2/A_1 is the total loss A_2 due to the set of second pulses only (area of $J = 4$ peak in the difference spectrum), divided by the total loss A_1 due to the set of single laser pulses per cycle (area of $J = 4$ peak in case a). Theoretical curves are shown for a set

of resonance lifetimes. The non-zero ratio at $T=0$ is due to tunneling during the laser pulses that is somewhat enhanced by the power broadening.

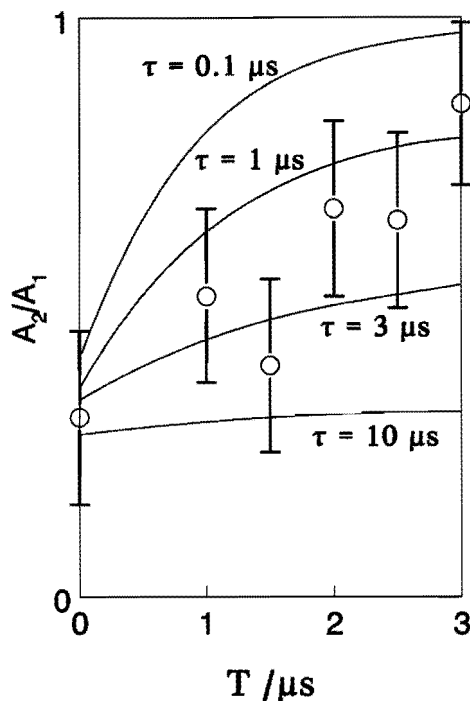


Figure 5.2: Time-dependent photoassociation signal A_2/A_1 as a function of delay time T for $I = 50 \text{ W/cm}^2$, $T = 0.35 \text{ mK}$, and $\gamma_{out}/\gamma_{so} = 2$. Experimental data with error bars are indicated as well as theoretical curves for various lifetimes of the shape resonance τ .

Presently, the most uncertain part of the inelastic decay is that induced by the second-order spin-orbit interaction ($V_{so}^{(2)}$) [11,12] between the valence electron spins of the colliding atoms, a 2-step spin-orbit effect where one spin influences the orbital motion of the charges which in turn influences the other spin. It has the same spin-angle structure as the magnetic dipole interaction [14], but a different dependence on the interatomic distance. Both the distance range where it is effective and its magnitude are only roughly known. As its strength increases rapidly with Z it is expected to play an increasingly important role for the heavier alkali atoms. Recent calculations predict the rates of decay of the condensate due to recombination [13] and dipolar relaxation [14]. Assuming opposite signs [12] for the partial width amplitudes $\gamma_{dip}^{1/2}$ and $\gamma_{so}^{1/2}$ due to dipolar and second-order spin-orbit decay

($\gamma_{inel}^{1/2} = \gamma_{dip}^{1/2} + \gamma_{so}^{1/2}$), and using the calculated value $1/\gamma_{dip} = 120\mu\text{s}$, we find a spin-orbit decay time $2 < 1/\gamma_{so} < 8\mu\text{s}$.

The rate γ_{so} enters γ_L via the same radial transition matrix element that occurs in the rate constant for the $V_{so}^{(2)}$ -induced relaxation of the doubly-polarized ^{87}Rb hyperfine state involved in the recent successful ^{87}Rb BEC experiment [1]. An analysis of resonance-enhanced time-independent $J=4$ photoassociation peaks would thus enable us to predict in a model-independent way the rate constant G_{so} for spin-orbit decay of the condensate in the BEC experiment. It turns out, however, that our result $G_{so} = (4 \pm 2) \times 10^{-14} \text{ cm}^3\text{s}^{-1}$ [18], is far larger than a recently measured value [19].

We believe that the most probable explanation for this discrepancy is our assumption that no shape resonances occur outside the $(F, l) = (6, 4)$ subspace. Taking into account the large number of angle-spin states outside this subspace, it would seem highly probable that one or more of them have positive energies below the top of the centrifugal barrier. The resulting strongly enhanced decay would lead to a much smaller value for γ_{inel} and thus to a smaller value of G_{so} .

Using peak areas of rotational lines for three subsequent vibrational levels in the low laser intensity limit, we determine an accurate value 4550 ± 100 a.u. for the van der Waals coefficient C_6 , in good agreement with a recent theoretical value 4426 a.u. [16]. Finally, with this C_6 -value and the above-mentioned resonance energy we determine the triplet scattering length to be in the range $-500a_0 < a_T(^{85}\text{Rb} + ^{85}\text{Rb}) < -300 a_0$, narrower than the range $-1000a_0 < a_T < -60a_0$ found in Ref. [10] and obtained with less input of theoretical parameters. The negative sign of a_T implies that a homogeneous ^{85}Rb gas sample will not form a stable condensate.

With additional experiments, we have found that doubly-polarized ^{87}Rb atoms exhibit a d -wave shape resonance, the details of which will be reported elsewhere [5]. For completeness we repeat here the most important result: the range $+99a_0 < a_T < +119a_0$ for the triplet scattering length, narrower than the range $+85a_0 < a_T < +140a_0$ obtained in Ref. [10], and again obtained with less input of theoretical parameters. Finally, we use the condition that mass-scaled results of separate ^{85}Rb and ^{87}Rb analyses are consistent to derive the number of bound states n_b in the $^{85}\text{Rb}_2$ and $^{87}\text{Rb}_2$ triplet ground states. We find $n_b = 38 \pm 1$ for $^{85}\text{Rb}_2$ and 39 ± 1 for $^{87}\text{Rb}_2$, the latter value being in good agreement with the theoretical value 38 derived in Ref. [17]. To our knowledge, there is no other experimental information on this quantity. The difference in n_b for the two isotopes is connected with the difference in sign of the respective scattering lengths: the state which becomes bound with the increasing atomic mass causes the $^{85}\text{Rb}_2$ scattering length to be negative and the $^{87}\text{Rb}_2$ scattering length to be positive.

In conclusion, by means of a pulsed photoassociation experiment we have observed the time-dependence of a collision of two cold ^{85}Rb atoms via a shape resonance. Combining this observation with time-independent data we have obtained new insight in elastic and inelastic processes, of importance for present and future cold atom experiments.

References

- [1] M.H. Anderson, J.R. Ensher, M.R. Matthews, C.E. Wieman, and E.A. Cornell, *Science* **269**, 198 (1995).
- [2] C.C. Bradley, C.A. Sacket, J.J. Tollet, and R.G. Hulet, *Phys. Rev. Lett.* **75**, 1687 (1995).
- [3] K.B. Davis, M-O Mewes, M.R. Anderson, N.J. van Druten, D.S. Durfee, D.M. Kurn, and W. Ketterle, *Phys. Rev. Lett.* **75**, 3969 (1995).
- [4] K. Gibble and S. Chu, *Metrologia* **29**, 201 (1992).
- [5] H.M.J.M. Boesten, C.C. Tsai, J.R. Gardner, D.J. Heinzen, and B.J. Verhaar (unpublished).
- [6] J. D. Miller, R. A. Cline, and D. J. Heinzen, *Phys. Rev. Lett.* **71**, 2204 (1994); R.A. Cline, J.D. Miller, and D.J. Heinzen, *Phys. Rev. Lett.* **73**, 632 (1994).
- [7] L.P. Ratliff, M.E. Wagshull, P.D. Lett, S.L. Rolston, and W.D. Phillips, *J. Chem. Phys.* **101**, 2638 (1994);
- [8] W.I. McAlexander, E.R.I. Abraham, N.W.M. Ritchie, C.J. Williams, H.T.C. Stoof, and R.G. Hulet, *Phys. Rev. A* **51**, 871 (1995).
- [9] R. Napolitano, J. Weiner, C. J. Williams, and P. S. Julienne, *Phys. Rev. Lett.* **73**, 1352 (1994).
- [10] J.R. Gardner, R.A. Cline, J.D. Miller, D.J. Heinzen, H.M.J.M. Boesten, and B.J. Verhaar, *Phys. Rev. Lett.* **74**, 3764 (1995).
- [11] A.M. Mizushima, *The theory of Rotating Diatomic Molecules* (Wiley & Sons, New York, 1975).
- [12] F.H. Mies, P.S. Julienne, and C.J. Williams (private communication); see also recent preprint by F.H. Mies, C.J. Williams, P.S. Julienne, and M. Krauss (1996), which came to the authors' attention after the completion of this work.
- [13] A.J. Moerdijk, H.M.J.M. Boesten, and B.J. Verhaar, *Phys. Rev. A* **53**, 916 (1996).
- [14] H.M.J.M. Boesten, A.J. Moerdijk, and B.J. Verhaar, *Phys. Rev. A* **54**, R29 (1996).
- [15] G. Herzberg, *Spectra of diatomic molecules*, 2nd ed. (Van Nostrand Reinhold, New York, 1950) p. 226; to our knowledge this is the first observed example of a Hund's case (e) structure.
- [16] M. Marinescu, H.R. Sadeghpour, and A. Dalgarno, *Phys. Rev. A* **49**, 982 (1994).

- [17] M. Krauss and W.J. Stevens, *J. Chem. Phys.* **93**, 4236 (1993).
- [18] This value is not yet corrected for the factor 2 reduction of two-body rates in a condensate.
- [19] C. Wieman (private communication).

Chapter 6

Dipolar decay in two recent Bose-Einstein condensation experiments

H.M.J.M. Boesten, A.J. Moerdijk, and B.J. Verhaar

Published in Physical Review A **54**, R29 (1996)

Abstract

In view of two recent Bose-Einstein condensation experiments, we have calculated the magnetic-dipolar decay-rate constants of the atomic density for the doubly polarized state in ^{87}Rb and ^{85}Rb , and for the highest state of the lower hyperfine manifold in ^{23}Na .

After the recent breakthrough to Bose-Einstein condensation (BEC) in dilute ultracold atomic gases of ^7Li , ^{23}Na , and ^{87}Rb [1–3], it has become a priority to try to understand the finite lifetime of the trapped gas sample, in particular below the transition temperature. Since the mechanism of the decay is not yet completely clarified, it is useful to consider the theoretical predictions for the various possible partial decay-rate constants. In this paper we present the decay-rate constants for the dipolar decay of the hyperfine states involved. For the case of ^7Li that result has been given in a previous paper [4]. The dipolar decay-rate constants for ^{23}Na and ^{87}Rb will be considered here. In Fig. 6.1 we show the ground-state hyperfine structure for ^{23}Na , ^{85}Rb , and ^{87}Rb as a function of magnetic field. In the following we refer to each of the hyperfine states in terms of the (lower-case) single-atom quantum numbers f, m_f , although f is a good quantum number only for $B = 0$. Capital quantum numbers F, M_F are reserved for two-atom states involved in collisions. Instead of the doubly polarized $f, m_f = 2, +2$ state in Na that we studied previously [4], we will concentrate here on the $1, -1$ state for which BEC was realized experimentally [3]. As Fig. 6.1 shows, special significance has to be attributed to the field range up to 316 G in which the $1, -1$ state can be trapped in a static magnetic trap as a low-field seeking state. Also in the case of ^{87}Rb we will concentrate on the dipolar decay of the state involved in the recent BEC experiment [1], the doubly polarized $2, +2$ state. For completeness we will give the analogous result also for the isotope

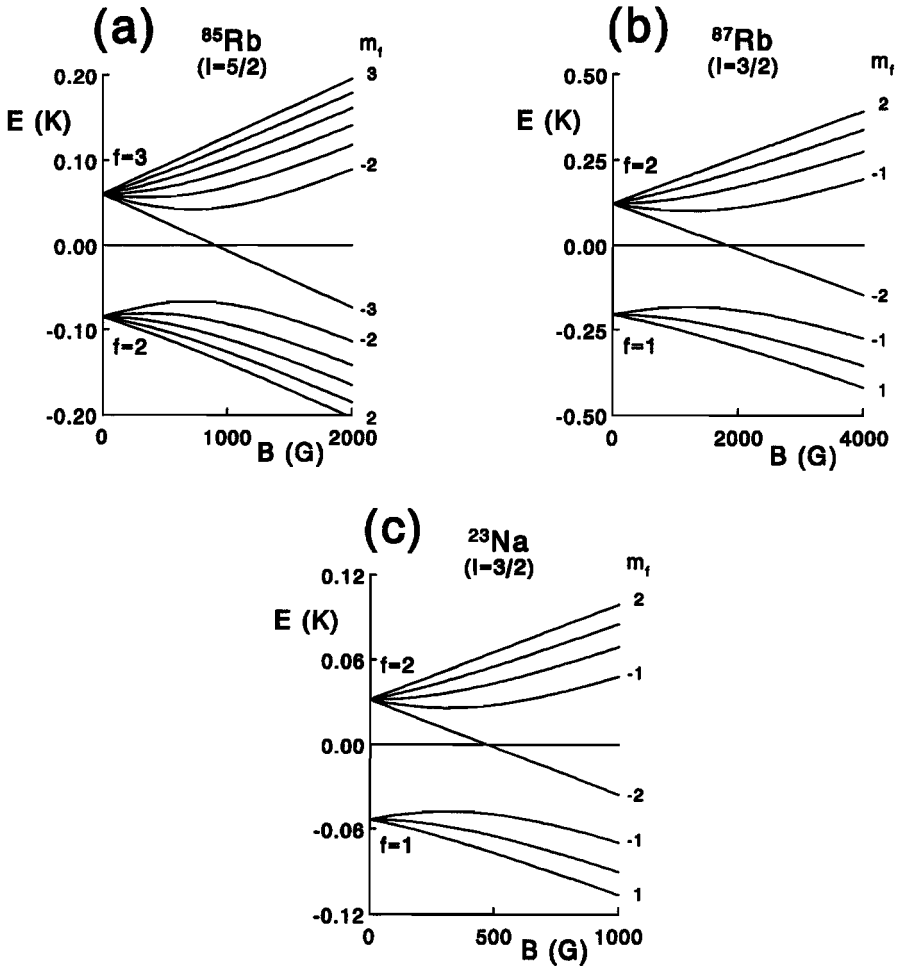


Figure 6.1: Ground-state hyperfine diagrams for (a) ^{85}Rb , (b) ^{87}Rb , and (c) ^{23}Na . The hyperfine states are labeled with f, m_f quantum numbers.

⁸⁵Rb. The method used has been sketched in Ref. [5]. Decay channels considered are all exothermal two-body decay channels not forbidden by selection rules, i.e., all are available combinations of lower-energy $f_1 m_{f_1}, f_2 m_{f_2}$ combinations with $M_F = m_{f_1} + m_{f_2}$ at most 2 different from the initial total M_F value, taking into account the possible transfer of $2\hbar$ of angular momentum between internal and external atomic degrees of freedom involved in an inelastic collision.

A reservation should be made in connection with the dipolar rate constant values to be presented in this Rapid Communication. For decades it has been known [6] that the magnetic dipole-dipole interaction V_{dip} among the valence-electron spins of interacting alkali-metal atoms is accompanied by a second type of spin-spin interaction with the same spin-angle structure that arises as a second-order effect in the valence-electron spin-orbit coupling and will be referred to here as V_{so}^2 . Both the (totally different) interatomic distance range, where V_{so}^2 is effective, and its magnitude are roughly known. Its strength increases rapidly with Z . Mies *et al.* [7] pointed to its possible role in the spin relaxation of alkali-metal atoms and made a preliminary study in the case of Rb atoms. A later study by Tiesinga *et al.* [8] concentrated on ¹³³Cs. Although a non-negligible V_{so}^2 contribution cannot be excluded in the present case of the Rb isotopes, we believe that a calculation of the purely magnetic dipolar part alone is useful, so that a comparison with the experimental decay rate might form the first experimental indication of a possible significant V_{so}^2 contribution.

In order to calculate the above-mentioned dipolar rate constants, detailed knowledge of the potentials involved is necessary. For Na the triplet and singlet potentials are very well known [9] and for the Rb isotopes the relevant part of the triplet potential has recently been determined by means of an analysis of two photoassociation experiments [10,11]. The influence of the singlet potential on the dipolar decay-rate constant for the fully stretched Rb state is expected to be small, because the dominant decay channels are almost pure triplet states. We use an experimental Rydberg-Klein-Rees potential [12] and obtain an indication of the associated range of uncertainty of each calculated rate constant by introducing a variable radial phase ϕ_S in the singlet wave function at an arbitrary point in the radial range where the WKB approximation is valid [9,10]. Upper and lower limits of the rate constants thus obtained by varying ϕ_S are indicated in the following figures.

In Fig. 6.2 we have given the dominant partial decay-rate constants and the total decay-rate constant for ⁸⁷Rb as a function of the magnetic field in the zero-temperature limit. Along the horizontal scale the quantity $1 + B/B_0$ is plotted logarithmically to combine the advantages of a linear scale at low B and a logarithmic scale at higher fields where the rate constants show a slower variation. The value of B_0 chosen, $a_{hf}/(64\mu_B)$, with a_{hf} the hyperfine constant, ensures a favorable separation between the linear and logarithmic parts. The upper horizontal scale indicates the actual B values. For each partial decay-rate constant two lines are presented, indicating upper and lower limits obtained by varying ϕ_S . Figure 6.2(a) shows the rate constants leaving the atoms in the highest hyperfine manifold $f = 2$, as well as the total rate constant. Figure 6.2(b) shows the remaining partial rate constants. A remarkable

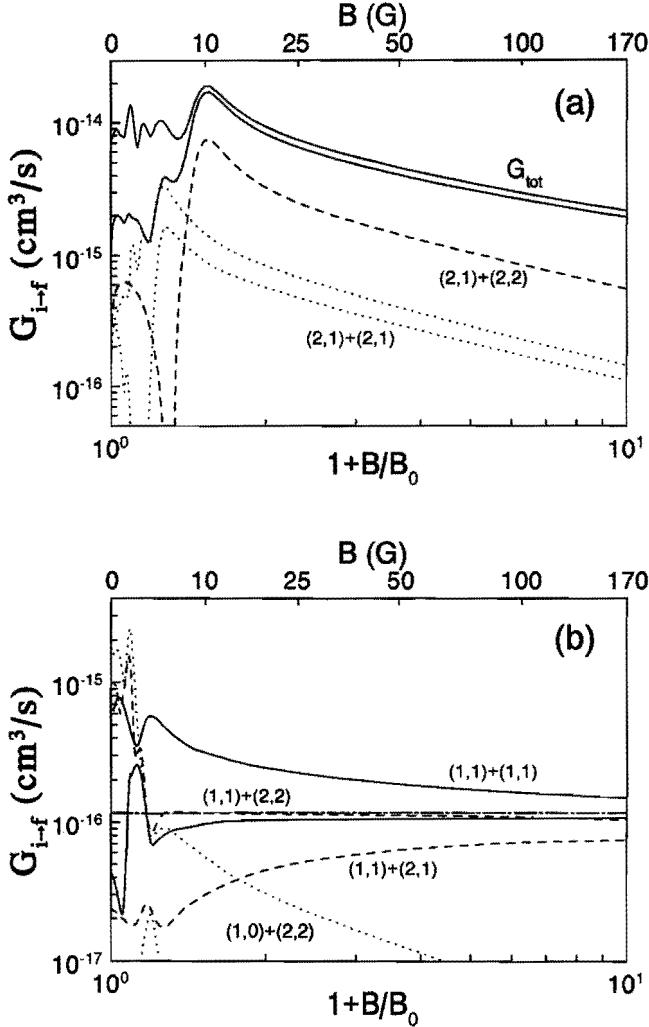


Figure 6.2: Zero-temperature dipolar relaxation-rate constants $G_{i \rightarrow f}$ for doubly polarized ^{87}Rb as a function of magnetic field, not including factor of 2 identical-particle reduction below BEC transition temperature. (a) Total rate constant G_{tot} and dominant partial rate constants for decay processes leaving both atoms in the upper ($f = 2$) hyperfine manifold; (b) remaining dominant partial rate constants. Horizontally the quantity $1 + B/B_0$ is plotted logarithmically with $B_0 = a_{h,f}/(128\mu_B) = 19.0$ G to combine the advantages of a linear and a logarithmic scale. For each partial decay-rate constant two lines are presented corresponding to the upper and lower limits obtained by varying singlet phase ϕ_S .

feature of the rate constants is the oscillatory behavior for small B values. This behavior is analogous to that of atomic H [5] and Na [4] and can be explained in terms of oscillations of the radial wave function in the final channel relative to that in the initial channel, as they occur in the integrand of the radial transition matrix element. The relative phase of these oscillations shifts with B .

Note that, in agreement with Ref. [4], zero-temperature decay-rate constants generally do not vanish. They vanish only in the extreme case of zero final phase-space volume, i.e., at $B = 0$ for final channels with both atoms in the upper hyperfine manifold. As a consequence, whereas the total decay-rate constant is dominated by such channels at the higher fields because of the overlap of initial and final radial wave functions, the remaining channels with at least one atom in the lower hyperfine manifold dominate for small B . The gradual decrease of the dominant rate constants and thus of the total rate constant at high fields is due to the growing disparity of initial and final kinetic energies with increasing B , leading to a decrease of overlap.

Note, furthermore, that the uncertainty in the singlet potential does not change the orders of magnitude of the dominant rate constants and the total rate constant at low B and is even negligible for the higher fields. The uncertainty in the triplet potential, which has not been included in the figures, corresponds to even smaller changes of the rate constants.

In the ^{87}Rb BEC experiment the magnetic field is about 5 G. For this field strength the predicted two-body dipolar decay-rate constant is $(6 \pm 3) \times 10^{-15} \text{ cm}^3\text{s}^{-1}$ and the dipolar lifetime of the condensate 90-300 s ($n = 2.5 \times 10^{12} \text{ cm}^{-3}$), including the factor of 2 reduction of the rate constant due to identical-particle effects [14]. The difference between the experimentally observed decay time of 15 s and this two-body dipolar decay time may be due to V_{so}^2 , in which case the amplitude due to V_{dip} and V_{so}^2 would be comparable in the case of Rb atoms. In a previous paper [13], we have calculated the rate of recombination to Rb_2 for spin-polarized ^{87}Rb leading to a lifetime of 24×10^4 s, completely negligible with respect to the two-body dipolar decay rate.

In Fig. 6.3 we have given the dominant partial decay-rate constants and total decay-rate constant for ^{85}Rb as a function of the magnetic field in the zero-temperature limit. Again the uncertainty in the rate constants due to the singlet potential is indicated. In contrast to the ^{87}Rb rate constants these rates show no oscillatory behavior. In general the ^{85}Rb rate constants are about a factor of 5 higher than the ^{87}Rb rate constants. This is due to the fact that the absolute value of the $^{85}\text{Rb} + ^{85}\text{Rb}$ scattering length is larger than that for $^{87}\text{Rb} + ^{87}\text{Rb}$. In the case of ^{85}Rb the range of variation of the rate constants associated with the uncertainty in the triplet potential is much larger than for ^{87}Rb , due to the much larger uncertainty in the ^{85}Rb scattering length [10,11]. Relative to the curves presented, the variations amount to an upward or downward shift by up to a factor of 3.

Figure 6.4 shows all three calculated partial dipolar decay-rate constants for ^{23}Na , as well as the total rate constant. Each of them tends to 0 for $B \rightarrow 0$ due to vanishing phase-space volume, in other words, due to the centrifugal potential which is more difficult for the

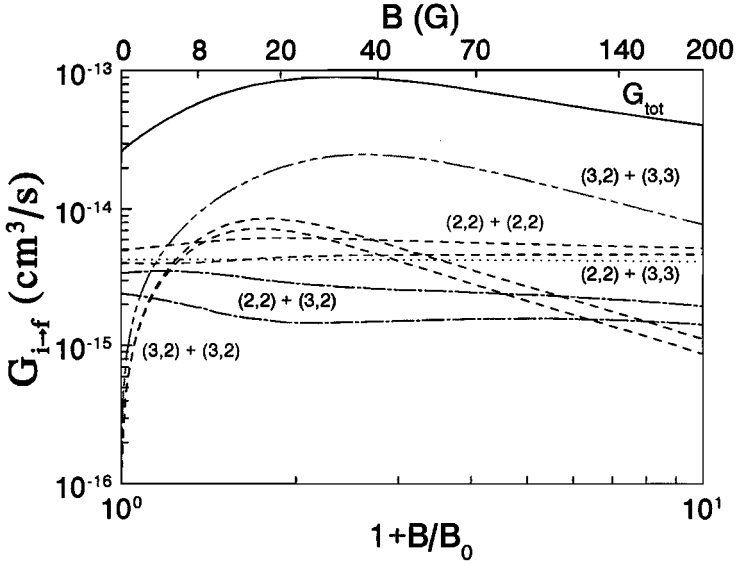


Figure 6.3: Same as Fig. 6.2 for ^{85}Rb , with $B_0 = a_{hf}/(32\mu_B) = 22.7 \text{ G}$.

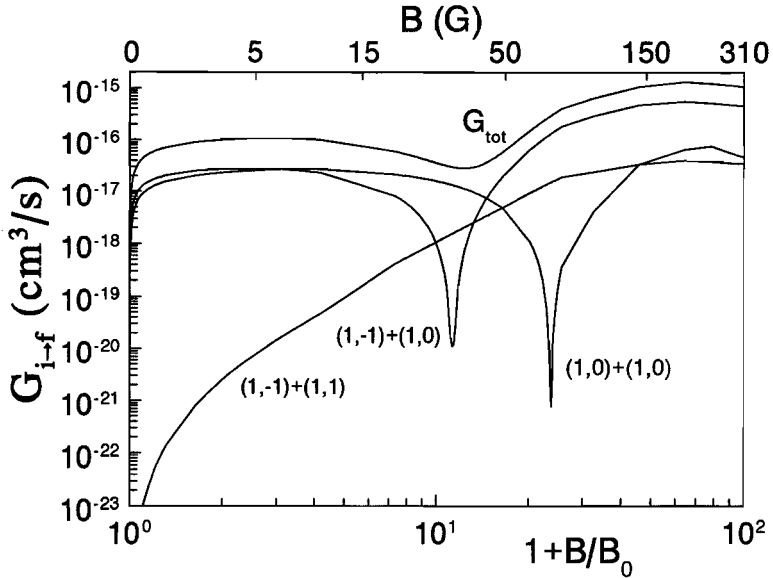


Figure 6.4: Zero-temperature dipolar relaxation-rate constants $G_{i\rightarrow f}$ and total rate constant for ^{23}Na atoms in the $|1, -1\rangle$ hyperfine state as a function of magnetic field with $B_0 = a_{hf}/(200\mu_B) = 3.16 \text{ G}$.

outgoing atoms to penetrate for decreasing kinetic energies. The pronounced minima as a function of field are again due to the varying phase relations of ingoing and outgoing radial waves.

The total dipolar decay-rate constant for ^{23}Na is thus calculated to be about $6 \times 10^{-17} \text{ cm}^3\text{s}^{-1}$ in the relevant field range around 1 G, again excluding the factor of 2 bosonic reduction of the rate constant in the BEC environment. We thus find the dipolar lifetime for the condensate to be 110 s ($n = 1.5 \times 10^{14} \text{ cm}^{-3}$), much longer than the experimentally observed 1-s lifetime. It may very well be that in the experiment of Ketterle *et al.* [3], with its much higher atom density, the condensate lifetime is primarily determined by the mechanism of recombination to Na_2 in three-body collisions. Indeed, since pairs of ^{23}Na atoms in the $1, -1$ hyperfine state interact predominantly via the triplet potential, the recombination rate can very well be estimated from the recombination rate for the collision of two spin-polarized atoms [13] leading to a lifetime of 1.3 s, in good agreement with the experimentally observed lifetime.

In conclusion, as a complement to previous studies that dealt with recombination rates or with dipolar rate constants for other states, we have calculated the dipolar rate constants for the hyperfine states of ^{87}Rb and ^{23}Na involved in two recent successful BEC experiments. The calculated rate constants are roughly consistent with the magnitude of the experimentally observed condensate lifetimes for ^{87}Rb , with a possible discrepancy due to V_{so}^2 . In the case of ^{23}Na , taking into account the high atomic density, the main decay mechanism of the condensate appears to be recombination to Na_2 .

References

- [1] M.H. Anderson, J.R. Ensher, M.R. Matthews, C.E. Wieman, and E.A. Cornell, *Science* **269**, 198 (1995).
- [2] C.C. Bradley, C.A. Sacket, J.J. Tollet, and R.G. Hulet, *Phys. Rev. Lett.* **75**, 1687 (1995).
- [3] K.B. Davis, M-O. Mewes, M.R. Andrews, N.J. van Druten, D.S. Durfee, D.M. Kurn, and W. Ketterle, *Phys. Rev. Lett.* **75**, 3969 (1995).
- [4] A.J. Moerdijk and B.J. Verhaar, *Phys. Rev. A* **53**, R19 (1996).
- [5] R.M.C. Ahn, J.P.H.W. van den Eijnde, and B.J. Verhaar, *Phys. Rev. B* **27**, 5424 (1983).
- [6] A M. Mizushima, *The Theory of Rotating Diatomic Molecules* (Wiley & Sons, New York, 1975).
- [7] F.H. Mies, P.S. Julienne, and C.J. Williams (private communication).
- [8] E. Tiesinga, A.J. Moerdijk, B.J. Verhaar, and H.T.C. Stoof, *Phys. Rev. A* **46**, R1167 (1992).

- [9] W.T. Zemke and W.C. Stwalley, *J. Chem. Phys.* **100**, 2661 (1994). The singlet potential has been improved using an inverse perturbation analysis by A.J. Moerdijk and B.J. Verhaar, *Phys. Rev. Lett.* **73**, 518 (1994).
- [10] J.R. Gardner, R.A. Cline, J.D. Miller, D.J. Heinzen, H.M.J.M. Boesten, and B.J. Verhaar, *Phys. Rev. Lett.* **74**, 3764 (1995).
- [11] H.M.J.M. Boesten, C.C. Tsai, J.R. Gardner, D.J. Heinzen, and B.J. Verhaar (unpublished).
- [12] C. Amiot, *J. Chem. Phys.* **93**, 8591 (1990).
- [13] A.J. Moerdijk, H.M.J.M. Boesten, and B.J. Verhaar, *Phys. Rev. A* **53**, 916 (1996).
- [14] H.T.C. Stoof, A.M.L. Janssen, J.M.V.A. Koelman, and B.J. Verhaar, *Phys. Rev. A* **39**, 3157 (1989).

Chapter 7

Properties of cold collisions of ^{39}K atoms and of ^{41}K atoms in relation to Bose-Einstein condensation

H.M.J.M. Boesten, J.M. Vogels, J.G.C. Tempelaars, and B.J. Verhaar

To be published in Physical Review A as a Rapid Communication

Abstract

We have determined properties of cold $^{39}\text{K} + ^{39}\text{K}$ and $^{41}\text{K} + ^{41}\text{K}$ collisions by a multichannel inverted perturbation approach applied to spectroscopic data of highly-excited ^{39}K singlet and triplet bound states. We predict positive scattering lengths for the $^{39}\text{K} + ^{39}\text{K}$ and $^{41}\text{K} + ^{41}\text{K}$ singlet potentials, as well as for the $^{41}\text{K} + ^{41}\text{K}$ triplet potential, and a negative value for $^{39}\text{K} + ^{39}\text{K}$ triplet scattering. From a study of the magnetic-field dependence we conclude that ^{41}K may be the first example of an alkali species with a Feshbach resonance in the magnetic-field range where these atoms can be trapped in the $f = 1, m_f = -1$ hyperfine state, thus providing a possibility to switch between stable and instable condensates in a Bose-Einstein condensation experiment.

The recent observation of Bose Einstein condensation (BEC) in weakly-interacting atomic gases of rubidium [1], lithium [2], and sodium [3] is an important step towards a more fundamental understanding of superfluidity and superconductivity in strongly interacting systems. A fascinating aspect of a Bose condensate in a dilute ultracold atomic gas is that its behavior is completely determined by one parameter only, the scattering length a , in contrast to the more complex systems. Recent work [4–6] shows that indeed various properties of a Bose condensate can be very well described by a nonlinear Schrödinger equation that contains a as a single parameter. In particular, it determines the stability of the condensate [7,8], a positive sign implying a stable and a negative sign an instable condensate [9]. The value of the scattering length is also a key ingredient of present methods to prepare the condensed phase, a large value being needed for efficient evaporative cooling [10]. Finally, two-body scattering properties play a crucial role also in other cold-atom experiments, for instance those dealing with laser-cooled atomic clocks [11].

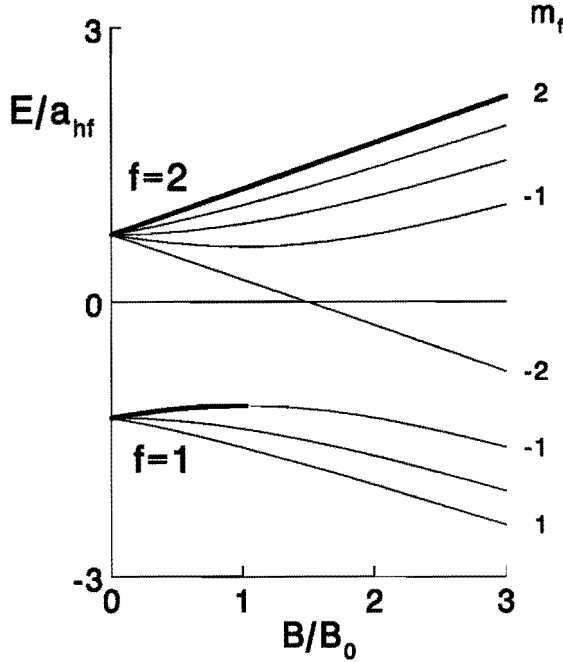


Figure 7.1: Ground-state hyperfine diagram for ^{39}K ($B_0 = 82.4\text{ G}$, $a_{hf} = 11.079\text{ mK}$) and ^{41}K ($B_0 = 45.3\text{ G}$, $a_{hf} = 6.097\text{ mK}$). Trappable states are indicated by bold lines.

In all successful BEC experiments thus far a cloud of atoms is trapped in a static magnetic field. In this kind of setup atoms can only be trapped for a reasonable time (larger than 1 s, for instance), when prepared in a specific hyperfine state. Figure 7.1 shows the ground-state hyperfine diagram for ^{39}K and ^{41}K , including the two states that are promising for observing BEC. The first of these is the ($f = 2, m_f = +2$) state with fully stretched electronic and nuclear spins, the second one is the highest state ($f = 1, m_f = -1$) of the lower hyperfine manifold, trappable for $B < B_0 = \frac{1}{2}a_{hf}/\mu_B$ with a_{hf} the atomic hyperfine constant and μ_B the Bohr magneton. An interesting aspect of atoms colliding in the $f = 1, m_f = -1$ hyperfine state is the possibility to effect a large change of the scattering length by varying the magnetic field, if a Feshbach-type resonance shows up in the collision process. Changing the field would enable one to directly control the magnitude and sign of the scattering length and thus the stability properties and dynamical behavior of the condensate [8]. Changing the sign of a as a function of time by variations of B , for instance, would offer possibilities for fascinating new experiments. Thus far theoretical predictions have been made for the

locations of Feshbach resonances for ^7Li and ^{23}Na [12] with reliable interaction potentials and for ^{133}Cs [13] with a less reliable interaction potential. Unfortunately, in ^7Li and ^{23}Na no resonances occur in the field regime where atoms can be trapped, while in the case of ^{133}Cs the interaction potential is too uncertain to definitely predict the locations of resonances.

Remarkably little has been published so far about the cold-collision properties of K atoms. This is surprising because this element has the attractive feature of having the two above-mentioned stable bosonic isotopes, as well as an almost stable fermionic isotope ^{40}K . In this paper we present a multichannel inverted perturbation approach of a combined set of singlet and triplet ^{39}K bound states, including their coupling by the hyperfine interaction, that enables us to determine the C_6 dispersion coefficient, exchange interaction parameters and scattering lengths. A simple mass-scaling rule subsequently enables us to derive the corresponding scattering properties of ^{41}K . Finally, we have used these potentials to predict the magnetic-field dependence of the scattering process of two ^{39}K and of two ^{41}K atoms in the $f = 1$, $m_f = -1$ hyperfine state.

The long-range singlet ($S=0$) and triplet ($S=1$) interaction potentials between two K atoms are written as

$$V_S(r) = -C_6/r^6 - C_8/r^8 - C_{10}/r^{10} - (-1)^S A e^{-\alpha r}, \quad (7.1)$$

with dispersion coefficients C_n and exchange parameters A, α . We select an interatomic distance r_0 as far out as possible, such that inside r_0 the energy separation between the $S = 0$ and $S = 1$ potentials is large enough for the singlet-triplet mixing by the hyperfine interaction to be negligible [12]. This enables us to summarize the entire $r < r_0$ part of the interaction potentials in terms of accumulated phases ϕ_S, ϕ_T of the oscillating singlet and triplet radial wave functions, which serve as a boundary condition for Schrödinger's equation in the range $r > r_0$.

We start by improving the inner part of the singlet potential, determined by Amiot [14], by a standard uncoupled inverted perturbation approach [15], making use of a code developed by Moerdijk [12]. We use measured energy differences of levels up to and including $v = 74$ with outer turning points up to $18.2a_0$. This yields a potential reproducing the measured bound-state energies to within the experimental uncertainties. We use this singlet potential and a published Rydberg-Klein-Rees triplet potential [16] to determine $\phi_S(E, l)$, $\phi_T(E, l)$ for arbitrary combinations of energy E and relative orbital angular momentum l by integrating the singlet and triplet radial Schrödinger equations from the origin outward to $r_0 = 16a_0$. The variation with E and l of the radial phases at r_0 is then used in the boundary condition for the $r > r_0$ problem and the values of the phases $\phi_T(0, 0)$, $\phi_S(0, 0)$ at $E = l = 0$ are varied together with the long-range potential parameters to optimally describe the highest energy levels [12], i.e., the singlet rovibrational levels of Ref. [14] with outer turning points between $17a_0$ and $29a_0$, and the triplet rovibrational levels of Ref. [16] with outer turning points between $17a_0$ and $20a_0$. The uncertainty in the variations of the phases over the E and l ranges involved in the following analysis has been estimated to be small and is included in the final error limits.

For this optimization problem we use a new multichannel inverted perturbation approach, which will be explained in more detail elsewhere [17]. Like the standard inverted perturbation approach (IPA) it searches for potential corrections that eliminate deviations between theoretical and experimental energy eigenvalues, using the expression for the first-order energy shift in perturbation theory. The essential difference is that the potential contains in addition singlet-triplet coupling terms, in our case the sum of the single-atom hyperfine interactions. Another advantage of the new method compared to the standard IPA is that triplet and singlet levels are included simultaneously, the parameter search comprising both dispersion and exchange parts and the triplet and singlet phases. It is emphasized that our analysis uses *differences* of experimental energy levels only [12]. On the other hand our analysis predicts *absolute* energies relative to the continuum.

We follow an iterative procedure in applying our multichannel IPA program to search for successively better singlet and triplet potentials. As a starting point we use long-range potentials described by the dispersion coefficients of Marinescu *et al.* [18], which are believed to be correct within 4% [19], and the exchange coefficients of Magnier [20]. With our multichannel IPA code we then search for the optimum phase values $\phi_S(0, 0)$, $\phi_T(0, 0)$. In the following step, using these as a starting point, we search for the optimum combination of C_6 and the phase values. It turns out that the data are not sensitive enough to C_8 and C_{10} to determine these higher-order dispersion coefficients. In further iterative steps these parameters are varied within their theoretical uncertainty bounds. Finally we vary C_6 , the exchange parameters and the phase parameters simultaneously to search for a least-squares minimum. As a result we find $C_6 = 3960 \pm 40$ a.u., in good agreement with the theoretical value of Marinescu *et al.* [18] but with an error bar of only 1%, and $\alpha = 0.845 \pm 0.015a_0^{-1}$, $A = (2.75 \pm 0.25) \times 10^{-6} \times \exp(-\alpha 20a_0)$ a.u., in reasonable agreement with Magnier's values [20]. We find that the terms included in the potential (7.1) give an excellent description in the radial range considered. It turns out that an analysis with r_0 shifted to $17a_0$ leads to values of C_6 , A and α within the above error limits.

From these coefficients and the corresponding phase parameters we then determine the scattering lengths for the collision of $^{39}\text{K} + ^{39}\text{K}$ atoms via a pure triplet or a (hypothetical) pure singlet collision channel. The results are summarized in Table 7.1. A simple mass-scaling law [21–23], transforming the phase values at r_0 , enables us to transform these results into the corresponding values for a $^{41}\text{K} + ^{41}\text{K}$ collision. The results are also presented in Table 7.1. We thus predict that the stability condition for the Bose condensate under homogeneous circumstances is fulfilled in the case of doubly spin-polarized ^{41}K atoms. For the analogous case of ^{39}K we predict that it is not fulfilled.

The other state that can be trapped in a static magnetic trap, the $f = 1, m_f = -1$ hyperfine state, is a field-dependent superposition of singlet and triplet eigenstates. The scattering length $a_{1,-1}$ will therefore depend on B . It is well-known that this dependence cannot be calculated by simply averaging a_S and a_T with weight factors equal to the singlet and triplet probabilities in the spin state of the incoming channel. This is only true in the degenerate-internal-states

Isotope	scattering length
^{39}K	$-1200 < a_T < -60$
^{39}K	$+130 < a_S < +146$
^{41}K	$+21 < a_T < +64$
^{41}K	$+78 < a_S < +90$

 Table 7.1: Triplet (a_T) and singlet (a_S) scattering lengths in a_0 for ^{39}K and ^{41}K

(DIS) limit, i.e., when the influence of the hyperfine splitting is negligible during a two-body collision [24]. The averaging prescription would lead to a smooth dependence on B with no resonances. A more realistic picture suggesting where Feshbach resonances might be expected arises as follows. For a fixed value of the field we separately diagonalize the spin Hamiltonian $V_{hf} + V_Z$, consisting of the hyperfine and Zeeman interactions, in the singlet and triplet two-atom subspace, i.e., we neglect the hyperfine-induced singlet-triplet mixing, replacing V_{hf} by its “symmetric” part $V_{hf}^+ = \frac{1}{4}a_{hf}\{F(F+1) - S(S+1) - I(I+1)\}$, depending on the two-atom spin-quantum numbers S, I, F . For ^{41}K the result is presented in Fig. 7.2(a). We restrict ourselves to the relevant highest vibrational levels v and to states with the two-atom magnetic-quantum number M_F equal to the value -2 in the incident channel. Note that the singlet levels are only weakly field-dependent via the nuclear Zeeman term. We give an indication for the error limits due to the uncertainties in the potential parameters and phase values by giving two extreme sets of curves (drawn and dashed lines). Also, we indicate the simple coupled $|(SI)FM_F\rangle$ and decoupled $|SM_SIM_I\rangle$ structures valid in the weak- and strong-field limits, and the B -dependent threshold of the continuum (dotted line), equal to the sum of the single-atom $f = 1, m_f = -1$ energies. Feshbach resonances are expected where a bound-state level crosses the threshold and becomes a quasi-bound state embedded in the continuum. Figure 7.2(a) suggests that a Feshbach resonance may exist close to or inside the field range where the atoms can be trapped. Note, however, that we have neglected the contribution $V_{hf}^- = \frac{1}{4}a_{hf}/\hbar^2\{(\vec{s}_1 - \vec{s}_2) \cdot (\vec{i}_1 - \vec{i}_2)\}$, antisymmetric in the atomic electron spins that couples singlet and triplet states. This might be a bad approximation when the energy distance between the latter is comparable to a_{hf} as is the case for low B . In fact we expect the $|v = 26, (11)2, -2\rangle$ state to be repelled by the higher $v = 87$ singlet level.

The result of a rigorous coupled channels calculation of $a_{1,-1}$ is presented in Fig. 7.2(b) for the same two extreme sets of potential parameters. Clearly, we predict at least one Feshbach resonance in the field range $B < B_0$ where the atoms are low-field seeking, for the whole range of possible potential parameters. Apparently, the V_{hf}^- coupling does play an important role for weak fields. A gas of ^{41}K atoms in the $f = 1, m_f = -1$ state may therefore very well be the first experimental example where the scattering length changes sign due to the existence of a Feshbach resonance in the interesting field-range. To illustrate the difference with the flat behavior of the simple DIS prediction Fig. 7.2(b) also shows

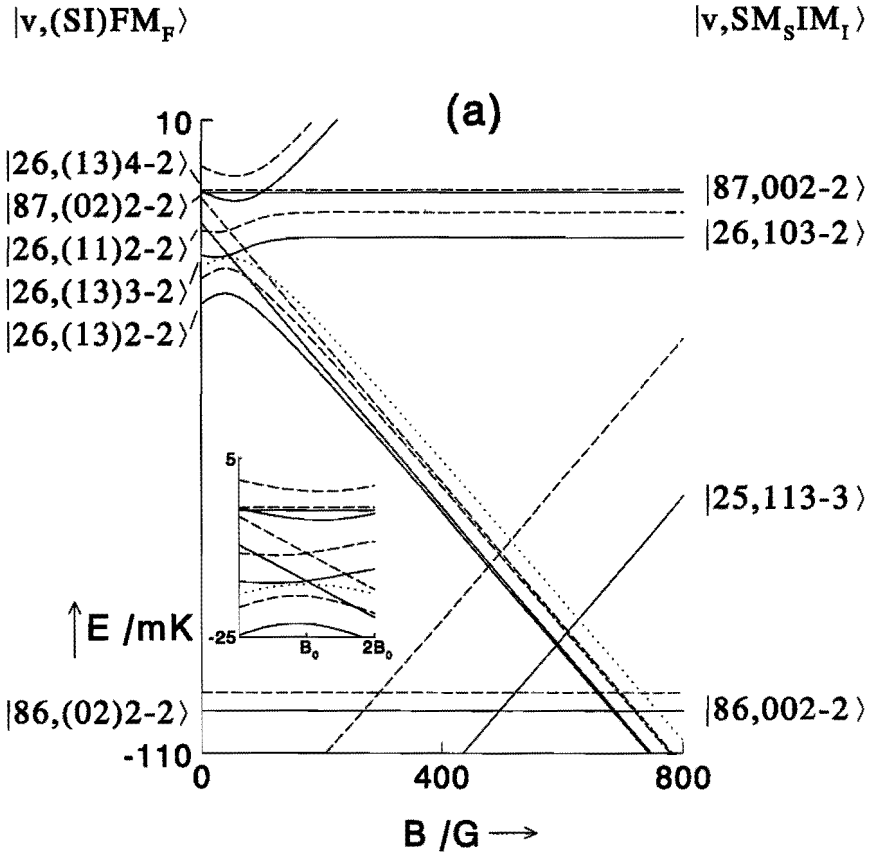


Figure 7.2: (a) Energies of highest singlet and triplet bound states for ^{41}K as a function of magnetic field for model neglecting V_{hf}^- . At $B = 0$ the splitting of the $S = 1$ levels is given by $V_{hf}^+ = \frac{1}{4}a_{hf}[F(F+1) - S(S+1) - I(I+1)]$. For each bound state two lines (drawn and dashed) are presented, corresponding to two extremes for the potential parameters. The dotted line shows the threshold energy of the $|1 - 1, 1 - 1\rangle$ collision channel. Resonances for ultralow collision energy occur where this line intersects with a bound state energy curve. Inset: bound-state energies in low-field regime.

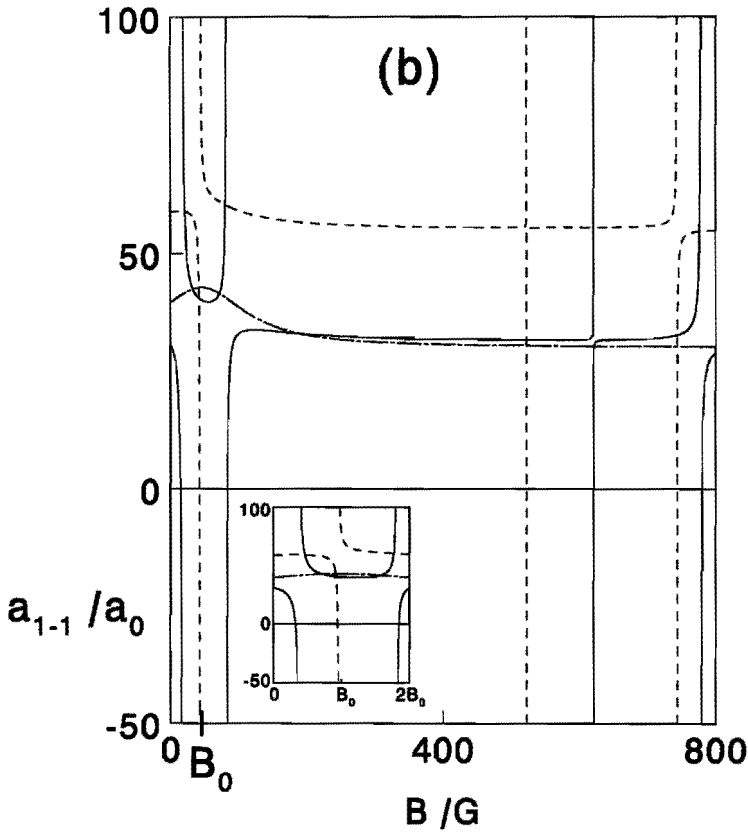


Figure 7.2: (b) Value of the scattering length for the $f = 1, m_f = -1$ state following from coupled channels calculation. The two lines are extreme results for different choices of the potentials. The dash-dotted line shows $a_{1,-1}$ in the DIS limit for one extreme choice. Inset: value of scattering length in low-field regime.

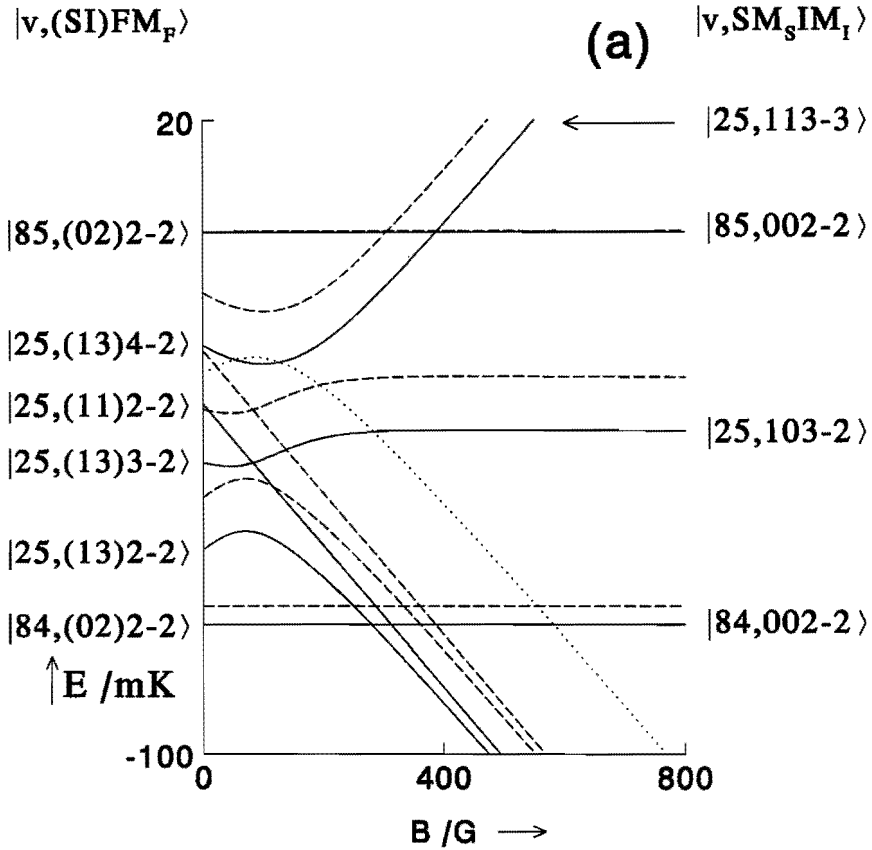


Figure 7.3: (a) Same as Fig. 7.2(a) for ^{39}K .

the above-mentioned average of a_S and a_T for one of the extreme sets of parameters (dash-dotted line, corresponding to drawn line for coupled channels). Another interesting feature visible in Fig. 7.2(b) is the interference of two nearby overlapping Feshbach resonances for a range of possible potential parameters. If this actually occurs experimentally, an intriguing time-dependent behavior with two competing time scales might show up in a measurement, especially when the field is varied as a function of time through the field range where the overlap occurs.

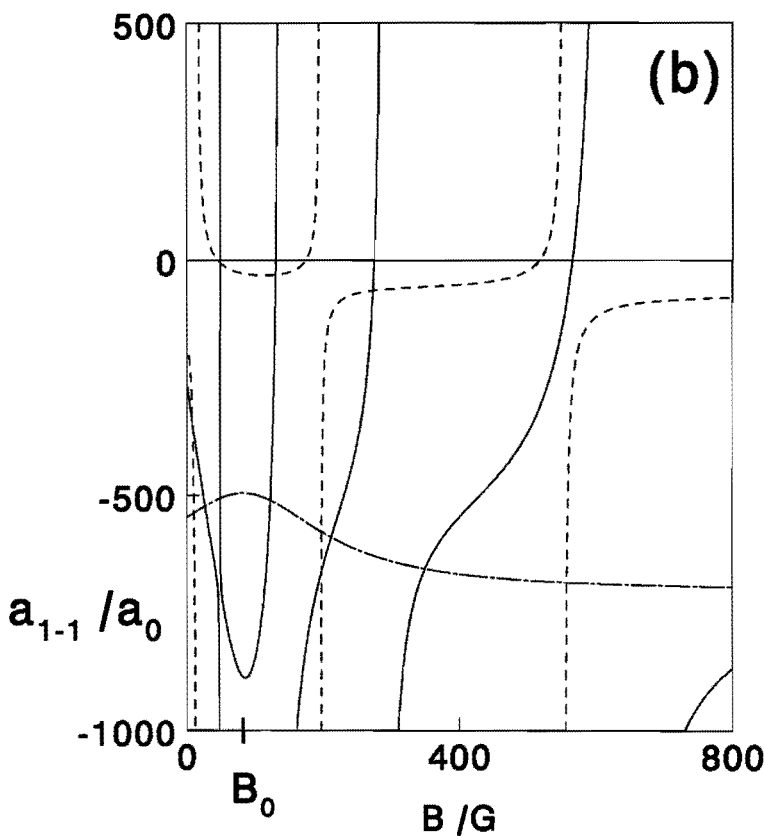


Figure 7.3: (b) Same as Fig. 7.2(b) for ^{39}K .

Taking into account the uncertainties in the potential parameters, the field ranges where the resonances are predicted to occur at threshold are:

$$16 < B_{S=1} < 44G, \quad (7.2)$$

$$515 < B_{S=1} < 630G, \quad (7.3)$$

$$740 < B_{S=0} < 785G, \quad (7.4)$$

where we indicate the resonances by their predominant singlet or triplet character. The interfering resonances are predicted to occur for $40 < B_{S=1} < 85G$.

Figure 7.3 shows analogous results for ^{39}K atoms. Note that due to the lower atomic mass the resonances are associated with vibrational states having lower v values. The coupled-channel results lead to the conclusion that the probability of finding a change of sign of a , either through $\pm\infty$ or 0, in the field range $B < B_0$, taking into account the uncertainty in the potential, is about 80%. A remarkable feature of the resonances is that they extend over a much wider field range than in ^{41}K . The field ranges where the resonances are predicted to occur at threshold turn out to be

$$0 < B_{S=1} < 16G, \quad (7.5)$$

$$195 < B_{S=1} < 295G, \quad (7.6)$$

$$550 < B_{S=0} < 630G. \quad (7.7)$$

In conclusion, we have studied collision properties of cold ^{39}K and ^{41}K atoms, relevant for BEC experiments. Despite the small hyperfine splittings we predict at least one Feshbach resonance for ^{41}K in the field range where the highest state of the lower hyperfine manifold can be trapped and a large probability for a change of sign of a in ^{39}K . The broadness of the resonance features in ^{39}K should make them more easily observable experimentally.

References

- [1] M.H. Anderson, J.R. Ensher, M.R. Matthews, C.E. Wieman, and E.A. Cornell, *Science* **269**, 198 (1995).
- [2] C.C. Bradley, C.A. Sacket, J.J. Tollet, and R.G. Hulet, *Phys. Rev. Lett.* **75**, 1687 (1995).
- [3] K.B. Davis, M-O Mewes, M.R. Anderson, N.J. van Druten, D.S. Durfee, D.M. Kurn, and W. Ketterle, *Phys. Rev. Lett.* **75**, 3969 (1995).
- [4] G. Baym and C.J. Pethick, *Phys. Rev. Lett.* **76**, 6 (1996).
- [5] M. Holland and J. Cooper, *Phys. Rev. A* **53**, R1954 (1996).
- [6] D.S. Jin, J.R. Ensher, M.R. Matthews, C.E. Wieman, and E.A. Cornell, *Phys. Rev. Lett.* **77**, 420 (1996).
- [7] A.L. Fetter and J.D. Walecka, *Quantum Theory of Many-Particle Systems* (McGraw-Hill, New York, 1971), p. 218.
- [8] E. Tiesinga, A.J. Moerdijk, B.J. Verhaar, and H.T.C. Stoof, *Phys. Rev. A* **46**, R1167 (1992); E.Tiesinga, B.J. Verhaar, and H.T.C. Stoof, *Phys. Rev. A* **47**, 4114 (1993).
- [9] This applies to a homogeneous condensate. For the inhomogeneous situation of a trapped gas the condition is different but again contains a .

- [10] W. Ketterle and N.J. van Druten, *Adv. At. Mol. Opt. Phys.* **37**, 181 (1996).
- [11] K. Gibble and S. Chu, *Metrologia* **29**, 201 (1992).
- [12] A.J. Moerdijk, W.C. Stwalley, R.G. Hulet, and B.J. Verhaar, *Phys. Rev. Lett.* **72**, 40 (1994); A.J. Moerdijk and B.J. Verhaar, *Phys. Rev. Lett.* **73**, 518 (1994); A.J. Moerdijk, B.J. Verhaar, and A. Axelsson, *Phys. Rev. A* **51**, 4852 (1995).
- [13] B.J. Verhaar, K. Gibble, and S. Chu, *Phys. Rev. A* **48**, R3429 (1993).
- [14] C. Amiot, J. Vergès, and C.E. Fellows, *J. Chem. Phys.* **103**, 3350 (1995).
- [15] C.R. Vidal and H. Scheingraber, *J. Mol. Spectrosc.* **65**, 46 (1977).
- [16] L. Li, A.M. Lyra, W.T. Luh, and W.C. Stwalley, *J. Chem. Phys.* **93**, 8452 (1990).
- [17] J.M. Vogels, H.M.J.M. Boesten, and B.J. Verhaar (to be published).
- [18] M. Marinescu, H.R. Sadeghpour, and A. Dalgarno, *Phys. Rev. A* **49**, 982 (1994).
- [19] W.T. Zemke, C.C. Tsai, and W.C. Stwalley, *J. Chem. Phys.* **101**, 10382 (1994).
- [20] S. Magnier, PhD Thesis, University of Paris, Orsay, France (1993).
- [21] J.R. Gardner, R.A. Cline, J.D. Miller, D.J. Heinzen, H.M.J.M. Boesten, and B.J. Verhaar, *Phys. Rev. Lett.* **74**, 3764 (1995).
- [22] H.M.J.M. Boesten, C.C. Tsai, J.R. Gardner, D.J. Heinzen, and B.J. Verhaar (unpublished).
- [23] H.M.J.M. Boesten, C.C. Tsai, D.J. Heinzen, and B.J. Verhaar (unpublished).
- [24] B.J. Verhaar, *Laser Phys.* **4**, 1054 (1994); B.J. Verhaar, in *Atomic Physics 14*, edited by D.J. Wineland, C.E. Wieman, and S.J. Smith (AIP Press, New York, 1995), p. 351.

Chapter 8

Introduction to optical collisions

H.M.J.M. Boesten, F.A. van Abeelen, and B.J. Verhaar

Abstract

In this chapter we will introduce and derive the optical-Bloch equations, necessary to describe collisions of two cold atoms in a laser field. This will be done starting from the Schrödinger equation for the total system, consisting of the two-atom system, the laser field, and the radiation reservoir (to describe spontaneous emission). The purpose of this chapter is to serve as an introduction to the final two chapters, which treat the first attempt in the literature to describe optical collisions entirely on the basis of quantum mechanics.

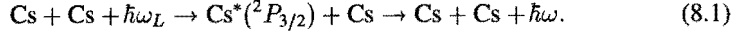
8.1 Introduction

Collisions between ultracold atoms are fundamentally different from collisions at room temperature because the de-Broglie wavelength Λ becomes larger than the range of the interaction potential between the atoms. Because of this, quantum-mechanical effects become important. This contrasts with, for instance, helium-neon collisions at room temperature, for which the relative motion of the atoms can be treated classically to a considerable extent [1]. Furthermore, at low temperatures the collision dynamics are influenced by the long-range part of the attractive potentials, which is unimportant for thermal collisions.

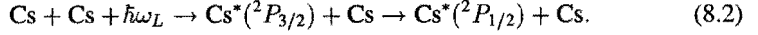
Ultracold collisions become especially interesting if one of the atoms is in an optically excited state. During such optical collisions the probability for spontaneous emission may very well become of order 1 due to the very long distance and time scales of the collision process. As a consequence, spontaneous emission can no longer be treated as a perturbation on the collision process.

Optical collisions occur for instance in optical traps, of which a large variety is used nowadays in laser cooling and laser trapping experiments. In such traps optical collisions give rise to decay of the atomic density. Two mechanisms which can lead to atom loss are [2]:

1. **Radiative decay:**



2. **Fine-structure change:**



In these equations and in the following we have, for the sake of definiteness, considered the case of two Cs atoms, although this chapter applies to any pair of identical alkali atoms. The basic idea of the radiative decay process is illustrated in Fig. 8.1. During the collision of two cesium atoms in the $^2S_{1/2} + ^2S_{1/2}$ ground state channel with relative kinetic energy $E_{k,in}$ one of the atoms is excited at an interatomic (i.e., internuclear) distance R by absorption of a laser photon, so that the molecular system is now in the $^2S_{1/2} + ^2P_{3/2}$ state (a similar description applies if the excitation occurs to the $^2S_{1/2} + ^2P_{1/2}$ channel). This process is possible if the laser frequency ω_L is equal to the distance between the potential curves of the ground state $E_g(R)$ and excited state $E_e(R)$. The interatomic distance at which the laser frequency fits exactly the transition from the $E_g(R)$ to the $E_e(R)$ potential is called the Condon radius R_C . The kinetic energy of the atoms is conserved during this transition, if the momentum of the absorbed photon is neglected. This is a satisfactory approximation for the circumstances of most of the present optical collision work. In addition, we confine ourselves to the case of red laser detuning relative to the atomic transition.

Next, the atoms are accelerated towards smaller R under the influence of the attractive resonant electric dipole-dipole interaction $E_e(R) = -C_3/R^3$. If, at a smaller interatomic distance $R < R_C$ spontaneous emission occurs, the frequency ω of the emitted photon will be smaller than the frequency ω_L of the absorbed photon because $E_g(R)$ is almost independent of R . The increase in kinetic energy $E_{k,fin} - E_{k,in}$ is equally distributed among both atoms. If this energy increase, $\hbar(\omega_L - \omega)/2$ per atom, is larger than the trap depth, both atoms can leave the trap.

In the fine-structure change loss process the laser excitation is followed by a fine-structure transition from the atomic $^2P_{3/2}$ to the atomic $^2P_{1/2}$ state when the atoms have moved to distances of roughly $20a_0$, because here curve crossings occur between molecular potentials asymptotically connecting with the $^2S_{1/2} + ^2P_{3/2}$ state and other molecular potentials, corresponding with the asymptotic $^2S_{1/2} + ^2P_{1/2}$ state. The asymptotic energy difference between both states is 797 K for cesium, 342 K for rubidium, and 25 K for sodium so that both atoms gain enough kinetic energy to leave the trap via a fine-structure transition.

Since these fine-structure changes occur at small R -values, for which the potential $E_e(R)$ is deep, the atoms move so rapidly during the transition that a classical description is sufficient for the collision process. The probability of a fine-structure transition during one passage through the crossing region, can be estimated from existing experimental data at room temperature [2], again because of the depth of $E_e(R)$.

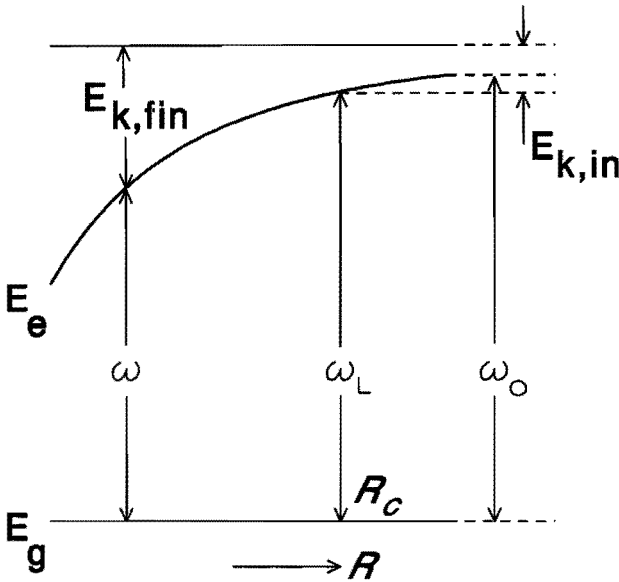


Figure 8.1: Radiative decay, ω_0 is the atomic transition frequency and $E_{k,in}$ ($E_{k,fin}$) the initial (final) collision energy.

Based on the above, we can divide the total range of interatomic distances into two regimes. One regime concerns the small distances up to $R_0 \approx 100a_0$. It includes the fine-structure crossing and can be treated classically. The other regime is that where the laser excitation and spontaneous emission occur: $R > R_0$ and needs to be described quantum mechanically. A very important question is whether the laser-excited atoms will be able to reach the small interatomic distances where they can undergo a fine-structure transition, i.e., one would like to know the probability that the atoms will survive in the excited molecular state all the way down to the radial range of the fine-structure curve crossings. This quantity can be calculated using the optical-Bloch equation which will be introduced in the third section. First we will look in some more detail at the potential curves involved.

For the description of optical collisions only large interatomic distances are relevant, for which the ground- and excited-state potential-curves can be treated very simply. In particular the $\text{Cs}(^2S_{1/2}) + \text{Cs}(^2S_{1/2})$ molecular potential is not split up and independent of R and the singlet and triplet molecular states are linear combinations of atomic product states. As mentioned above, in the excited-state potential curves asymptotically connecting with the $^2S_{1/2} + ^2P_{3/2}$ or $^2S_{1/2} + ^2P_{1/2}$ fine-structure limits are important. The radial dependence can be derived from the Hamiltonian consisting of the sum of the R -independent $^2P_{3/2} - ^2P_{1/2}$

fine-structure splitting and the electric dipole-dipole interaction [3]

$$\begin{aligned} V_{d-d}(R) &= \frac{1}{4\pi\epsilon_0} \left(\vec{D}_1 \cdot \vec{D}_2 - 3(\vec{D}_1 \cdot \hat{R})(\vec{D}_2 \cdot \hat{R}) \right) / R^3 \\ &= \frac{1}{4\pi\epsilon_0} (D_{1x'}D_{2x'} + D_{1y'}D_{2y'} - 2D_{1z'}D_{2z'}) / R^3, \end{aligned} \quad (8.3)$$

with D_{ij} the j -component (along body-fixed x', y', z' axes) of the electrostatic dipole operator of atom i . The resulting eigenvalues E_n are shown in Fig. 8.2. In this figure we used the notation Ω_σ^\pm , with $\Omega = |M_J(z')|$, the absolute value of the projection of the total electronic momentum on the interatomic axis, $\sigma = g/u$, the parity of the total electronic wave function and \pm the symmetry character under reflection in a plane through the internuclear axis (only if $\Omega = 0$).

Of the five attractive curves in Fig. 8.2 the 0_u^+ excited state is expected to be the dominant channel in fine-structure loss processes [4]. Due to selection rules of the electric dipole operator this excited state couples with the 0_g^+ ground state only. In the following we will restrict ourselves to this choice of channels: $|e\rangle = 0_u^+(^2P_{3/2} + ^2S_{1/2})$ and $|g\rangle = 0_g^+(^2S_{1/2} + ^2S_{1/2})$. The value of the C_3 dispersion coefficient follows from the slope of the $0_u^+(^2P_{3/2} + ^2S_{1/2})$ -curve in Fig. 8.2 at small X . It is also important to notice that in this entire chapter the nuclear spin is left out of consideration. Incorporation of the nuclear spin and of more fine-structure channels in the following derivation of the optical-Bloch equation, however, is straightforward.

8.2 Schrödinger equation for optical collisions

In this section we will derive the (infinite) set of coupled-channels equations describing the evolution of the total system, consisting of two atoms with an internuclear distance vector \vec{R} , the laser field and a radiation reservoir necessary for the description of spontaneous emission.

The Schrödinger equation for our two-level system, interacting with one (laser)mode (frequency ω_L) of the radiative field and an infinite number of modes (frequency ω_k) of the reservoir, can be written as

$$i\hbar \frac{d}{dt} |t\rangle = H |t\rangle, \quad (8.4)$$

with

$$H = T_{\vec{R}} + H_{mol}(R) + H_{em} + H_{int}, \quad (8.5)$$

in which

$$\begin{aligned} T_{\vec{R}} &= -\frac{\hbar^2}{2\mu} \Delta_{\vec{R}}, \\ H_{mol}(R) &= \sigma_+ \sigma_- \hbar \omega_{eg}(R) \\ &= \sigma_+ \sigma_- (\hbar \omega_0 - C_3/R^3), \\ H_{em} &= \hbar \omega_L a_L^\dagger a_L + \sum_{\vec{k}\epsilon} \hbar \omega_k a_{\vec{k}\epsilon}^\dagger a_{\vec{k}\epsilon}, \\ H_{int} &= -\sigma_+ \vec{d}^*(\hat{R}) \cdot (\vec{\mathcal{E}}_L + \vec{\mathcal{E}}_R) - \sigma_- \vec{d}(\hat{R}) \cdot (\vec{\mathcal{E}}_L^\dagger + \vec{\mathcal{E}}_R^\dagger). \end{aligned} \quad (8.6)$$

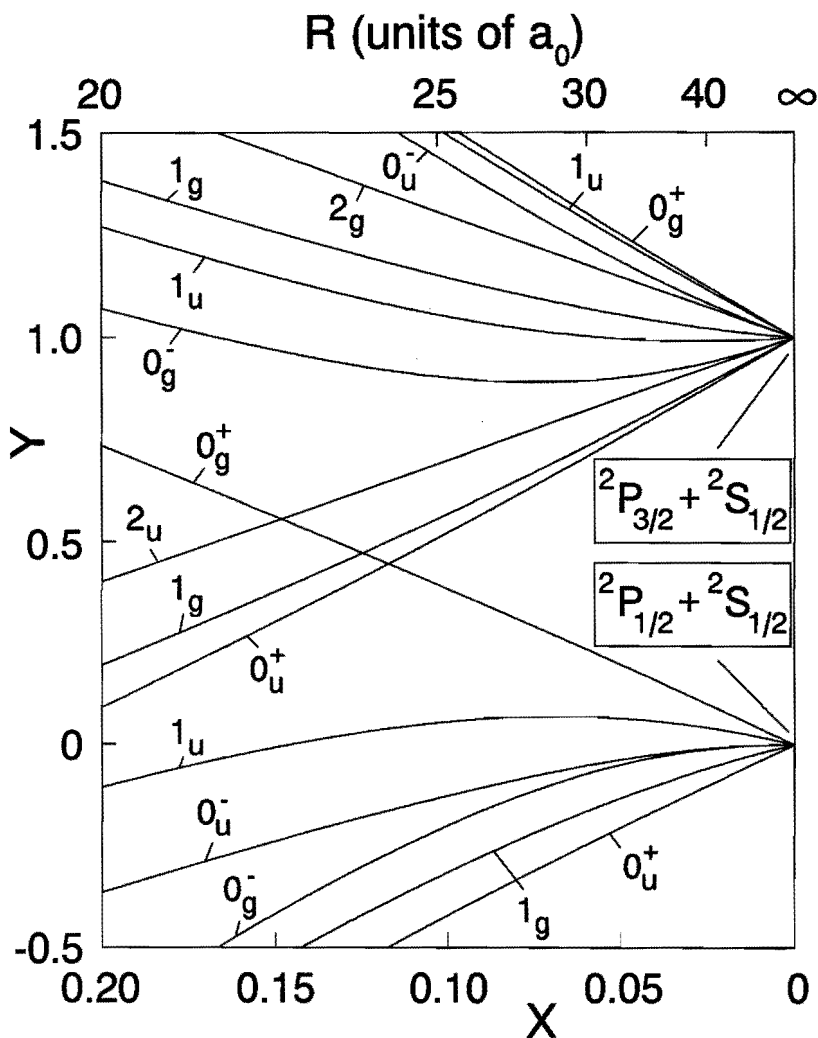


Figure 8.2: Potential energy curves for the $^2P_{3/2} + ^2S_{1/2}$ and $^2P_{1/2} + ^2S_{1/2}$ states of Cs_2 ; $X = d^2/(12\pi\epsilon_0\Delta R^3)$, $Y = (E_n - E_{1/2}^0)/\Delta$, with $d = \langle ^2S, M_L = 0 | D_z | ^2P, M_L = 0 \rangle$, the atomic electric-dipole matrix element, and Δ the atomic fine-structure splitting, $E_{1/2}^0$ is the molecular energy of the asymptotic $^2P_{1/2} + ^2S_{1/2}$ states.

The symbol μ denotes the reduced mass, equal to $m/2$, ω_0 the atomic transition frequency and $\sigma_- = \sigma_+^\dagger = |g\rangle\langle e|$. The operators a_L^\dagger (a_L) and $a_{\vec{k}\vec{\epsilon}}^\dagger$ ($a_{\vec{k}\vec{\epsilon}}$) in the free hamiltonian H_{em} of the electromagnetic field are the photon creation (annihilation) operators of the laser mode and of the reservoir modes. The occupation number of the laser mode with polarization vector $\vec{\epsilon}_L$ is called N , the occupation number of the reservoir mode with wave number \vec{k} and polarization vector $\vec{\epsilon}$ is called $N_{\vec{k}\vec{\epsilon}}$, etcetera. The Hamiltonian H_{int} describes the interaction between the molecular system and the radiation field. In it the vector \vec{d} represents the molecular electric-dipole matrix element

$$\vec{d}(\hat{R}) = \langle \phi_g(\vec{R}) | \vec{D}_1 + \vec{D}_2 | \phi_e(\vec{R}) \rangle, \quad (8.7)$$

in which $|\phi_{g/e}(\vec{R})\rangle$ is the electronic wave function for molecules with interatomic distance \vec{R} . The phases of the e - and g -states are chosen in such a way that, for all values of \hat{R} , $\vec{d}^* \cdot \vec{\epsilon}_L = \vec{d} \cdot \vec{\epsilon}_L^*$ is a negative real number.

The vectors $\vec{\mathcal{E}}_L$ ($\vec{\mathcal{E}}_L^\dagger$) and $\vec{\mathcal{E}}_R$ ($\vec{\mathcal{E}}_R^\dagger$) are the annihilation (creation) parts of the electric-field-strength operators of the laser and the reservoir [5]:

$$\vec{\mathcal{E}}_L = \sqrt{\frac{\hbar\omega_L}{2\epsilon_0 L^3}} \vec{\epsilon}_L a_L, \quad (8.8)$$

$$\vec{\mathcal{E}}_R = \sum_{\vec{k}\vec{\epsilon}} \sqrt{\frac{\hbar\omega_k}{2\epsilon_0 L^3}} \vec{\epsilon} a_{\vec{k}\vec{\epsilon}}. \quad (8.9)$$

In the above expressions the laser field is described by an electromagnetic field mode in a cubic cavity with edge L and periodic boundary conditions. The frequency of this mode is equal to the laser frequency ω_L . The reservoir is represented by the collection of all modes that can exist in this cavity (we will refer to these modes as reservoir modes). In the Hamiltonian H_{int} nonresonant terms like $\sigma_- \vec{d}^*(\hat{R}) \cdot (\vec{\mathcal{E}}_L + \vec{\mathcal{E}}_R)$, for which an $e \rightarrow g$ transition and a photon absorption take place simultaneously, or $\sigma_+ \vec{d}(\hat{R}) \cdot (\vec{\mathcal{E}}_L^\dagger + \vec{\mathcal{E}}_R^\dagger)$, for which during a $g \rightarrow e$ transition a photon is created, are omitted (rotating-wave approximation [6]).

Taking into account all modes in expression (8.9) leads to divergences. Furthermore, the coupling between the molecular system and the relativistic reservoir modes is not correctly described by H_{int} in combination with (8.9). A correct treatment of the interaction with these modes requires a relativistic description of the molecular system. These problems are avoided by limiting the summation over the reservoir modes to modes with a frequency smaller than a certain cutoff frequency ω_c . This cutoff frequency has to be chosen in such a way that only those modes that are important for the description of laser excitation and spontaneous emission are taken into account, while the relativistic modes are excluded. We take [5] $\omega_0 \ll \omega_c \ll m_e c^2 / \hbar \approx 8 \times 10^{20}$ Hz. The atomic transition frequency ω_0 is of the order of 10^{15} Hz and thus $\omega_c = 10^{17}$ Hz is a good choice. In the remaining part of this chapter all summations are limited by this cutoff frequency.

In the coupled equations to be derived, laser-coupling matrix elements of the form

$$\langle g, N | \sigma_- \vec{d}(\hat{R}) \cdot \vec{\mathcal{E}}_L^\dagger | e, N-1 \rangle = \vec{d}(\hat{R}) \cdot \vec{\epsilon}_L^* \sqrt{\frac{\hbar\omega_L}{2\epsilon_0 L^3}} \sqrt{N} \quad (8.10)$$

occur. To make these matrix elements independent of N , we make the following substitutions in the expressions for $\vec{\mathcal{E}}_L$ and $\vec{\mathcal{E}}_L^\dagger$,

$$\begin{aligned} a_L &\rightarrow \sqrt{\bar{N}} \hat{a}_L, \\ a_L^\dagger &\rightarrow \sqrt{\bar{N}} \hat{a}_L^\dagger, \end{aligned} \quad (8.11)$$

with \bar{N} the expectation value of the number of laser photons, related to the laser intensity I via $I = \bar{N}\hbar\omega_L/L^3c$. The operators \hat{a}_L and \hat{a}_L^\dagger are defined by

$$\begin{aligned} \hat{a}_L|N\rangle &= |N-1\rangle, \quad \hat{a}_L|0\rangle = 0, \\ \hat{a}_L^\dagger|N\rangle &= |N+1\rangle. \end{aligned} \quad (8.12)$$

Because of the choice of phases of $\phi_e(\vec{R})$ and $\phi_g(\vec{R})$ introduced above all laser-coupling matrix elements now have the following negative real value

$$\vec{d}(\vec{R}) \cdot \vec{\mathcal{E}}_L^* \sqrt{\frac{\hbar\omega_L}{2\varepsilon_0L^3}} \sqrt{\bar{N}} \equiv -\frac{\hbar\Omega_r(\vec{R})}{2}. \quad (8.13)$$

The quantity Ω_r is called the Rabi frequency and is a positive real number.

To derive the set of coupled-channels equations for the total system we write the total state vector $|t\rangle$ as a linear combination of eigenstates of the free part of H without the kinetic energy operator ($H_{mol}(\vec{R}) + H_{em}$):

$$\begin{aligned} |t\rangle &= \sum_{N, N_{\vec{k}_1\vec{\varepsilon}_1}, \dots} \left[F_{e, N, N_{\vec{k}_1\vec{\varepsilon}_1}, \dots}(\vec{R}, t) |e, N, N_{\vec{k}_1\vec{\varepsilon}_1}; N_{\vec{k}_2\vec{\varepsilon}_2}; \dots\rangle + \right. \\ &\quad \left. F_{g, N, N_{\vec{k}_1\vec{\varepsilon}_1}, \dots}(\vec{R}, t) |g, N, N_{\vec{k}_1\vec{\varepsilon}_1}; N_{\vec{k}_2\vec{\varepsilon}_2}; \dots\rangle \right]. \end{aligned} \quad (8.14)$$

The equations for the coefficients $F_{g/e, N, N_{\vec{k}_1\vec{\varepsilon}_1}, \dots}(\vec{R}, t)$ are found by substituting the expansion (8.14) for $|t\rangle$ in the Schrödinger equation and taking the inner product with $|g/e, N, N_{\vec{k}_1\vec{\varepsilon}_1}; N_{\vec{k}_2\vec{\varepsilon}_2}; \dots\rangle$ on the left and right hand sides:

$$\begin{aligned} i\hbar \frac{\partial}{\partial t} F_{g, N, \mathcal{O}}(\vec{R}, t) &= [T_{\vec{R}} + N\hbar\omega_L] F_{g, N, \mathcal{O}}(\vec{R}, t) + \frac{1}{2}\hbar\Omega_r F_{e, N-1, \mathcal{O}}(\vec{R}, t), \\ i\hbar \frac{\partial}{\partial t} F_{e, N-1, \mathcal{O}}(\vec{R}, t) &= [T_{\vec{R}} + (N-1)\hbar\omega_L + \hbar\omega_{eg}(R)] F_{e, N-1, \mathcal{O}}(\vec{R}, t) + \\ &\quad \frac{1}{2}\hbar\Omega_r F_{g, N, \mathcal{O}}(\vec{R}, t) - \vec{d}^* \cdot \sum_{\vec{k}\vec{\varepsilon}} \langle \mathcal{O} | \vec{\mathcal{E}}_R | \vec{k}\vec{\varepsilon} \rangle F_{g, N-1, \vec{k}\vec{\varepsilon}}(\vec{R}, t), \end{aligned} \quad (8.15)$$

$$\begin{aligned} i\hbar \frac{\partial}{\partial t} F_{g, N-1, \vec{k}\vec{\varepsilon}}(\vec{R}, t) &= [T_{\vec{R}} + (N-1)\hbar\omega_L + \hbar\omega_k] F_{g, N-1, \vec{k}\vec{\varepsilon}}(\vec{R}, t) + \\ &\quad \frac{1}{2}\hbar\Omega_r F_{e, N-2, \vec{k}\vec{\varepsilon}}(\vec{R}, t) - \vec{d} \cdot \langle \vec{k}\vec{\varepsilon} | \vec{\mathcal{E}}_R^\dagger | \mathcal{O} \rangle F_{e, N-1, \mathcal{O}}(\vec{R}, t), \\ i\hbar \frac{\partial}{\partial t} F_{e, N-2, \vec{k}\vec{\varepsilon}}(\vec{R}, t) &= [T_{\vec{R}} + (N-2)\hbar\omega_L + \hbar\omega_k + \hbar\omega_{eg}(R)] F_{e, N-2, \vec{k}\vec{\varepsilon}}(\vec{R}, t) + \\ &\quad \frac{1}{2}\hbar\Omega_r F_{g, N-1, \vec{k}\vec{\varepsilon}}(\vec{R}, t) - \\ &\quad \vec{d}^* \cdot \sum_{\vec{k}'\vec{\varepsilon}'} \langle \vec{k}\vec{\varepsilon} | \vec{\mathcal{E}}_R | \vec{k}'\vec{\varepsilon}' \rangle F_{g, N-2, \vec{k}'\vec{\varepsilon}'}(\vec{R}, t), \end{aligned} \quad (8.16)$$

etcetera. The notation $|\vec{k}\vec{e}\rangle$ has been introduced as an abbreviated notation for the state $|N_{\vec{k}\vec{e}} = 1; \text{ all other reservoir modes unoccupied}\rangle$. The state $|\mathcal{O}\rangle$ is the vacuum state of the reservoir.

The equations are ordered in sets of two equations. Each set contains the equations of the coefficients of eigenstates which are coupled by the laser field only. One of these eigenstates contains the combined molecule-laser state $|g, M\rangle$ for certain M , the other $|e, M - 1\rangle$. The pair $\{|g, M\rangle, |e, M - 1\rangle\}$ is called the M^{th} manifold. Attached to each manifold is a collection of eigenstates which can be populated by subsequent laser excitations and spontaneous emissions from the state $|g, N, \mathcal{O}\rangle$:

$$\left\{ |e, M - 1, N_{\vec{k}_1\vec{e}_1}; N_{\vec{k}_2\vec{e}_2}; \dots\rangle, |g, M, N_{\vec{k}_1\vec{e}_1}; N_{\vec{k}_2\vec{e}_2}; \dots\rangle \middle| M + \sum_{\vec{k}\vec{e}} N_{\vec{k}\vec{e}} = N \right\}.$$

This process of subsequent excitations and emissions is called a radiative cascade. Equations (8.15) describe the first step in the cascade of the N^{th} manifold (to be referred to hereafter as the highest level of the cascade), Eqs. (8.16) the second step (second level). The radiative cascade is schematically drawn in Fig. 8.3. The above set of equations is the starting point for the derivation of the quantum-mechanical optical-Bloch equation in the following section.

8.3 Quantum-mechanical optical-Bloch equation

Equations (8.4), (8.5), and (8.6) in the previous section describe the time evolution of the total system, including the relative motion of the atoms, the laser, and the reservoir. However, we are only interested in the evolution of the degrees of freedom of the molecular system. The state of this subsystem is obtained by taking the partial trace over the laser and reservoir degrees of freedom of the density operator $\rho_{tot}(t) = |t\rangle\langle t|$ which represents the total system:

$$\rho(t) = \text{Sp}_R \text{Sp}_L \rho_{tot}(t). \quad (8.17)$$

In general, the resulting state $\rho(t)$ of the molecular system is a mixed state. An equation describing the evolution of such a subsystem is called “master equation”. In this section the master equation for $\rho(t)$ will be derived.

The terms in the Hamiltonian H containing the electric-field operators $\vec{\mathcal{E}}_R$ and $\vec{\mathcal{E}}_R^\dagger$ are the largest obstacles in the derivation of this equation. They are responsible for the coupling between the different levels in the radiative cascade. To include these terms in the description we follow Mollow’s approach [7], but with an essential generalization: in contrast to Mollow we take the relative collisional motion of the atoms into account.

We start by rewriting Eqs. (8.4), (8.5), and (8.6) in the interaction picture by applying the transformation

$$\begin{cases} |t\rangle^I = e^{iH_0 t/\hbar} |t\rangle, \\ O^I(t) = e^{iH_0 t/\hbar} O e^{-iH_0 t/\hbar}, \end{cases} \quad (8.18)$$

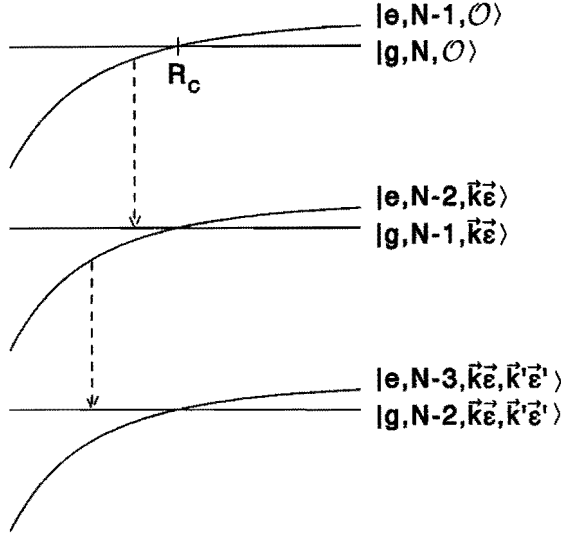


Figure 8.3: Radiative cascade. The curves illustrate the ground- and excited-state potential curves. Within each level the states are coupled by the laser field. Vertical arrows represent spontaneous decay to lower levels in the cascade. For the sake of clarity we have given only the sum of the potential energy and the energy of the laser field.

where $H_0 = H_{em} + H_{mol}(R)$ and O an arbitrary operator. Equation (8.4) transforms into

$$i\hbar \frac{d}{dt} |t\rangle^I = H_1^I(t) |t\rangle^I, \quad (8.19)$$

with

$$H_1^I(t) = T_{\vec{R}}^I(t) + H_{int}^I(t). \quad (8.20)$$

Furthermore,

$$H_{int}^I(t) = -\sigma_+^I(t) \vec{d}^*(\hat{R}) \cdot [\vec{\mathcal{E}}_L^I(t) + \vec{\mathcal{E}}_R^I(t)] - \sigma_-^I(t) \vec{d}(\hat{R}) \cdot [\vec{\mathcal{E}}_L^I(t) + \vec{\mathcal{E}}_R^I(t)], \quad (8.21)$$

$$\sigma_-^I(t) = \sigma_- e^{-i\omega_{eg}(R)t}, \quad (8.22)$$

$$\vec{\mathcal{E}}_L^I(t) = \sqrt{\frac{\hbar\omega_L}{2\varepsilon_0 L^3}} \sqrt{N} \vec{e}_L \hat{a}_L e^{-i\omega_L t}, \quad (8.23)$$

$$\vec{\mathcal{E}}_R^I(t) = \sum_{\vec{k}\vec{e}} \sqrt{\frac{\hbar\omega_k}{2\varepsilon_0 L^3}} \vec{e} a_{\vec{k}\vec{e}} e^{-i\omega_k t}. \quad (8.24)$$

The advantage of this interaction picture is that the evolution of $|t\rangle^I$ is only determined by the relative kinetic energy of the atoms and the interaction between the molecular system and the radiation field. The state $|t\rangle^I$ no longer contains the free-evolution exponents of the internal molecular state and the radiation field.

The solution of (8.19) can be expanded in powers of H_1^I :

$$|t\rangle^I = \sum_{n=0}^{\infty} |t\rangle_n^I, \quad (8.25)$$

where the n^{th} term is related to the preceding one via the recursion relation

$$|t\rangle_n^I = \frac{1}{i\hbar} \int_{t_0}^t dt' H_1^I(t') |t'\rangle_{n-1}^I, \quad |t\rangle_0^I = |t_0\rangle^I. \quad (8.26)$$

We assume that at the reference time t_0 the density operator $\rho_{tot}(t_0)$ can be written as

$$\rho_{tot}(t_0) = \text{Sp}_R \rho_{tot}(t_0) \otimes |\mathcal{O}\rangle\langle\mathcal{O}|, \quad (8.27)$$

the product of an arbitrary state of the molecular system and the laser on the one hand and the vacuum state of the reservoir on the other hand. This means that we neglect the correlations which exist at time t_0 between the reservoir and the rest of the system. The idea behind this is that such correlations disappear in a very short time τ_c ($\ll 1/\Gamma$) and that new correlations arise that are independent of the previous history. The assumption that the reservoir is in the vacuum state at time t_0 is justified by the consideration that spontaneously emitted photons rapidly move far away from the radiating system; the interaction with the molecular system will hardly change the state of the reservoir. As a result

$$\vec{\mathcal{E}}_R^I(t) |t_0\rangle^I = \vec{\mathcal{E}}_R^I(t) |t_0\rangle^I = 0, \quad (8.28)$$

in which we used $a_{\vec{k}\epsilon} |\mathcal{O}\rangle = 0$.

The time τ_c can be estimated using the function

$$\begin{aligned} \phi(t-t') &\equiv \langle \mathcal{O} | \left(\mathcal{E}_{Ri}^I(t) + \mathcal{E}_{Ri}^{I\dagger}(t) \right) \left(\mathcal{E}_{Ri}^I(t') + \mathcal{E}_{Ri}^{I\dagger}(t') \right) | \mathcal{O} \rangle \\ &= \langle \mathcal{O} | \mathcal{E}_{Ri}^I(t) \mathcal{E}_{Ri}^{I\dagger}(t') | \mathcal{O} \rangle \\ &= \langle \mathcal{O} | e^{iH_{em}t/\hbar} e^{-iH_{em}t'/\hbar} \mathcal{E}_{Ri} e^{-iH_{em}(t-t')/\hbar} \mathcal{E}_{Ri}^\dagger e^{-iH_{em}t'/\hbar} e^{iH_{em}t/\hbar} | \mathcal{O} \rangle \\ &= \langle \mathcal{O} | \mathcal{E}_{Ri}^I(t-t') \mathcal{E}_{Ri}^{I\dagger}(0) | \mathcal{O} \rangle, \end{aligned} \quad (8.29)$$

with $i = x, y, z$. The last identity also follows from the fact that in the vacuum state no preferential time exists, so that ϕ can only depend on the difference $t - t'$ between the two times t and t' . In addition, it does not depend on i . This follows from symmetry arguments. The real part of $\phi(t-t')$ equals the correlation function of the components of the electric-field operator $\vec{E}_R = \vec{\mathcal{E}}_R + \vec{\mathcal{E}}_R^\dagger$, i.e., the reservoir part of the operator describing the interaction between the reservoir and the molecular system:

$$\text{Re } \phi(t-t') = \text{Re} \langle \mathcal{O} | E_{Ri}^I(t) E_{Ri}^I(t') | \mathcal{O} \rangle \quad (8.30)$$

$$= \frac{1}{2} \langle \mathcal{O} | E_{Ri}^I(t) E_{Ri}^I(t') + E_{Ri}^I(t') E_{Ri}^I(t) | \mathcal{O} \rangle. \quad (8.31)$$

Again, we have assumed that the reservoir is in the vacuum state. As a consequence, the time interval for which $\phi(\tau) \neq 0$ is a measure for the time scale of the influence of fluctuations in the reservoir, and thus for τ_c . In order to determine this width, Eq. (8.29) will be worked out in more detail in the following paragraphs.

Using (8.24) and the properties of the photon-creation and annihilation operators we find

$$\begin{aligned}\phi(\tau) &= \sum_{\vec{k}\vec{z}} \sum_{\vec{k}'\vec{z}'} \frac{\hbar}{2\varepsilon_0 L^3} \sqrt{\omega_k \omega_{k'}} \epsilon_i(\hat{k}) \epsilon_i^*(\hat{k}') e^{-i\omega_k \tau} \langle \mathcal{O} | a_{\vec{k}\vec{z}} a_{\vec{k}'\vec{z}'}^\dagger | \mathcal{O} \rangle \\ &= \sum_{\vec{k}\vec{z}} \frac{\hbar \omega_k}{2\varepsilon_0 L^3} \epsilon_i(\hat{k}) \epsilon_i^*(\hat{k}) e^{-i\omega_k \tau}.\end{aligned}\quad (8.32)$$

In this expression we have explicitly indicated that the polarization vectors $\vec{\epsilon}$ depend on the direction of the wave number \vec{k} ; each \vec{k} corresponds with two basis polarization vectors $\vec{\epsilon}^1$ and $\vec{\epsilon}^2 \perp \hat{k}$. We now take the limit $L \rightarrow \infty$, so that

$$\phi(\tau) = \frac{L^3}{(2\pi)^3} \int d\hat{k} \sum_{m=1}^2 \epsilon_i^m(\hat{k}) \epsilon_i^{m*}(\hat{k}) \int k^2 dk \frac{\hbar \omega_k}{2\varepsilon_0 L^3} e^{-i\omega_k \tau}.\quad (8.33)$$

The \hat{k} -integral is independent of i and can therefore be easily determined:

$$\int d\hat{k} \sum_{m=1}^2 \epsilon_i^m(\hat{k}) \epsilon_i^{m*}(\hat{k}) = \frac{1}{3} \int d\hat{k} \sum_{m=1}^2 \vec{\epsilon}^m(\hat{k}) \vec{\epsilon}^{m*}(\hat{k}) = \frac{8\pi}{3}.\quad (8.34)$$

Finally, we replace the k -integral by an integral over all frequencies of the reservoir modes and obtain the result

$$\phi(\tau) = \int_0^{\omega_c} d\omega G(\omega) e^{-i\omega \tau},\quad (8.35)$$

where

$$G(\omega) = \frac{\hbar \omega^3}{6\pi^2 \varepsilon_0 c^3}.\quad (8.36)$$

In Eq. (8.35) we again encounter the cutoff frequency ω_c which was introduced in the previous section. From this expression one can directly see that $\phi(\tau)$ is only nonvanishing in a time interval around $\tau = 0$ with a duration of the order of $1/\omega_c$. For $\tau \gg 1/\omega_c$ the exponents interfere destructively. In conclusion,

$$\tau_c \approx 1/\omega_c \approx 10^{-17} \text{ s}.\quad (8.37)$$

Before continuing with the treatment of $\vec{\mathcal{E}}_R$ we will carry out some preparatory work. First we calculate the commutator $[\mathcal{E}_{Ri}^I(t), \mathcal{E}_{Rj}^{I\dagger}(t')]$. From Eq. (8.24) and $[a_{\vec{k}\vec{z}}, a_{\vec{k}'\vec{z}'}^\dagger] = \delta_{\vec{k}\vec{k}'} \delta_{\vec{z}\vec{z}'}$ it follows that

$$[\mathcal{E}_{Ri}^I(t), \mathcal{E}_{Rj}^{I\dagger}(t')] = \sum_{\vec{k}\vec{z}} \frac{\hbar \omega_k}{2\varepsilon_0 L^3} \epsilon_i(\hat{k}) \epsilon_j^*(\hat{k}) e^{-i\omega_k(t-t')},\quad (8.38)$$

with $i = x, y, z$. After introducing a third ‘‘polarization vector’’ $\vec{\epsilon}^3(\hat{k}) = \hat{k}$ we find

$$\sum_{m=1}^3 \epsilon_i^m(\hat{k}) \epsilon_j^{m*}(\hat{k}) = \delta_{ij},\quad (8.39)$$

so that

$$\sum_{m=1}^2 \epsilon_i^m(\hat{k}) \epsilon_j^{m*}(\hat{k}) = \delta_{ij} - (\hat{k} \cdot \hat{i})(\hat{k} \cdot \hat{j}), \quad (8.40)$$

in which \hat{i} and \hat{j} are direction vectors. The contributions to the sum over \vec{k} in (8.38) cancel if $i \neq j$. If $i = j$ Eq. (8.38) equals $\phi(t - t')$, so that

$$[\mathcal{E}_{Ri}^I(t), \mathcal{E}_{Rj}^{I\dagger}(t')] = \phi(t - t') \delta_{ij}. \quad (8.41)$$

Secondly, we introduce the function

$$\begin{aligned} F(t - t') &\equiv \int_{-\infty}^{t'} dt'' e^{i\omega_{eg}(R)(t-t'')} \phi(t - t'') \\ &= \int_{\tau}^{\infty} dt'' e^{i\omega_{eg}(R)t''} \phi(t''), \end{aligned} \quad (8.42)$$

with $\tau = t - t'$. Just as $\phi(\tau)$, $F(\tau)$ is only $\neq 0$ in a small interval around $\tau = 0$ of order τ_c . The real part of $F(0)$ follows from

$$\begin{aligned} \text{Re } F(0) &= \frac{1}{2} \int_0^{\omega_c} d\omega G(\omega) 2\pi \frac{1}{2\pi} \int_0^{\infty} dt'' [e^{i(\omega_{eg}(R)-\omega)t''} + e^{-i(\omega_{eg}(R)-\omega)t''}] \\ &= \frac{1}{2} \int_0^{\omega_c} d\omega G(\omega) 2\pi \delta(\omega_{eg}(R) - \omega) \\ &= \frac{1}{2} \frac{\hbar^2}{d^2} \Gamma(R), \end{aligned} \quad (8.43)$$

where

$$d^2 = \vec{d}(\hat{R}) \cdot \vec{d}^*(\hat{R}), \quad (8.44)$$

$$\Gamma(R) = \frac{d^2 \omega_{eg}^3(R)}{3\pi \epsilon_0 c^3 \hbar}. \quad (8.45)$$

The quantity d^2 is a constant for $R > 30a_0$ and $\Gamma(R)$ is the molecular spontaneous emission rate, which can be expressed easily in the atomic rate Γ_{at} . For the specific choice of g and e states that we made in section 8.1 the rate $\Gamma(\infty) = \frac{4}{3}\Gamma_{at}$. Furthermore, we define

$$\text{Im } F(0) \equiv \frac{\hbar^2}{d^2} \delta\omega. \quad (8.46)$$

This term causes a shift $\delta\omega$ in the frequency of the $e \rightarrow g$ transition and is assumed to be included in ω_{eg} .

The last preparatory work concerns an estimate of the order of magnitude of the change of the state $|t\rangle^I$ in a time interval τ_c . Using (8.22), (8.23), and (8.13) we find that the laser part of $H_1^I(t)|t\rangle^I$ has the order of magnitude $\hbar\Omega_\tau|t\rangle^I$. The order of magnitude of $T_{\hat{R}}^I(t)|t\rangle^I$ is $E_{kin}|t\rangle^I$, in which E_{kin} is the relative kinetic energy of the atoms which depends on the stage in which the collision process has arrived. In our case an upper limit of E_{kin} is given

by the depth of the e -potential D_e . An upper limit for the “relative” change $\chi(\tau_c)$, defined by $\| |t + \tau_c\rangle^I - |t\rangle^I \| = \chi(\tau_c) \| |t\rangle^I \|$ is therefore

$$\chi(\tau_c) < (\Omega_r + D_e + \Gamma) \tau_c, \quad (8.47)$$

in which we used (8.19), (8.20), and the well known fact that the time scale of the evolution of $|t\rangle^I$ due to the coupling with the reservoir is $1/\Gamma$, which will turn out to be consistent with the equations to be derived in the remaining part of this section. In practice the Rabi frequency Ω_r is of the same order of magnitude as Γ . For cesium atoms $\Gamma = 44$ MHz and $C_3 = 12.2$ a.u., leading to $\chi(\tau_c) < 10^{-3}$.

Now multiplying both parts of Eq. (8.26) with $\tilde{\mathcal{E}}_R^I(\bar{t})$ we find using the commutator (8.41) and the fact that $[\mathcal{E}_{Ri}^I(t), T_{R\bar{r}}^I(t')] = 0$:

$$\begin{aligned} \tilde{\mathcal{E}}_R^I(\bar{t})|t\rangle_n^I &= \frac{1}{\hbar} \int_{t_0}^t dt' \tilde{\mathcal{E}}_R^I(\bar{t}) H_1^I(t') |t'\rangle_{n-1}^I \\ &= \frac{1}{\hbar} \int_{t_0}^t dt' [\tilde{\mathcal{E}}_R^I(\bar{t}), T_{R\bar{r}}^I(t')] |t'\rangle_{n-1}^I + \frac{1}{\hbar} \int_{t_0}^t dt' [\tilde{\mathcal{E}}_R^I(\bar{t}), H_{int}^I(t')] |t'\rangle_{n-1}^I + \\ &\quad \frac{1}{\hbar} \int_{t_0}^t dt' H_1^I(t') \tilde{\mathcal{E}}_R^I(\bar{t}) |t'\rangle_{n-1}^I \\ &= i \frac{\vec{d}(\hat{R})}{\hbar} \int_{t_0}^t dt' \phi(\bar{t} - t') \sigma_-^I(t') |t'\rangle_{n-1}^I + \frac{1}{\hbar} \int_{t_0}^t dt' H_1^I(t') \tilde{\mathcal{E}}_R^I(\bar{t}) |t'\rangle_{n-1}^I. \end{aligned} \quad (8.48)$$

If we take $\bar{t}, t > t_0 + \tau_c$ (this means that we only look at the system when the influence of the correlations between the reservoir and the remaining part of the system at time t_0 has disappeared), the integration limit t_0 in the first term on the right hand side of (8.48) can be replaced by $-\infty$ because of the width τ_c of the time interval for which $\phi(\bar{t} - t') \neq 0$. Furthermore (see Eq. (8.22))

$$\sigma_-^I(t') = \sigma_- e^{-i\omega_{eg}(R)\bar{t}} e^{i\omega_{eg}(R)(\bar{t}-t')} = \sigma_-^I(\bar{t}) e^{i\omega_{eg}(R)(\bar{t}-t')}. \quad (8.49)$$

Because also $\chi(\tau_c) \ll 1$, we can write

$$\begin{aligned} i \frac{\vec{d}(\hat{R})}{\hbar} \int_{t_0}^t dt' \phi(\bar{t} - t') \sigma_-^I(t') |t'\rangle_{n-1}^I &\approx i \frac{\vec{d}(\hat{R})}{\hbar} \int_{-\infty}^t dt' \phi(\bar{t} - t') e^{i\omega_{eg}(R)(\bar{t}-t')} \sigma_-^I(\bar{t}) |t'\rangle_{n-1}^I \\ &= i \frac{\vec{d}(\hat{R})}{\hbar} F(\bar{t} - t) \sigma_-^I(\bar{t}) |t\rangle_{n-1}^I. \end{aligned} \quad (8.50)$$

The second term on the right hand side of (8.48) is negligible [8,9]. We now take $\bar{t} = t$ and sum over all orders n . The result is

$$\tilde{\mathcal{E}}_R^I(t)|t\rangle^I \approx i \frac{\vec{d}(\hat{R})}{\hbar} F(0) \sigma_-^I(t) |t\rangle^I, \quad (8.51)$$

in which we used again (8.28).

In physical terms this can be understood as follows. The left hand side of (8.51) yields a nonvanishing result if a previously spontaneously emitted photon is present in the state $|t\rangle^f$ which can be annihilated by the operator $\vec{\mathcal{E}}_R^f(t)$. The second member of (8.48) expresses that this can be the last spontaneously emitted photon (second term) or an earlier emitted photon (third term). If it concerns in the last case a photon emitted at $t'' < t' < \bar{t}$, then the integrand contains a factor $\phi(\bar{t} - t'')$ due to the involved commutator. Because ϕ has only significant values in a time interval $\tau_c = 1/\omega_c$ this means that at least two spontaneous emissions should have occurred within a time interval τ_c . The corresponding probability is of order $\Gamma\tau_c = \Gamma/\omega_c$ and thus negligible.

Finally, we return to the Schrödinger picture and conclude

$$\vec{\mathcal{E}}_R|t\rangle \approx \frac{1}{2}i\hbar \frac{d(\hat{R})}{dt} \Gamma(R)\sigma_-|t\rangle, \quad (8.52)$$

$$-\sigma_+ \vec{d}^*(\bar{R}) \cdot \vec{\mathcal{E}}_R|t\rangle \approx -\frac{1}{2}i\hbar \Gamma(R)\sigma_+\sigma_-|t\rangle. \quad (8.53)$$

We thus find that $|t\rangle$ obeys approximately the modified Schrödinger equation

$$i\hbar \frac{d}{dt}|t\rangle = \tilde{H}|t\rangle, \quad (8.54)$$

with

$$\tilde{H} = \tilde{H}_0 + \tilde{H}_1, \quad (8.55)$$

where

$$\tilde{H}_0 = H_{em} + H_{mol}(R) - \frac{1}{2}i\hbar \Gamma(R)\sigma_+\sigma_-, \quad (8.56)$$

$$\tilde{H}_1 = T_{\bar{R}} - \sigma_+ \vec{d}^*(\hat{R}) \cdot \vec{\mathcal{E}}_L - \sigma_- \vec{d}(\hat{R}) \cdot \{\vec{\mathcal{E}}_R^\dagger + \vec{\mathcal{E}}_L^\dagger\}. \quad (8.57)$$

The photon-annihilation part of the interaction between the molecular system and the reservoir has become a potential term in the e channel. We can also see that the imaginary part of $F(0)$ would have led to the term $\delta\omega\sigma_+\sigma_-$, which can indeed be interpreted as a frequency shift in ω_{eg} .

In Mollow's approach the laser is represented by a harmonically oscillating electric field which enters in the Hamiltonian after a canonical transformation. This transformation can be avoided although, without it, it is impossible to derive a master equation for $\rho(t)$ as defined by the standard definition (8.17). In that definition the e - g and space representation of $\rho(t)$ has the components

$$\begin{aligned} \rho_{nm}(\vec{R}, \vec{R}', t) &= \langle n, \vec{R} | \rho(t) | m, \vec{R}' \rangle \\ &= \langle t | (|m, \vec{R}'\rangle \langle n, \vec{R}|) | t \rangle \\ &= \sum_{N, N_{\vec{k}_1 \vec{\epsilon}_1}, \dots} F_{n, N, N_{\vec{k}_1 \vec{\epsilon}_1}, \dots}(\vec{R}, t) F_{m, N, N_{\vec{k}_1 \vec{\epsilon}_1}, \dots}^*(\vec{R}', t). \end{aligned} \quad (8.58)$$

We now introduce an alternative definition of $\rho(t)$ in which the sum of products of F -coefficients with an equal photon number in (8.58) is replaced by a sum of products of F -coefficients that belong to one manifold:

$$\rho_{eg}(\vec{R}, \vec{R}', t) = \langle t | (|\vec{R}'\rangle\sigma_- \langle \vec{R} | \hat{a}_L^\dagger) | t \rangle, \quad (8.59)$$

$$\rho_{ge}(\vec{R}, \vec{R}', t) = \langle t | (\hat{a}_L |\vec{R}'\rangle\sigma_+ \langle \vec{R} |) | t \rangle, \quad (8.60)$$

$$\rho_{ee}(\vec{R}, \vec{R}', t) = \langle t | (\hat{a}_L |\vec{R}'\rangle\sigma_+\sigma_- \langle \vec{R} | \hat{a}_L^\dagger) | t \rangle, \quad (8.61)$$

$$\rho_{gg}(\vec{R}, \vec{R}', t) = \langle t | (\hat{a}_L^\dagger |\vec{R}'\rangle\sigma_-\sigma_+ \langle \vec{R} | \hat{a}_L) | t \rangle. \quad (8.62)$$

The components $\rho_{ee}(\vec{R}, \vec{R}', t)$ and $\rho_{gg}(\vec{R}, \vec{R}', t)$, which are the relevant quantities in the calculation of loss rates, are the same as in the standard definition. Only the nondiagonal components $\rho_{eg}(\vec{R}, \vec{R}', t)$ and $\rho_{ge}(\vec{R}, \vec{R}', t)$ have been changed. This new definition enables us to derive directly the desired master equation.

Differentiating Eq. (8.59) with respect to time and using the modified Schrödinger equation (8.54) we find

$$\frac{\partial}{\partial t} \rho_{eg}(\vec{R}, \vec{R}', t) = \frac{1}{i\hbar} \langle t | (|\vec{R}'\rangle\sigma_- \langle \vec{R} | \hat{a}_L^\dagger \hat{H} - \hat{H}^\dagger |\vec{R}'\rangle\sigma_- \langle \vec{R} | \hat{a}_L^\dagger) | t \rangle. \quad (8.63)$$

The $T_{\vec{R}}$ terms in the above expression lead to

$$\frac{1}{i\hbar} \left\{ -\frac{\hbar^2}{2\mu} \Delta_{\vec{R}} + \frac{\hbar^2}{2\mu} \Delta_{\vec{R}'} \right\} \rho_{eg}(\vec{R}, \vec{R}', t). \quad (8.64)$$

The \hat{H}_0 term leads to

$$-i \left\{ \omega_{eg}(R) - \omega_L - \frac{1}{2} i \Gamma(R) \right\} \rho_{eg}(\vec{R}, \vec{R}', t), \quad (8.65)$$

because $\sigma_-^2 = 0$ and $[\hat{a}_L^\dagger, \hat{a}_L^\dagger \hat{a}_L] = -\hat{a}_L$. All σ_- terms of \hat{H}_1 and \hat{H}_1^\dagger are zero because $\sigma_-^2 = 0$. The laser-coupling terms with σ_+ in \hat{H}_1 and \hat{H}_1^\dagger yield

$$\begin{aligned} & -\frac{1}{i\hbar} \vec{d}^*(\hat{R}) \cdot \vec{\epsilon}_L \sqrt{\frac{\hbar\omega_L}{2\varepsilon_0 L^3}} \sqrt{N} \langle t | (|\vec{R}'\rangle\sigma_-\sigma_+ \langle \vec{R} | \hat{a}_L^\dagger \hat{a}_L) | t \rangle + \\ & \frac{1}{i\hbar} \vec{d}^*(\hat{R}') \cdot \vec{\epsilon}_L \sqrt{\frac{\hbar\omega_L}{2\varepsilon_0 L^3}} \sqrt{N} \langle t | (|\vec{R}'\rangle\sigma_+\sigma_- \langle \vec{R} | \hat{a}_L \hat{a}_L^\dagger) | t \rangle \\ & = -i \frac{1}{2} \Omega_r(\hat{R}) \rho_{gg}(\vec{R}, \vec{R}', t) + i \frac{1}{2} \Omega_r(\hat{R}') \rho_{ee}(\vec{R}, \vec{R}', t). \end{aligned} \quad (8.66)$$

The $\vec{\mathcal{E}}_R$ term of \hat{H}_1^\dagger yields zero because

$$\begin{aligned} & \langle t | (\sigma_+ \vec{d}^*(\hat{R}') \cdot \vec{\mathcal{E}}_R \sigma_- |\vec{R}'\rangle \langle \vec{R} | \hat{a}_L^\dagger) | t \rangle = \\ & \langle t | (|\vec{R}'\rangle \langle \vec{R} | \hat{a}_L^\dagger \sigma_+ \sigma_- \vec{d}^*(\hat{R}') \cdot \vec{\mathcal{E}}_R) | t \rangle \approx \\ & \langle t | \left(|\vec{R}'\rangle \langle \vec{R} | \hat{a}_L^\dagger \sigma_+ \sigma_-^2 \frac{1}{2} \frac{\vec{d}^*(\hat{R}') \cdot \vec{d}(\hat{R})}{d^2} \Gamma(R) \right) | t \rangle = 0, \end{aligned} \quad (8.67)$$

in which we used Eq. (8.52). The result is:

$$\begin{aligned} \frac{\partial}{\partial t} \rho_{eg}(\vec{R}, \vec{R}', t) &= \frac{i\hbar}{2\mu} (\Delta_{\vec{R}} - \Delta_{\vec{R}'}) \rho_{eg}(\vec{R}, \vec{R}', t) - \\ & i \left\{ \omega_{eg}(R) - \omega_L - \frac{1}{2} i \Gamma(R) \right\} \rho_{eg}(\vec{R}, \vec{R}', t) - \\ & i \frac{1}{2} \Omega_r(\hat{R}) \rho_{gg}(\vec{R}, \vec{R}', t) + i \frac{1}{2} \Omega_r(\hat{R}') \rho_{ee}(\vec{R}, \vec{R}', t). \end{aligned} \quad (8.68)$$

In this way we have obtained one component of the quantum-mechanical optical-Bloch equation. By taking the complex conjugate of Eq. (8.68) we find for $\partial \rho_{ge}/\partial t$:

$$\begin{aligned} \frac{\partial}{\partial t} \rho_{ge}(\vec{R}, \vec{R}', t) &= \frac{i\hbar}{2\mu} (\Delta_{\vec{R}} - \Delta_{\vec{R}'}) \rho_{ge}(\vec{R}, \vec{R}', t) + \\ & i \left\{ \omega_{eg}(R') - \omega_L + \frac{1}{2} i \Gamma(R') \right\} \rho_{ge}(\vec{R}, \vec{R}', t) + \\ & i \frac{1}{2} \Omega_r(\hat{R}) \rho_{gg}(\vec{R}, \vec{R}', t) - i \frac{1}{2} \Omega_r(\hat{R}') \rho_{ee}(\vec{R}, \vec{R}', t). \end{aligned} \quad (8.69)$$

The $T_{\vec{R}}$ terms of $\partial \rho_{ee}/\partial t$ and $\partial \rho_{gg}/\partial t$ are treated as above. The \vec{H}_0 term yields zero in $\partial \rho_{gg}/\partial t$ because $\sigma_-^2 = \sigma_+^2 = 0$ and $[a_L^\dagger a_L, \hat{a}_L^\dagger \hat{a}_L] = 0$, and yields

$$\left\{ -i\omega_{eg}(R) - \frac{1}{2} \Gamma(R) + i\omega_{eg}(R') - \frac{1}{2} \Gamma(R') \right\} \rho_{ee}(\vec{R}, \vec{R}', t) \quad (8.70)$$

in $\partial \rho_{ee}/\partial t$. The \vec{E}_R^\dagger term in \vec{H}_I and the \vec{E}_R term in \vec{H}_I^\dagger yield zero in $\partial \rho_{ee}/\partial t$, again because of the identity $\sigma_-^2 = \sigma_+^2 = 0$. In $\partial \rho_{gg}/\partial t$ these terms lead via (8.52) to

$$\begin{aligned} & -\frac{1}{i\hbar} \langle t | (\vec{E}_R^\dagger \cdot \vec{d}(\hat{R}) \sigma_- \sigma_+ \sigma_- | \vec{R}' \rangle \langle \vec{R} | \hat{a}_L^\dagger \hat{a}_L | t \rangle \\ & + \frac{1}{i\hbar} \langle t | (| \vec{R}' \rangle \langle \vec{R} | \sigma_+ \sigma_- \sigma_+ \vec{d}^*(\hat{R}') \cdot \vec{E}_R \hat{a}_L^\dagger \hat{a}_L | t \rangle \\ & \approx \frac{1}{2} (\Gamma(R) + \Gamma(R')) \frac{\vec{d}^*(\hat{R}') \cdot \vec{d}(\hat{R})}{d^2} \rho_{ee}(\vec{R}, \vec{R}', t). \end{aligned} \quad (8.71)$$

Finally, we give the contributions of the laser-coupling terms. In $\partial \rho_{ee}/\partial t$ the laser-coupling terms lead to

$$-i \frac{1}{2} \Omega_r(\hat{R}) \rho_{ge}(\vec{R}, \vec{R}', t) + i \frac{1}{2} \Omega_r(\hat{R}') \rho_{eg}(\vec{R}, \vec{R}', t), \quad (8.72)$$

and in $\partial \rho_{gg}/\partial t$ to

$$-i \frac{1}{2} \Omega_r(\hat{R}) \rho_{eg}(\vec{R}, \vec{R}', t) + i \frac{1}{2} \Omega_r(\hat{R}') \rho_{ge}(\vec{R}, \vec{R}', t). \quad (8.73)$$

In total we thus find

$$\begin{aligned} \frac{\partial}{\partial t} \rho_{ee}(\vec{R}, \vec{R}', t) &= \frac{i\hbar}{2\mu} (\Delta_{\vec{R}} - \Delta_{\vec{R}'}) \rho_{ee}(\vec{R}, \vec{R}', t) + \\ & i \left\{ \omega_{eg}(R') + \frac{1}{2} i \Gamma(R') - \omega_{eg}(R) + \frac{1}{2} i \Gamma(R) \right\} \rho_{ee}(\vec{R}, \vec{R}', t) - \\ & i \frac{1}{2} \Omega_r(\hat{R}) \rho_{ge}(\vec{R}, \vec{R}', t) + i \frac{1}{2} \Omega_r(\hat{R}') \rho_{eg}(\vec{R}, \vec{R}', t), \end{aligned} \quad (8.74)$$

$$\begin{aligned} \frac{\partial}{\partial t} \rho_{gg}(\vec{R}, \vec{R}', t) &= \frac{i\hbar}{2\mu} (\Delta_{\vec{R}} - \Delta_{\vec{R}'}) \rho_{gg}(\vec{R}, \vec{R}', t) + \\ & \frac{1}{2} (\Gamma(R) + \Gamma(R')) \frac{\vec{d}^*(\hat{R}') \cdot \vec{d}(\hat{R})}{d^2} \rho_{ee}(\vec{R}, \vec{R}', t) - \\ & i \frac{1}{2} \Omega_r(\hat{R}) \rho_{ge}(\vec{R}, \vec{R}', t) + i \frac{1}{2} \Omega_r(\hat{R}') \rho_{ge}(\vec{R}, \vec{R}', t). \end{aligned} \quad (8.75)$$

Equations (8.68), (8.69), (8.74), and (8.75) can be written in the form

$$\begin{aligned} \frac{\partial}{\partial t} \underline{\underline{\rho}}(\vec{R}, \vec{R}', t) &= \frac{i\hbar}{2\mu} (\Delta_{\vec{R}} - \Delta_{\vec{R}'}) \underline{\underline{\rho}}(\vec{R}, \vec{R}', t) - \\ & \frac{i}{\hbar} \left[\underline{\underline{V}}(\vec{R}) \underline{\underline{\rho}}(\vec{R}, \vec{R}', t) - \underline{\underline{\rho}}(\vec{R}, \vec{R}', t) \underline{\underline{V}}^\dagger(\vec{R}') \right] + \\ & \underline{\underline{\Gamma}}(\underline{\underline{\rho}}(\vec{R}, \vec{R}', t)), \end{aligned} \quad (8.76)$$

with

$$\underline{\underline{V}}(\vec{R}) = \hbar \begin{pmatrix} -\Delta(R) - \frac{1}{2} i \Gamma(R) & \frac{1}{2} \Omega_r(\hat{R}) \\ \frac{1}{2} \Omega_r(\hat{R}) & 0 \end{pmatrix} \quad (8.77)$$

and

$$\underline{\underline{\Gamma}}(\underline{\underline{\rho}}(\vec{R}, \vec{R}', t)) = \hbar \begin{pmatrix} 0 & 0 \\ 0 & \frac{1}{2} (\Gamma(R) + \Gamma(R')) \frac{\vec{d}(\hat{R}) \cdot \vec{d}^*(\hat{R}')}{d^2} \rho_{ee}(\vec{R}, \vec{R}', t) \end{pmatrix}. \quad (8.78)$$

The upper left term in the above matrices corresponds to the ee -component, $\Delta(R)$ is the local laser detuning

$$\Delta(R) = \omega_L - \omega_{eg}(R) = \Delta_\infty \left[1 + \frac{C_3}{\hbar \Delta_\infty R^3} \right], \quad (8.79)$$

where $\Delta_\infty = \omega_L - \omega_0$ is the detuning of the laser with respect to the atomic transition frequency. Since the detuning is zero at the Condon radius, we can write

$$\Delta(R) = \Delta_\infty \left[1 - \left(\frac{R_C}{R} \right)^3 \right]. \quad (8.80)$$

In Eq. (8.76) we can distinguish the coherent evolution described by the effective Hamiltonian

$$H_{eff} = -\frac{\hbar^2}{2\mu} \Delta_{\vec{R}} + \underline{\underline{V}}(\vec{R}), \quad (8.81)$$

and the incoherent evolution described by $\underline{\Gamma}(\underline{\rho})$. According to the definitions (8.59)–(8.62) $\underline{\rho}(\vec{R}, \vec{R}', t)$ consists of a sum of contributions each of which comes from one level in the radiative cascade. The effective Hamiltonian H_{eff} describes the evolution of one such level including the loss of probability to lower levels due to spontaneous emission, but excluding the gain of probability from higher levels. The V and V^\dagger terms in the right hand side of (8.76) therefore lead to “trace loss” in $\underline{\rho}(\vec{R}, \vec{R}', t)$. This loss is compensated for by $\underline{\Gamma}(\underline{\rho})$ which accounts for the gain in probability from higher cascade levels. This term is therefore called “gain term”. Finally, we notice that the above master equation has been derived for the reduced density matrix corresponding to a pure state $|t\rangle$. If the total system has to be described by a mixed state we find the same equation after averaging over all $\underline{\rho}$ -matrices.

The master equation describes the evolution of a collision of two atoms in a laser field for arbitrary laser intensities. The only restriction we made in the derivation of this master equation is the limitation to a two-level system. However, including more (internal) degrees of freedom, is a straightforward extension of Eq. (8.76). An interesting limiting situation is the low laser intensity limit. If the laser intensity is small enough the gain term in (8.76) can be neglected and the collision can be described with a Schrödinger equation with the effective Hamiltonian H_{eff} . This limit will be extensively studied in the following two chapters.

References

- [1] J.P.J. Driessen, Thesis Eindhoven University, 1989.
- [2] A. Gallagher and D.E. Pritchard, Phys. Rev. Lett. **63**, 957 (1989).
- [3] M. Movre and G. Pichler, J. Phys. B **10**, 2631 (1977).
- [4] Y.B. Band and P.S. Julienne, Phys. Rev. A **46**, 330 (1992).
- [5] C. Cohen-Tannoudji, J. Dupont-Roc, and G. Grynberg, *Photons and atoms* (Wiley, New York, 1989).
- [6] C. Cohen-Tannoudji, J. Dupont-Roc, and G. Grynberg, *Atom-Photon Interactions* (Wiley, New York, 1992).
- [7] B.R. Mollow, Phys. Rev. A **12**, 1919 (1975).
- [8] H.M.J.M. Boesten, Master Thesis Eindhoven University, 1992.
- [9] F.A. van Abeelen, Master Thesis Eindhoven University, 1996.

Chapter 9

Quantum suppression of collisional loss rates in optical traps

H.M.J.M. Boesten, B.J. Verhaar, and E. Tiesinga

Published in Physical Review A **48**, 1428 (1993)

Abstract

We present a coupled-channel study of optical collisions, restricted to a single atom-laser manifold. Outside of a resonance region around the Condon point, we find a simple representation of the solution in terms of propagating complex dressed states. The probability flux for the $^2P_{3/2} + S$ state at small interatomic distances can be interpreted in terms of two such interfering dressed states. The coupled-channel solution displays some features that have previously been obtained with semiclassical optical-Bloch-equation methods. An important quantum effect, however, is a strong reduction of atom loss rates at low collision energies that is roughly proportional to E^{-2} .

9.1 Introduction

In recent years a rapid development has taken place in the field of cooling atomic gases and storing them in optical and magnetic traps. The interest is stimulated by exciting opportunities offered by such cold gases, such as the possible realization of Bose-Einstein condensation and precision experiments such as the construction of an ultrastable Cs clock. The interest also comes from the expectation that collisions between atoms proceed in an unusual way at the temperatures which are now being achieved. At low temperatures, the collision between a ground-state atom and an optically excited atom proceeds differently due to the fact that the spontaneous-emission time becomes comparable with the collision time, which makes it essential to include spontaneous emission in a more fundamental way in the description of the collision (for an overview of research in this area, see Julienne, Smith, and Burnett [1]).

A crucial aspect determining to a great extent the possibilities of carrying out experiments on atoms in traps is the existence of loss mechanisms which shorten the half-life of the atom density. For (magneto-)optical traps Gallagher and Pritchard [2] first pointed to the existence of two important mechanisms, both of which occur in atom-atom collisions. The basic process involved is resonant laser excitation

$$A(S) + A(S) + \hbar\omega \rightarrow A(^2P_{3/2}) + A(S) \quad (9.1)$$

at large interatomic distance and subsequent acceleration along a $-C_3/R^3$ attractive excited-state-potential surface. This is followed by either spontaneous emission and the possibility of a subsequent escape of the fast-moving ground-state atoms, or, more importantly, by an exothermal fine-structure transition $^2P_{3/2} \rightarrow ^2P_{1/2}$ at close interatomic distance giving the atoms enough energy to escape.

After the basic description by Gallagher and Pritchard the theory was further developed in two papers [3,4], which clearly demonstrated the rich variety of physical phenomena involved in optical collisions. In these papers the atomic motion was treated classically, which introduces an ambiguity as to the choice of the relative atomic velocity on the excited potential. This type of ambiguity can be avoided in a purely quantum-mechanical theory. It is clear, however, that a rigorous fully quantum-mechanical theory of optical collisions is beyond present computational possibilities. Therefore it is of interest to investigate partial aspects of the full problem in order to obtain so much insight that adequate approximative descriptions can eventually be developed. One such study was recently carried out in the nonsaturated regime on the basis of the WKB and a stationary-phase-like approximation for the atomic motion [5]. The result was written in the form of a product of an absorption line shape and a survival probability on the excited potential with an excited-state velocity determined by energy conservation.

In this paper the treatment will be fully quantum mechanical, but limited to a single manifold [6] of coupled states $|e, N\rangle$ and $|g, N + 1\rangle$ of the combined molecule-laser system and a single combination of relative orbital angular momentum quantum numbers l' and l for the excited and unexcited two-atom system, respectively. Here e and g denote optically coupled excited and unexcited internal states of the combined two-atom system, while N and $N + 1$ stand for the associated numbers of laser photons.

9.2 Method of calculation

For the sake of definiteness we concentrate on the optical collision of Cs atoms, and on the 0_u^+ and 0_g^+ excited and ground states, respectively [3,5]. We thus deal with a simple two-channel model of an optical collision, but believe that the conclusions shed light on more realistic situations with complications such as a number of subsequent radial avoided crossings due to hyperfine structure or a number of excited potential curves besides 0_u^+ . We consider collision energies from the mK range down to values around $10 \mu\text{K}$, where recoil effects can still

be neglected both for linear and angular momentum. In view of the predominance of the $-C_3/R^3$ potential, the centrifugal effects in the e channel do not depend on the precise value of l , which may therefore be taken equal to l .

The above restriction to a single manifold allows us to take into account the loss of probability flux due to spontaneous emission but we do not consider the “recycling” of ground-state atoms thereby produced on the next lower manifold, i.e., their subsequent laser excitation. This first-order treatment in the spontaneous-emission rate is valid as long as the depletion of the original manifold is small. In practice, this also implies a small depletion of the ground state, i.e., a restriction to the unsaturated regime. The implied near-linear intensity dependence is indeed indicated by experimental data of Sesko *et al.* [7] and is also reproduced by optical Bloch equation calculations [4]. Also for the more general case, where the depletion of the original manifold is not small, the present single-manifold study is of interest, since the waves generated in lower- N manifolds by spontaneous emission again behave according to the same coupled-channel equations, so that the properties of the solution may be used to develop an approach for the total problem.

We thus solve the system of coupled radial equations

$$\left[-\frac{\hbar^2}{2\mu} \frac{d^2}{dR^2} + \frac{\hbar^2 l(l+1)}{2\mu R^2} + \hbar \underline{\omega}(R) \right] \underline{F}(R) = E \underline{F}(R), \quad (9.2)$$

with μ the reduced mass and

$$\underline{F}(R) = \begin{pmatrix} F_e(R) \\ F_g(R) \end{pmatrix} \quad (9.3)$$

the coupled radial wave functions associated with the $|e, N\rangle$ and $|g, N+1\rangle$ states. Furthermore,

$$\underline{\omega}(R) = \begin{pmatrix} -\Delta(R) - i\Gamma & \frac{1}{2}\Omega_r \\ \frac{1}{2}\Omega_r & 0 \end{pmatrix}, \quad (9.4)$$

in which $\Delta(R) = \Delta(1 - R_C^3/R^3)$ is the local laser detuning with R_C the Condon point. For simplicity we neglect the long-range retardation and the $1/R^6$ van der Waals potential at the large distances involved, while the spontaneous-emission rate $\Gamma = 32.7 \times 10^6 \text{ s}^{-1}$ and the Rabi frequency Ω_r are taken independent of R [4,5]. Including R -dependent corrections in our coupled-channel calculations is straightforward but is not expected to change the basic conclusions. We solve the set of coupled equations (9.2), subject to boundary conditions to be specified below.

It turns out that our coupled-channel solution has a simple behavior outside the resonance region around R_C . It can be described to a very good approximation in terms of decoupled solutions in a local- R basis of complex dressed states consisting of the eigenvectors of the

non-Hermitian matrix $\underline{\omega}$:

$$\begin{aligned} |1(N)\rangle &= \cos(\theta) |e, N\rangle + \sin(\theta) |g, N+1\rangle, \\ |2(N)\rangle &= -\sin(\theta) |e, N\rangle + \cos(\theta) |g, N+1\rangle \end{aligned} \quad (9.5)$$

with complex coefficients determined by $\tan(2\theta) = -\Omega_r / [\Delta(R) + i\Gamma]$ and the complex eigenvalues $-\frac{1}{2}\hbar [\Delta(R) + i\Gamma] \pm \frac{1}{2}\hbar\Omega(R)$ in which $\Omega(R) = \left\{ \Omega_r^2 + [\Delta(R) + i\Gamma]^2 \right\}^{1/2}$, the sign of the square root being chosen in such a way that $\text{Re}[\Omega(R)]$ is positive right of R_C . The associated damped radial wave functions $F_{i(N)}(R)$ satisfy the equations

$$\left[-\frac{\hbar^2}{2\mu} \frac{d^2}{dR^2} + \frac{\hbar^2 l(l+1)}{2\mu R^2} - \frac{1}{2}\hbar [\Delta(R) + i\Gamma] \pm \frac{1}{2}\hbar\Omega(R) \right] F_{i(N)}(R) = E F_{i(N)}(R) \quad (9.6)$$

with the + or - sign for $i = 1$ or 2.

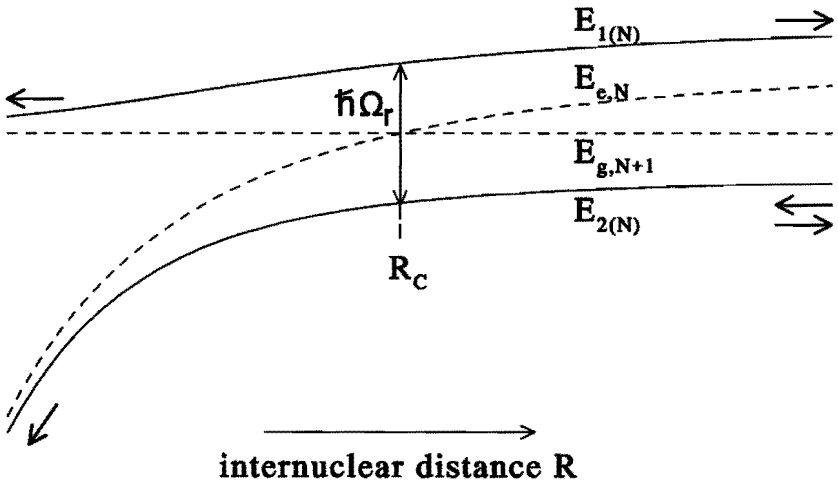


Figure 9.1: Boundary conditions for collision problem ($\Gamma = 0$): an incoming wave in the $|2(N)$ -channel right of R_C and outgoing waves in all channels.

In terms of the above decoupled solutions the boundary conditions for the collision problem are an incoming $|2(N)\rangle$ wave right of R_C and $|1(N)\rangle, |2(N)\rangle$ waves leaving the environment of R_C both to the left and right. For the collision energy E less than the threshold energy $E_{th} = -\frac{1}{2}\hbar\Delta + \frac{1}{2}\hbar\text{Re}[\Omega(\infty)]$ the $|1(N)\rangle$ radial wave function should go to 0 as $R \rightarrow \infty$. Our main conclusions remain valid for other boundary conditions, in particular for waves approaching R_C from the direction of the origin and thus also for the coupled problem where the reflection of radially ingoing waves from the small- R region calculated

in Ref. [3] is taken into account. For the simple case without spontaneous emission ($\Gamma = 0$, $E_{i(N)}$ real) the boundary conditions are illustrated in Fig. 9.1. We solve the set of complex coupled equations (9.2) in the uncoupled basis in the resonance region around R_C with a width of a few hundred a_0 to find a set of linearly independent coupled basis solutions. Subsequently, we form a linear combination to satisfy the above conditions at the boundaries of this region.

In the first instance we restrict ourselves to $l = 0$. The program has been checked by applying it to a simple model in which the actual $-C_3/R^3$ potential is replaced by a rectilinear potential having the same derivative at R_C . For such a simple avoided crossing analytical expressions for reflection and transmission coefficients can be derived [8] which agree excellently with our numerical results.

9.3 Results and discussion

Figure 9.2 shows the probability fluxes J_g , J_e , and their sum in the uncoupled basis, following from the coupled-channel solution for initial kinetic energy $E = 1$ mK, detuning $\Delta = -\Gamma$, and Rabi frequency $\Omega_r = 0.8 \Gamma$. For reasons to be explained below we normalize to $J_g + J_e = 1$ at small R . We see a behavior with an interesting physical interpretation: a decreasing J_g at large R due to laser excitation on approaching $R_C = 2950a_0$, an excited-state flux J_e starting at somewhat lower values, then first decreasing slowly due to the combined effect of laser excitation and spontaneous emission and subsequently, after the passage of the resonance region around R_C , decaying more rapidly due to disappearing laser excitation. Around $2000a_0$, J_g (as well as $J_g + J_e$) reaches a plateau, with Rabi oscillations in antiphase in J_e and J_g . It turns out that in all our $l = 0$ calculations the passage through the avoided crossing leads to negligible reflection of waves back to large R . This applies even to the lowest collision energies considered. This is in agreement with Ovchinnikova's analytical results [8] for rectilinear crossing potentials, which can be readily extended to the present calculations including spontaneous emission, as we will show elsewhere. It also turns out that the Rabi oscillations do not appear in the sum $J_g + J_e$, in agreement with classical expectations. The decrease of $J_g + J_e$ right of the plateau is due to the loss of probability flux from the considered manifold by spontaneous emission. In principle, one would have to go to the next lower manifold in order to follow the recycling of this incoherent part of the scattering state.

It turns out that the oscillating J_e pattern is in its totality rather accurately proportional to Ω_r^2 , within wide intensity limits to be given below, provided the solution is normalized to a prescribed value for the total atom flux $J_g + J_e$ in the region left of R_C where this sum has reached a constant plateau. Figure 9.3 shows the J_e pattern for $\Omega_r = 0.4 \Gamma$, i.e., for one-fourth of the original intensity. Clearly, apart from a nonlinear interval around R_C , the J_e pattern is simply shifted along the logarithmic axis relative to that in Fig. 9.2.

The linear intensity dependence can be explained in the same way that the absence of

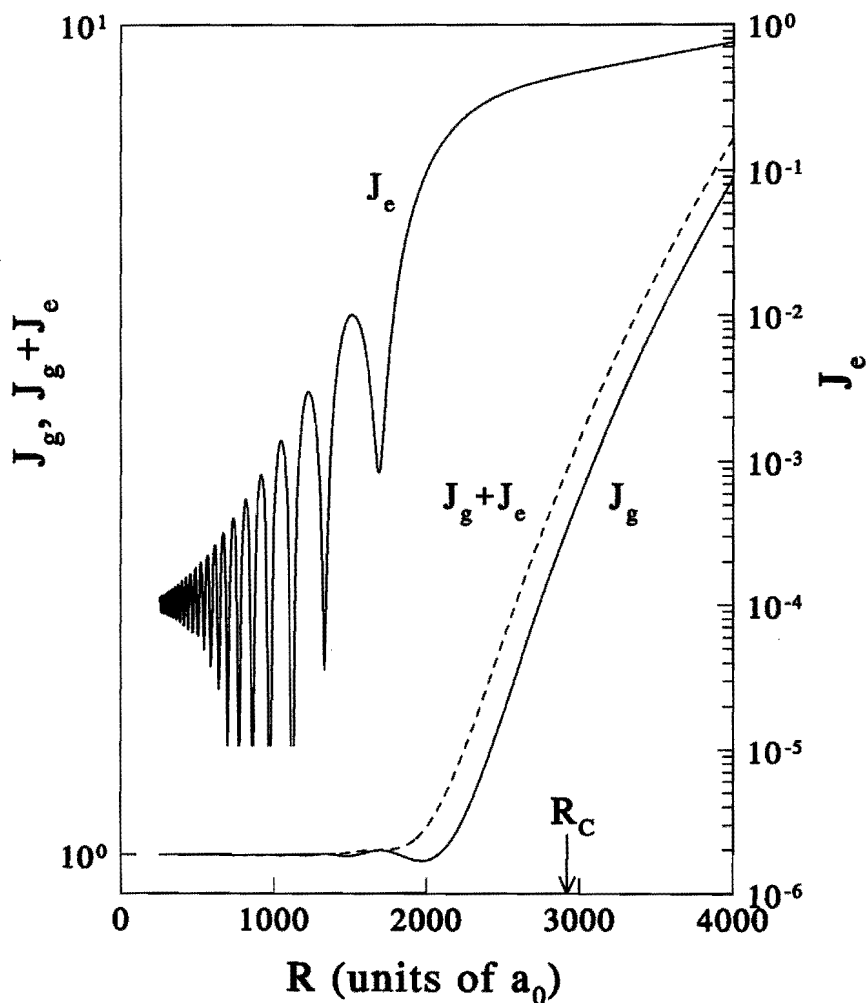


Figure 9.2: Probability fluxes J_g , $J_g + J_e$ (left scale), and J_e (right scale) in uncoupled basis as a function of internuclear distance, following from coupled-channel calculations for $E = 1$ mK, $\Delta = -\Gamma$, and $\Omega_r = 0.8 \Gamma$.

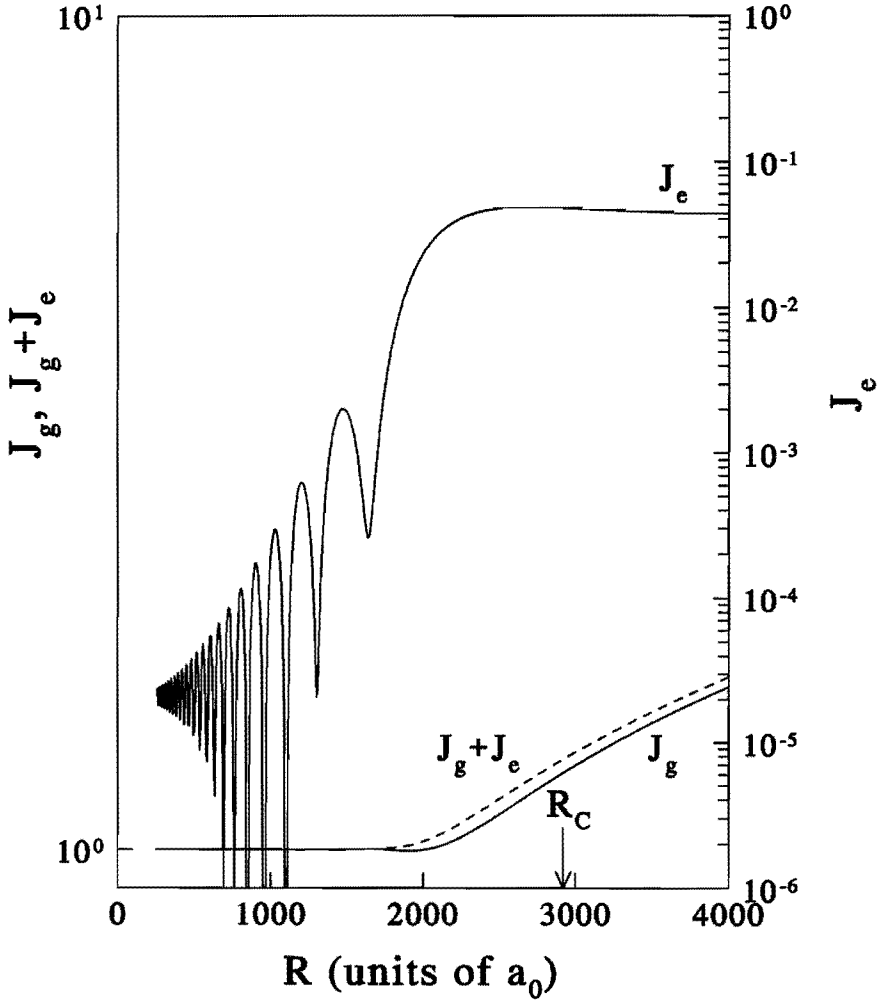


Figure 9.3: Fluxes J_g , $J_g + J_e$ (left scale), and J_e (right scale) in uncoupled basis, following from coupled-channel calculations for $E = 1$ mK, $\Delta = -\Gamma$, and $\Omega_r = 0.4 \Gamma$.

saturation in the experimental Cs loss rate of Ref. [7] is explained in Ref. [1]: in the plateau region most of the excited-state amplitude is due to off-resonant excitation occurring well inside R_C , as this process is favored by improved survival. The flux lost previously to the lower manifold by spontaneous emission is recycled according to the same off-resonant excitation probability. In this respect it is of importance that the atomic velocity increase after the first excitation-spontaneous-emission cycle is still rather low. The new J_g , J_e combination on the next lower manifold is therefore expected to be proportional to that of the original manifold and can consequently be considered to be part of the same total pure state, for which J_g and J_e behave in the plateau region as given in Fig. 9.2.

On the basis of this near linearity it is the ratio J_e/Ω_r^2 that in the limit $\Omega_r \rightarrow 0$ is relevant for the comparison with experiment. Then normalization with respect to the plateau value of $J_g + J_e$ is completely equivalent to normalization relative to the incident value of $J_g + J_e$, since the sum does not change near R_C in this limit. Figure 9.4 shows the functions J_e/Ω_r^2 , J_g , and $J_g + J_e$ in the zero-intensity limit for $\Delta = -\Gamma$ and $E = 1$ mK. We now see a maximum of the excited-state flux near R_C . To illustrate the accuracy of the theoretical linear intensity dependence of our J_e we give in Fig. 9.5 the value of J_e at $R = 10a_0$ as a function of $(\Omega_r/\Gamma)^2$ for $E = 1$ mK and $\Delta = -\Gamma$. Clearly, the linear dependence is very accurate until $\Omega_r/\Gamma = 0.6$.

It turns out that the period of the Rabi oscillations in Figs. 9.2 and 9.3 agrees rather precisely with the local precession frequency $\Omega_{eff}(R) = \sqrt{\Delta^2(R) + \Omega_r^2}$ if one assumes the effective velocity to be the average $\{v_g + v_e(R)\}/2$ of the velocities on the g and e potentials. Another interesting feature can also be seen, for instance, in Fig. 9.2. The oscillation is seen to be sharper at the bottom than at the top. This can be explained classically in terms of the fact that part of the population oscillates between the g and e states. The instantaneous velocity therefore oscillates between the values v_g and v_e of the local velocities.

Similar properties are obtained at lower energies. In Fig. 9.6 we show as an example the radial fluxes for $E = 10$ μ K and $\Delta = -\Gamma$. In general, for the same detuning and intensity the main J_e/Ω_r^2 maximum increases with decreasing energies, corresponding to the slower motion of the atoms through the resonance region, with the associated more effective excitation. Other features seen for lower energies are a smaller amplitude of the Rabi oscillations, arising from a better adiabatic following of the polarization vector. The much stronger damping of J_e left of R_C is discussed below.

In Fig. 9.5 we have also presented the intensity dependence of J_e at $R = 10a_0$ for $E = 300$ μ K and $E = 10$ μ K. We notice that the linearity of J_e persists to lower maximum intensities for decreasing energies, again corresponding to more effective laser excitation.

The J_e pattern in the foregoing Figs. 9.2 and 9.3 can be understood more in detail in terms of the interference of two radial waves in the complex dressed-state basis $|1(N)\rangle$ and $|2(N)\rangle$. For an intuitive picture of these radial waves it is useful to calculate the radial fluxes in this (nonorthogonal) basis. Figure 9.7 shows $J_{1(N)}$ and $J_{2(N)}$ as functions of R for $E = 1$ mK, $\Delta = -\Gamma$, and $\Omega_r = 0.4\Gamma$. The flux $J_{1(N)}$ starts from zero right of R_C , in agreement with the

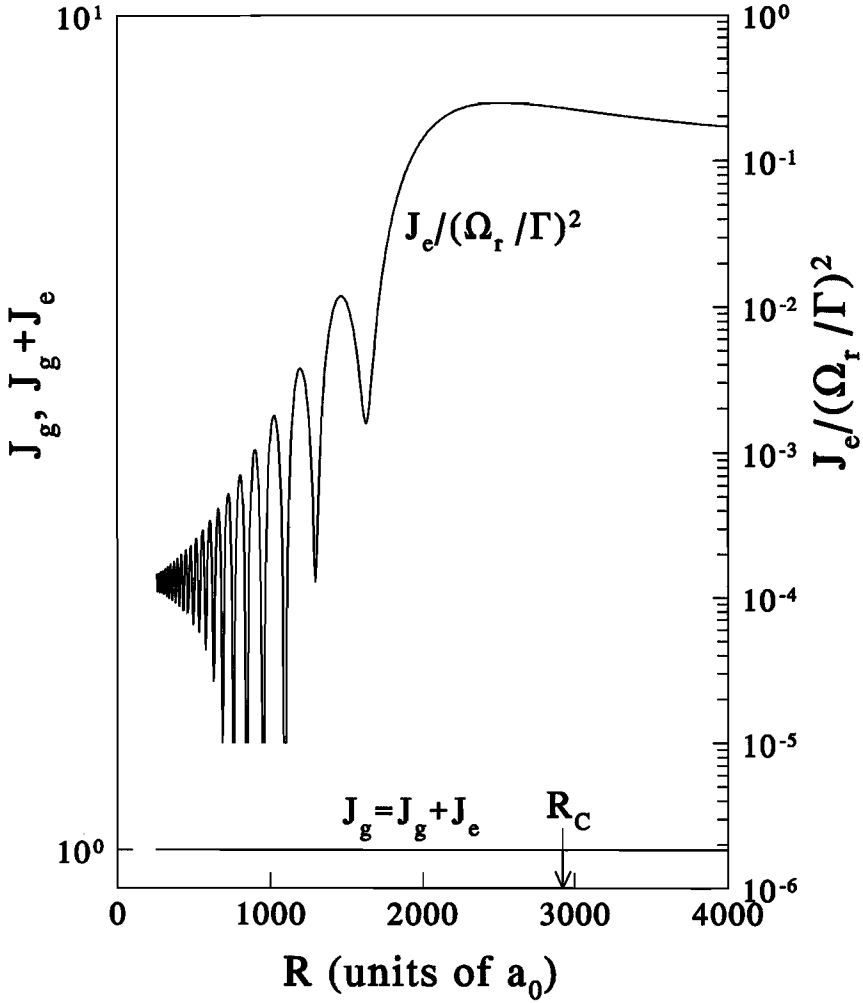


Figure 9.4: Fluxes J_g , $J_g + J_e$, and $J_e / (\Omega_r / \Gamma)^2$ in the zero-intensity limit for $E = 1$ mK and $\Delta = -\Gamma$.

boundary conditions in Fig. 9.1. Near R_C , $J_{1(N)}$ increases strongly and reaches a maximum

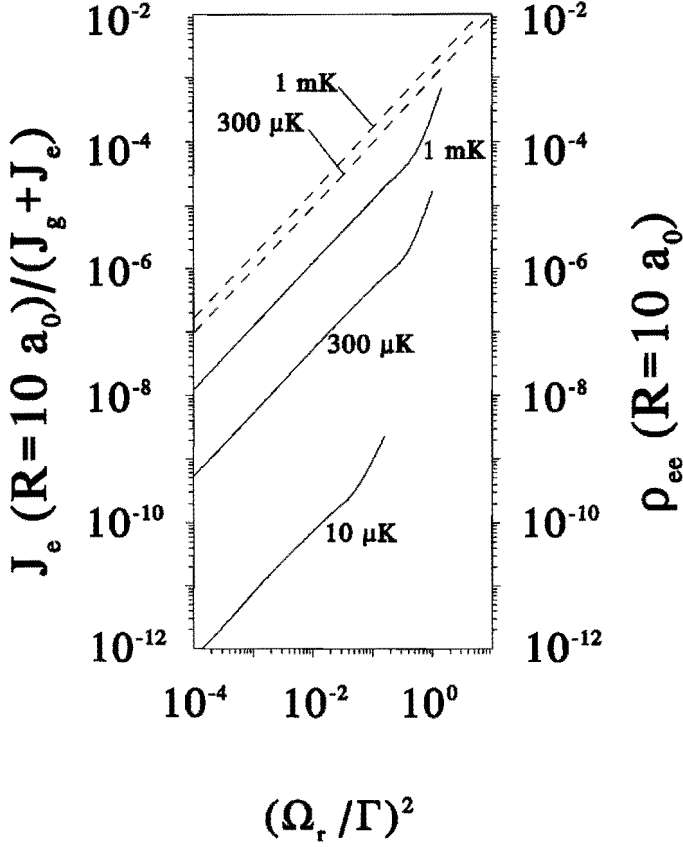


Figure 9.5: Normalized flux J_e (solid lines) and ρ_{ee} (dashed lines), obtained with OBE, at $R = 10a_0$ as a function of $(\Omega_r/\Gamma)^2$ for some selected energies and $\Delta = -\Gamma$, illustrating near-linear intensity dependence.

$600a_0$ left of R_C . For all interatomic distances, however, $J_{1(N)}$ is much smaller than $J_{2(N)}$. Although $J_{1(N)}$ still shows some remnants of a Rabi-type oscillation it is much smoother than J_e . A similar remark applies to $J_{2(N)}$ compared to J_g . This already illustrates that the complex dressed states are a suitable basis to obtain radial waves with as regular behavior as possible. It is also confirmed by the behavior which develops starting at the plateau region towards smaller distances: the $1(N)$ and $2(N)$ components of the coupled channel solution turn out to be uncoupled exponentially damped waves converging to $R = 0$, with regularly changing complex wave numbers. A simple calculation based on such locally exponential

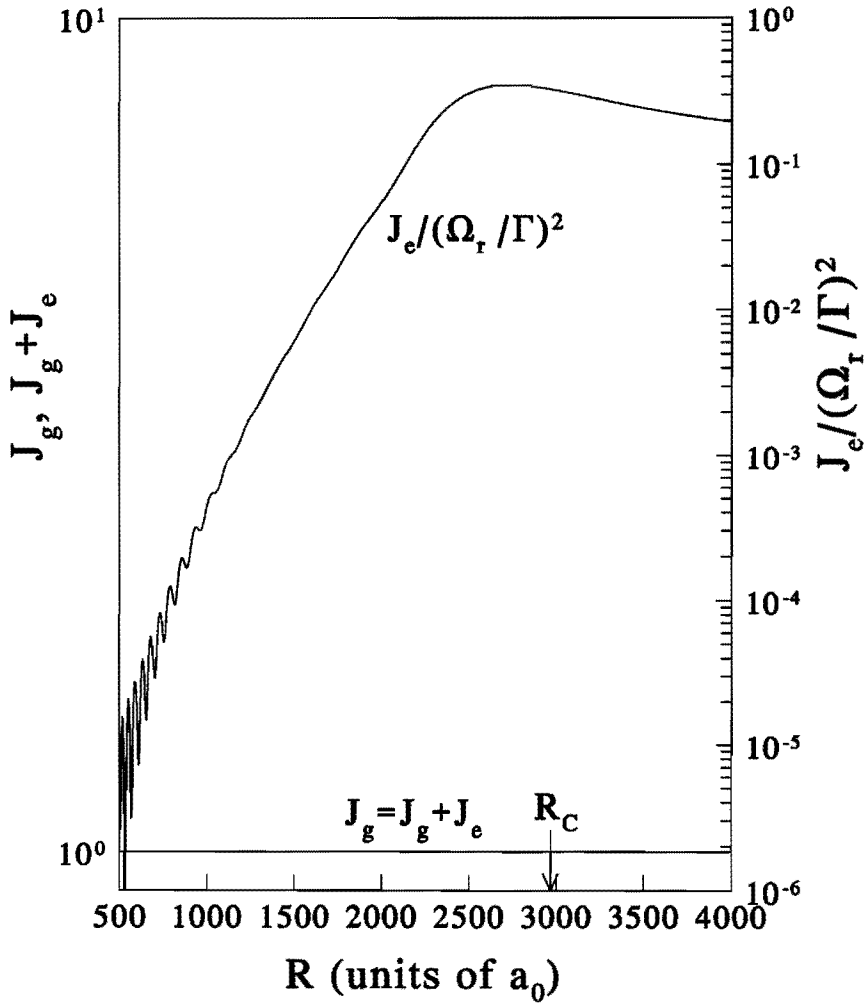


Figure 9.6: Fluxes J_g , $J_g + J_e$, and $J_e / (\Omega_r / \Gamma)^2$ in the zero-intensity limit for $E = 10 \mu\text{K}$ and $\Delta = -\Gamma$.

waves shows that the amplitude of the strongly oscillating J_e pattern is roughly equal to $[J_{1(N)}J_{2(N)}]^{1/2}(\hbar\Omega_r/2)(\hbar\Delta)^{-3/4}E^{-1/4}(R/R_C)^{9/4}$. On the other hand, we find the oscillations to take place around an average value equal to $\cos^2(\theta) J_{1(N)} + \sin^2(\theta) J_{2(N)}$, which tends to $J_{1(N)}$ near $R = 10a_0$. Both predictions are confirmed by the actual J_e patterns.

We thus find that $J_{1(N)}$ is the physically interesting quantity for the fine-structure changing loss rate, since it is equal to the flux J_e of excited atoms at the corresponding avoided crossing near $10a_0$. The $J_{2(N)}$ flux determines the radiative escape loss, because its contribution to J_e dominates in the wider range of interatomic distances where radiative escape is most probable as the final fate of the atoms.

For the physical interpretation of our coupled-channel solutions it is of importance to compare $J_{1(N)}$ and $J_{2(N)}$ with uncoupled adiabatic solutions $J_{1(N)}^0$ and $J_{2(N)}^0$. This will make clear to which radial region the nonadiabatic excitation is confined. Figure 9.8 shows $J_{1(N)}/J_{1(N)}^0$ and $J_{2(N)}/J_{2(N)}^0$ for $E = 10 \mu\text{K}$, $\Delta = -\Gamma$, and $\Omega_r = 0.2 \Gamma$. The uncoupled fluxes are normalized in such a way that the two ratios tend to 1 for $R \rightarrow 0$. Clearly, most of the excitation of $J_{1(N)}$ occurs left of R_C due to the finite radial velocity. For the same reason the ratio $J_{2(N)}/J_{2(N)}^0$ grows for decreasing R : the $2(N)$ dressed state is depleted more slowly than for zero velocity.

At this point we make a comparison with treatments based on the optical-Bloch-equation (OBE) method [4]. In Fig. 9.5 we compare our J_e flux at $R = 10a_0$ for $\Delta = -\Gamma$, normalized as above, to the OBE value of the excited-state population ρ_{ee} at the same radius. For higher energies, not shown in the figure, where the radial motion can be treated classically, these quantities are equal. For the 1-mK and 300- μK OBE calculations we used the “energy conserving” trajectory choice [5]. For lower collision energies, below E_{th} , we adopted the “switched” and “asymptotic” trajectory choices, which lead to almost identical results (within 15 %). We find a suppression of the excited-state occupation probability, due to the quantum-mechanical nature of the radial motion, by about one order of magnitude already at 1 mK and increasing strongly with decreasing energy, roughly proportional to E^{-2} .

The origin of this tremendous suppression is the destructive interference of the radial waves on the excited potential, arising from excitation at the various radii left of R_C . Adding these wavelets as they arrive for instance at $10a_0$, their phase difference is larger for lower collision energies: the velocity increase along the excited-state potential during the passage through the excitation region becomes more and more important compared to the initial velocity. This destructive interference is fully taken into account in our approach and is left out in a classical treatment of radial motion. Apparently, it is a dominating quantum effect at low collision energies. The experimental relevance is associated with a strongly reduced atom loss in the unsaturated regime, both for the fine-structure and radiative-escape loss mechanisms.

All previous results were restricted to $l = 0$. In order to get an impression of the influence of centrifugal effects, we concentrate on a single l value equal to $kR_C/2$, with k the asymptotic wave number, and solve the coupled equations. Far left of R_C we include the

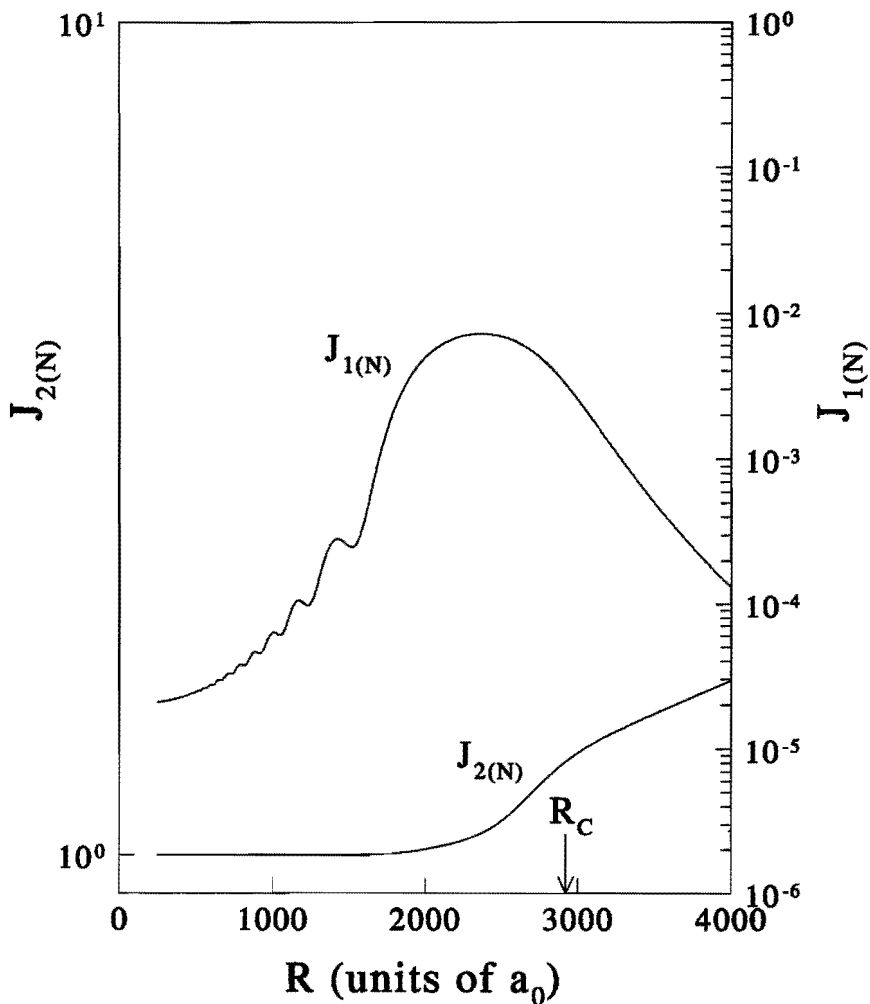


Figure 9.7: Dressed-state fluxes $J_{2(N)}$ (left scale) and $J_{1(N)}$ (right scale) in coupled basis for $E = 1$ mK, $\Delta = -\Gamma$, and $\Omega_r = 0.4 \Gamma$.

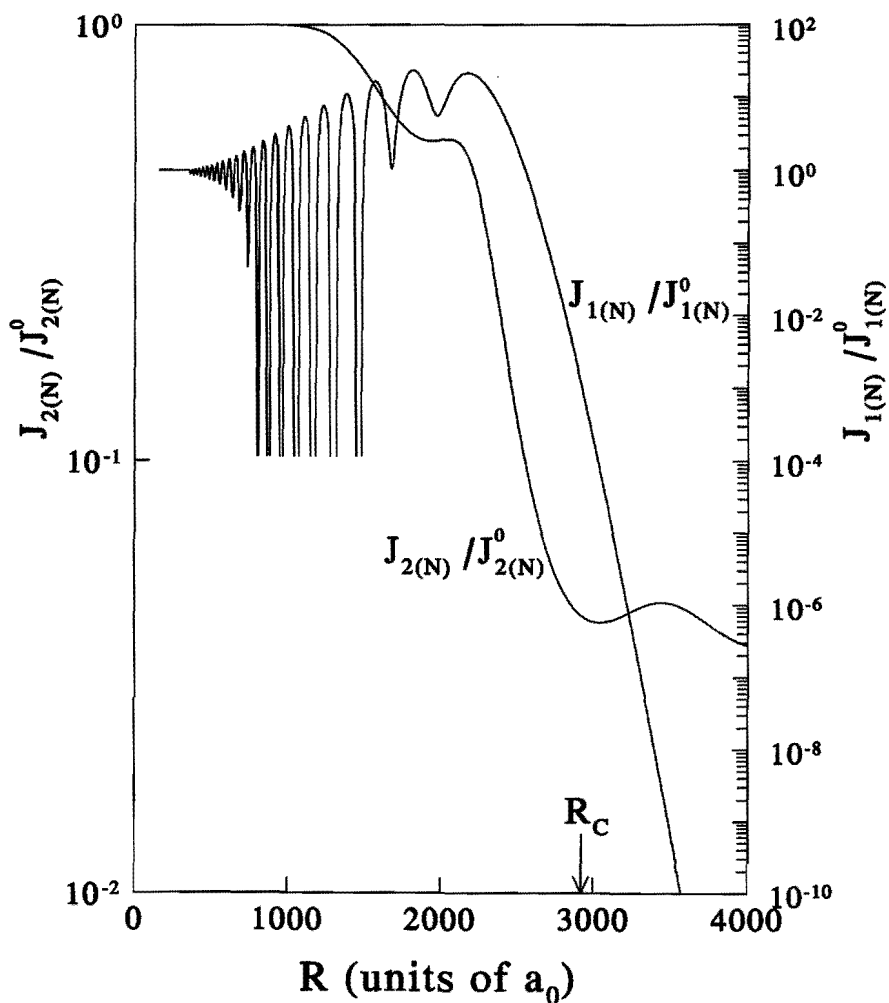


Figure 9.8: Ratios $J_{1(N)}/J_{1(N)}^0$ (left scale) and $J_{2(N)}/J_{2(N)}^0$ (right scale) of fluxes in dressed-state basis and adiabatic fluxes as a function of R for $E = 10 \mu\text{K}$, $\Delta = -\Gamma$, and $\Omega_r = 0.2 \Gamma$.

reflection from the centrifugal barrier in the $2(N)$ channel and normalize with respect to the

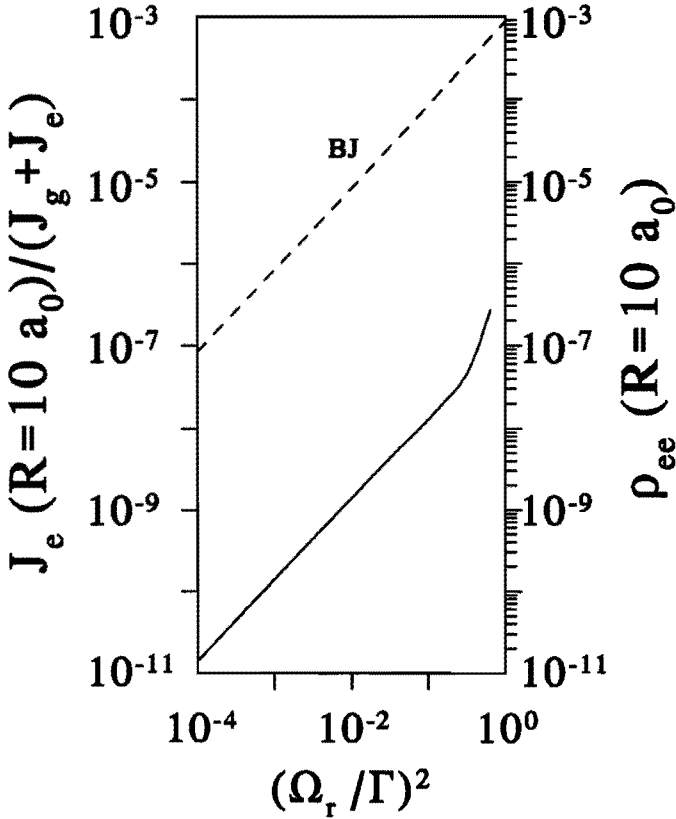


Figure 9.9: Normalized flux J_e (solid line) and ρ_{ee} (dashed line), obtained with OBE, at $R = 10a_0$ as a function of $(\Omega_r/\Gamma)^2$ for $E = 300 \mu\text{K}$, $\Delta = -\Gamma$, and $l = 30$.

flux of the left-going wave.

Again we find a linear intensity dependence of the J_e pattern. This is illustrated in Fig. 9.9, where we present the probability flux J_e at $R = 10a_0$ as a function of $(\Omega_r/\Gamma)^2$ for $E = 300 \mu\text{K}$, $\Delta = -\Gamma$, and $l = 30$. We see a linear behavior up to $\Omega_r/\Gamma = 0.6$ in agreement with the previously mentioned off-resonant excitation. Comparing J_e in Fig. 9.9 with J_e in Fig. 9.5 for $l = 0$, we note that the survival rate is about one order of magnitude lower at $l = kR_C/2$. Again, we compare also with the OBE survival. Apparently, the quantum suppression is now even larger than for $l = 0$. This may be ascribed to the lower local radial velocity v_j , taking into account the centrifugal barrier, which leads to an increased

destructive interference.

Our calculations thus show that higher l and lower E survival rates are strongly suppressed relative to OBE values. It should be noted that in our coupled-channel calculations the unsaturated domain is restricted to much lower intensities than suggested for instance by the Rb experiments in Refs. [7,9]. This is probably due to the fact that the inclusion of nuclear spin leads to a considerable reduction of Rabi frequencies Ω_r , the total optical dipole strength being distributed over the individual anticrossings with the various $^2P_{3/2} + S$ hyperfine states. We are developing the computational scheme for the inclusion of hyperfine structure both in the $S + S$ and the $^2P_{3/2} + S$ channels, needed for the description of such optical collisions.

References

- [1] P.S. Julienne, A.M. Smith, and K. Burnett, in *Advances in Atomic, Molecular and Optical Physics*, edited by D.R. Bates and B. Bederson (Academic, San Diego, CA, 1992), p. 141.
- [2] A. Gallagher and D.E. Pritchard, *Phys. Rev. Lett.* **63**, 957 (1989).
- [3] P.S. Julienne and J. Vigué, *Phys. Rev. A* **44**, 4464 (1991).
- [4] Y.B. Band and P.S. Julienne, *Phys. Rev. A* **46**, 330 (1992).
- [5] A.M. Smith, K. Burnett, and P.S. Julienne, *Phys. Rev. A* **46**, 4091 (1992).
- [6] C. Cohen-Tannoudji, J. Dupont-Roc, and G. Grynberg, *Atom-Photon Interactions* (Wiley, New York, 1992).
- [7] D. Sesko, T. Walker, C. Monroe, A. Gallagher, and C. Wieman, *Phys. Rev. Lett.* **63**, 961 (1989).
- [8] M. Ya. Ovchinnikova, *Opt. Spektrosk.* **17**, 821 (1964) [*Opt. Spectrosc. (USSR)* **17**, 447 (1964)].
- [9] P. Feng, D. Hoffmann, and T. Walker, *Phys. Rev. A* **47**, R3495 (1993).

Chapter 10

Simple quantum-mechanical picture of cold optical collisions

H.M.J.M. Boesten and B.J. Verhaar

Published in Physical Review A **49**, 4240 (1994)

Abstract

We present a quantum-mechanical study of the dynamics of collisions of cold atoms in a (magneto-) optical trap valid in the linear intensity regime. We find further evidence for a discrepancy with results of the semiclassical optical-Bloch-equation method at lower collision energies and detunings, referred to as "quantum suppression" in previous work. We find a strong dependence on the detuning: for the lowest energies considered the suppression factor ranges from more than three orders of magnitude for $\Delta = -\Gamma_{a1}$ to a factor 2 at $\Delta = -10\Gamma_{a1}$. The fraction of atoms surviving at small interatomic distances for a single l value can in good approximation be described by a simple formula in the form of a product of a Landau-Zener excitation function and a WKB survival factor. Summed over partial waves this formula allows a relatively easy calculation of loss rates in a two-channel linear-intensity description. The role of such an approach in a future more complete treatment including hyperfine channels is pointed out.

Cold-atom collisions have become an intensively studied research subject since the advent of laser cooling techniques applicable to alkali-metal atoms. This development was preceded by studies of both two- and three-dimensional cold collisions of spin-polarized hydrogen atoms, cooled cryogenically by contact with superfluid helium. A number of fascinating phenomena have been observed in these studies, which are caused by the remarkable properties of collisions between ground-state atoms in the quantum regime where the atomic de Broglie wavelength extends beyond the range of the interatomic potential. In this paper we will deal exclusively with another type of cold collisions, sometimes referred to as "optical collisions", which play an important role in optical traps. In such collisions one of the two collision partners is optically excited near the distance of approach where the laser frequency is resonant with the energy separation of a pair of optically coupled internal two-body states.

A general description of this type of collision poses special problems because of the role of both laser field and spontaneous emission during the collision process.

Gallagher and Pritchard (GP) [1] presented a quasistatic theory and identified two types of mechanisms contributing to loss of atoms from an optical trap. To go beyond the quasistatic description of the laser excitation, Band and Julienne proposed an optical-Bloch-equation (OBE) theory [2]. Both of these approaches are based on a classical treatment of the orbital motion of the colliding atoms. Recently, to explore the bounds of validity of such a description, a quantum-mechanical (QM) two-channel model [3] was investigated for the special but experimentally interesting case where the losses are linear in the laser intensity I . A central result of this study was a “quantum suppression” of loss rates, most prominent at lower collision energies, of QM relative to OBE values.

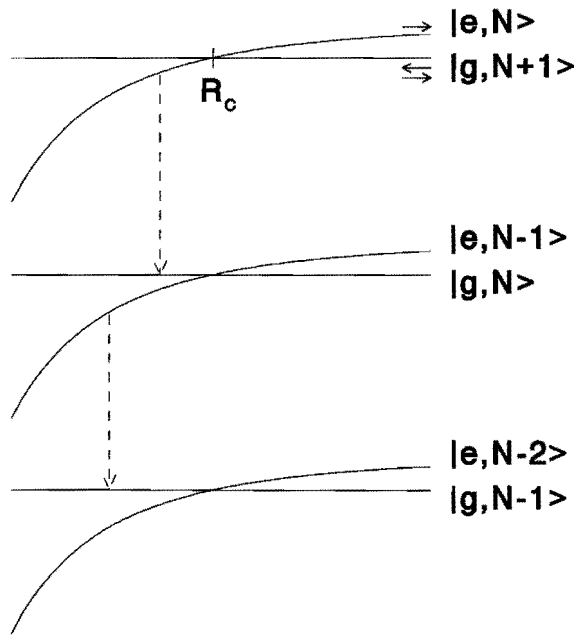


Figure 10.1: Dressed-state manifolds and decay by spontaneous emission.

The basic reason why our method is restricted to first-order I effects is explained in Fig. 10.1, showing a few of the dressed-states manifolds $\{|e, N\rangle, |g, N+1\rangle\}$, $\{|e, N-1\rangle, |g, N\rangle\}$, \dots in which g and e stand for the two-atom ground state and optically excited state, while N is the number of laser photons in the mode considered. We include the coupling of the diabatic states within each of the manifolds by the laser field, as well as the spontaneous decay to the next lower manifold indicated in the figure. The latter can be shown [4] to give rise to an absorptive term equal to $-i\Gamma$ in the e channel which does

not destroy the coherence of the coupled-channel state. The flux of ground-state atoms in the next lower manifold, however, which again undergoes laser excitation, would represent a new, incoherent, contribution to the total state and is omitted since the coupled-channel theory deals with a single coherent state. The OBE theory is more complete in that it does take such (at least second-order I) “recycling” contributions into account, but at the expense of a classical description of the translational motion. For details of our model we refer to Ref. [3]. To be specific we again restrict our calculations to the case of cesium atoms and consider the pair of $g = 0_g^+$ and $e = 0_u^+$ molecular states with $\Gamma = \Gamma_{mol}/2 = (2/3) \Gamma_{at}$.

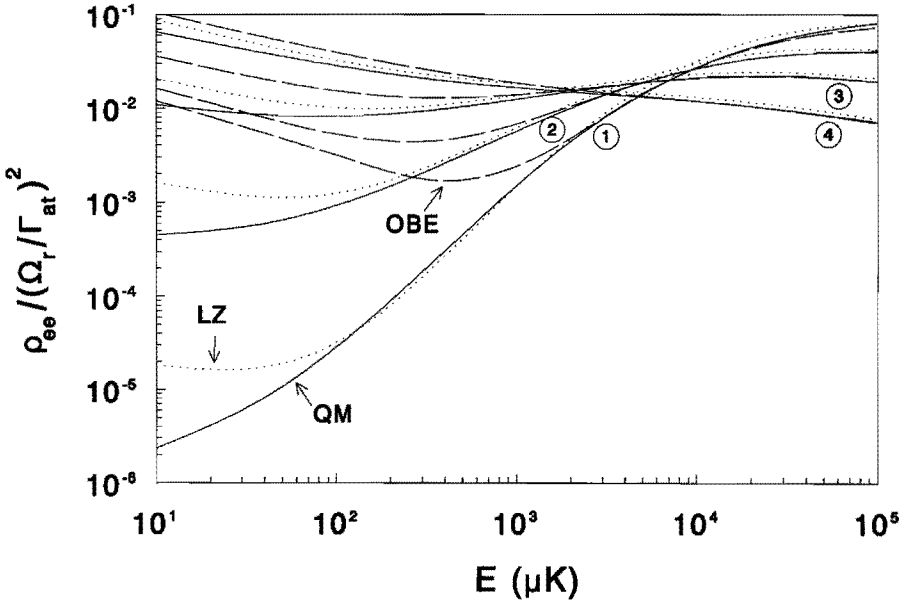


Figure 10.2: Excited-state fraction of atoms at $R = 10 a_0$ as a function of collision energy for $l = 0$ and (1) $\Delta = -\Gamma_{at}$, (2) $\Delta = -2\Gamma_{at}$, (3) $\Delta = -4\Gamma_{at}$, (4) $\Delta = -10\Gamma_{at}$. Solid lines: QM. Dotted lines: LZ. Dashed lines: OBE.

In this paper we study the detuning and partial-wave dependence of the quantum suppression. The important quantity for loss processes is the fraction $\rho_{ee} = J_e/(J_g + J_e)$ of atoms in the excited channel at interatomic distance R , where J_e (J_g) is the radial probability flux in the excited (ground-state) channel. To eliminate the intensity dependence we consider the value of $\rho_{ee}/(\Omega_r/\Gamma_{at})^2$ in the limit of zero intensity. Fig. 10.2 shows this quantity for s -wave scattering at $R = 10 a_0$ as a function of collision energy for four values of the detuning (QM curves). We also show the corresponding OBE predictions. The OBE description contains an ambiguity as to the choice of the relative atomic velocity on the excited-state potential.

For collision energies $E > \hbar|\Delta|$, the excited-state population ρ_{ee} is insensitive to the specific choice. For lower energies the dependence on the trajectory is considerable. Smith, Burnett, and Julienne [5] showed by an analytical treatment of quantum-mechanical equations using the stationary-phase approximation that the energy-conserving excited-state trajectory is to be preferred in general. However, this energy-conserving trajectory choice is not applicable for $E < \hbar|\Delta|$. We used the “switched trajectory” choice because it is applicable for all collision energies and gives better results at low E . Note that the quantum suppression relative to the OBE increases rapidly with decreasing detuning. This is connected with the role of the radial phase in a quantum-mechanical description. For low Δ the width $\hbar\Gamma/(V'_{ee} - V'_{gg})$ of the excitation region, where $V'_{ee} - V'_{gg}$ is the difference in slope of the e and g potentials, is so large that it contains a large number of wavelengths in the excited channel, giving rise to destructive interference for low energies. The Landau-Zener approach includes this interference. Since the amplitude of the radial wave excited locally in the upper channel is proportional to the product of decoupled g and e radial waves, the destructive interference disappears for the higher energies.

In Fig. 10.2 we also give the results for a simple Landau-Zener approximation to our QM results (LZ). Except for some discrepancy at low E we find ρ_{ee} to be rather accurately described by the product of an excitation and a survival factor,

$$\rho_{ee}(R) = T(E, l = 0)S(E, l = 0, R). \quad (10.1)$$

The excitation function T is the Landau-Zener formula [6] for the transition probability in a crossing of two linear potential curves,

$$T(E) = 1 - \exp(-v_{ref}/v_0) \approx \frac{\pi\hbar\Omega_r^2 R_C^4}{6C_3 v_0}. \quad (10.2)$$

Here v_l is the radial velocity at the crossing for partial wave l , equal to the collision velocity for $l = 0$, and v_{ref} is the reference velocity defined by $v_{ref} = 2\pi V_{eg}^2/(\hbar|V'_{ee} - V'_{gg}|)$ with $V_{eg} = \hbar\Omega_r/2$. In Eq. (10.2) we have used that $v_{ref} \ll v_0$ for the relevant experimental circumstances.

The survival function S for reaching R from R_C is the WKB expression

$$S(E, R) = \exp \left[-2 \int_R^{R_C} \text{Im} \kappa(R') dR' \right], \quad (10.3)$$

with $\kappa(R')$ the local complex wave number [3]. The above-mentioned discrepancy at low E is due to the curvature of the $-C_3/R^3$ potential which is not included in the LZ formula. Band and Julienne [2] give an analogous single-pass LZ expression valid for the weak-coupling, high detuning ($\Delta \gg \Gamma$) limit and notice that it is in agreement with both GP and OBE results. In the present paper we compare it in addition to a full quantum-mechanical calculation and find also agreement in the $\Delta = O(\Gamma)$ regime where the earlier approaches fail. Furthermore, we also consider the nonvanishing partial waves.

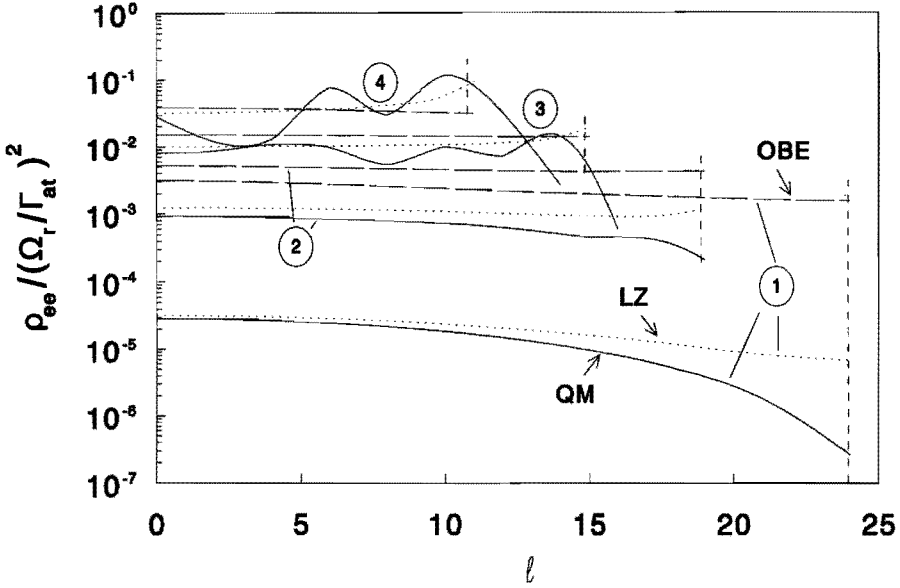


Figure 10.3: Excited-state fraction of atoms at $R = 10 a_0$ as a function of l for $E = 100 \mu\text{K}$ and detunings as in Fig. 10.2. Solid lines: QM. Dotted lines: LZ. Dashed lines: OBE. Vertical dashed lines indicate l_{max} for which the outer turning point of the ground-state channel equals R_C .

Since most of the trap loss comes from $l \neq 0$ partial waves, we now proceed with the influence of the centrifugal barrier on the collision. In Fig. 10.3 we present QM and OBE values of ρ_{ee} at $R = 10 a_0$ as a function of l for $E = 100 \mu\text{K}$ and the same four detunings as in Fig. 10.2. Vertical lines indicate the value l_{max} for which the outer turning point of the ground-state channel is equal to R_C . We see oscillations in the QM curves for the higher detunings, due to nodes and antinodes in the ground-state wave function leading to an oscillating Frank-Condon factor at R_C . These oscillations are related to similar oscillations as a function of laser frequency in the analogous process of photoassociation described by Thorsheim *et al.* [7] which have recently been observed experimentally [8]. Their disappearance for low detunings is probably due to the broadening of the Frank-Condon enhancement region. The Frank-Condon oscillations exhibited by our fully quantum-mechanical calculations are absent both in the OBE and the LZ curves. Apart from this and some discrepancy at the high l values, we again see good agreement with our simple LZ formula for $l \neq 0$ while the OBE results deviate by one to two orders of magnitude for small detunings. Experimentally measured loss rates contain a summation over angular momentum. Replacing the partial-

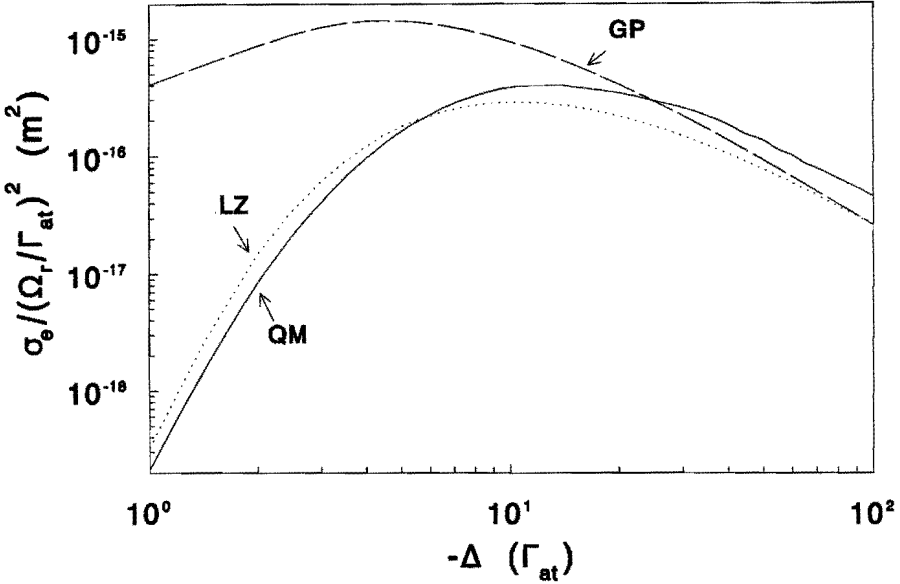


Figure 10.4: Cross section for excited-state survival at $R = 10 a_0$, divided by $(\Omega_r/\Gamma_{at})^2$, as a function of detuning for $E = 100 \mu\text{K}$. Solid line: QM. Dotted line: LZ. Dashed line: GP.

wave sum by an integral, the effective cross section for reaching the interatomic distance R in the excited channel reduces to

$$\begin{aligned} \sigma_e(R) &= \frac{\pi}{k^2} \int_0^{l_{\max}} dl (2l+1) T(E, l) S(E, l, R) \\ &= \frac{\pi}{k^2} \int_0^{l_{\max}} dl (2l+1) \frac{\pi \hbar \Omega_r^2 R_C^4}{6C_3 v_l} S(E, l, R), \end{aligned} \quad (10.4)$$

with k the asymptotic wave number. In Fig. 10.4 we present this expression, divided by $(\Omega_r/\Gamma_{at})^2$, for $R = 10 a_0$ and $E = 100 \mu\text{K}$ as a function of detuning, together with the coupled-channel QM curves and the prediction of the GP model. Note the maximum at $\Delta \approx -10\Gamma_{at}$ which comes from the competition between excitation and survival, i.e., the decrease of the survival factor at lower detunings (see Fig. 10.2) and the decrease of the excitation probability at high detunings leading to a Δ^{-2} behavior. Figure 10.4 shows good agreement of the LZ formula with the QM results. This agreement is enhanced by the disappearance of the Frank-Condon oscillations in the l summation. The GP result also shows good agreement for the higher detunings, where the excitation is more localized near R_C . In this frequency regime the GP model has been shown to be in excellent agreement

with experiment [9]. In Fig. 10.4 we have continued the GP curve into the low Δ region, although it has not been claimed to be valid there in Ref. [1].

Expression (10.4) is a central result of the present paper. It allows the calculation of fine-structure and radiative-escape loss processes. Despite its simplicity it describes the quantum-mechanical flux in the excited channel to much lower energies and detunings than both the OBE and GP models. The validity of such a simplified approach is of great importance in view of future attempts to describe optical collisions including the effect of hyperfine interactions relevant for smaller detunings [10,11]. If one wants to deal with the complexity of potential curves arising from the hyperfine splitting in both ground and excited states and wants to keep track of the interplay of the various Condon crossings for different hyperfine states at different radii, it is probably inevitable to use a simplified approach. A LZ type of approach may be very helpful in that connection, especially because it allows one to take into account also the phase of the radial channel wave functions in between crossings, contrary to a description based on classical treatments of the translational motion, such as the OBE or GP description.

It is also of importance to repeat that our quantum-mechanical approach, which includes loss of radial flux due to spontaneous emission but omits recycling, is only valid in the regime where losses are (more or less) linear in intensity. One should keep in mind, however, that such a restriction may also be unavoidable in a more complete OBE approach, a treatment to higher order in I implying a too complicated simultaneous coupling of more than one excited electronic state and more than one associated l' value in the excited channel.

References

- [1] A.Gallagher and D.E. Pritchard, *Phys. Rev. Lett.* **63**, 957 (1989).
- [2] Y.B. Band and P.S. Julienne, *Phys. Rev. A* **46**, 330 (1992).
- [3] H.M.J.M. Boesten, B.J. Verhaar, and E. Tiesinga, *Phys. Rev. A* **48**, 1428 (1993).
- [4] R. Dum, P. Zoller and H. Ritsch, *Phys. Rev. A* **45**, 4879 (1992).
- [5] A.M. Smith, K. Burnett, and P.S. Julienne, *Phys. Rev. A* **46**, 4091 (1992).
- [6] E.E. Nikitin and S.Y. Umanskii, *Theory of Slow Atomic Collisions* (Springer-Verlag, New York, 1984).
- [7] H.R. Thorsheim, J. Weiner, and P.S. Julienne, *Phys. Rev. Lett.* **58**, 2420 (1987).
- [8] J.D. Miller, R.A. Cline, and D.J. Heinzen, *Phys. Rev. Lett* **71**, 2204 (1993).
- [9] M.G. Peters, D. Hoffmann, J.D. Tobiasson, and T. Walker, *Phys. Rev. A* **50**, R906 (1994).

- [10] C.D. Wallace, T.P. Dinneen, K-Y. N. Tan, T.T. Grove, and P.L. Gould, *Phys. Rev. Lett.* **69**, 897 (1992).
- [11] P. Feng, D. Hoffmann, and T. Walker, *Phys. Rev. A* **47**, R3495 (1993).

Summary

Rapid developments in the field of cooling and trapping of atomic gasses in free space using laser beams have culminated in the realization of a very precise atomic clock in 1989, based on a fountain of laser cooled cesium atoms, and of Bose-Einstein condensation (BEC), a macroscopic quantum phenomenon, first in a cold ^{87}Rb gas (JILA, Boulder, June 1995) and quickly after that in cold ^7Li (Rice University, Houston, July 1995) and ^{23}Na (MIT, Cambridge, October 1995) gasses. The observations of BEC are an important step towards a more fundamental understanding of superfluidity and superconductivity in strongly interacting systems.

In both applications collisions between particles in the cold gas play a crucial role. It appears that the precision of the cesium atomic clock is limited by a frequency shift caused by collisions, which fundamentally do not disappear if the sample is cooled down further. In the BEC experiments collisions play an important role from several points of view. To start with, the behavior of the condensate can be fully described by one parameter, the scattering length, which is determined by the collisional behavior of the atoms at very low energies. In particular, it appears that the sign of the scattering length determines the (in)stability of a homogeneous condensate. Also, a large scattering length is necessary for efficient evaporative cooling, the final cooling stage in the complete cooling process from room temperature (300 K) down to BEC temperatures (nK- μK). Finally, exothermal inelastic collisions determine the lifetime of the condensate.

In chapter 2 of this thesis the basic principles of the photoassociation process are explained. We have used this process to determine collision properties of cold ^{85}Rb and ^{87}Rb atoms. In chapter 3, we present results as derived from a ^{85}Rb experiment. In this experiment the atoms are doubly spin-polarized, so that they only collide via a triplet potential. Furthermore, the laser can be tuned in such a way that one specific electronic state is excited. The 0_g^- state we used has the great advantage that the complications of the hyperfine "spaghetti" do not play a role: the hyperfine shifts are negligible and the nuclear spins are decoupled to very good approximation. The double spin polarization and the choice of the 0_g^- excited state have made the theoretical analysis of the photoassociation spectra feasible. On the basis of these spectra we concluded that the sign of the scattering length for a ^{85}Rb gas is negative and, using a mass-scaling law, that this sign is positive for a ^{87}Rb gas. A positive sign indicates a stable and a negative sign an instable homogeneous condensate. Shortly after the publication of these results BEC was indeed observed at Boulder.

In chapters 4 and 5 shape resonances in the d -wave scattering of ^{87}Rb atoms and in the g -wave scattering of ^{85}Rb atoms are reported. The observations of these shape resonances enable a very precise determination of the above-mentioned scattering lengths and also an experimental value for the C_6 van der Waals dispersion coefficient. The g -wave shape resonance appears to live so long that it has turned out possible to measure the time dependence of the tunneling process, building up the shape resonance state. Furthermore, the analysis of the g -wave shape resonance has led to an upper limit for the decay rate of a possible decay

mechanism of the condensate, due to the so-called second order spin-orbit interaction, an interaction between the valence electrons of the interacting atoms. Up to now no experimental value was known.

In chapter 6 decay rates of ^{87}Rb and ^{23}Na condensates due to the magnetic dipolar interaction are theoretically determined. In the ^{23}Na BEC experiment the most important limitation of the lifetime of the condensate does not seem to be this mechanism but a 3-body process. According to very recent experimental data the decay rate of the ^{87}Rb condensate agrees roughly with the calculated magnetic dipolar relaxation rate. For completeness we also present the decay rate for a ^{85}Rb gas in this chapter.

Besides the previously mentioned doubly-spin polarized state another hyperfine state exists which is suitable for BEC experiments in a magnetic trap. An interesting aspect of atoms prepared in this state is the possibility of changing the sign of the scattering length by varying the magnetic field if a Feshbach resonance occurs in the collision process. Making use of this, properties of the condensate could be drastically changed by an external “knob”. In chapter 7 an analysis of ^{39}K bound states is presented for which we used a new multichannel inverted perturbation approach. On the basis of this approach we have determined properties of the collision between two ^{39}K and the collision between two ^{41}K atoms in the hyperfine states that are relevant for BEC-experiments. It now appears that, despite the small hyperfine interaction, in a ^{41}K gas of $f = 1, m_f = -1$ atoms a Feshbach resonance occurs at magnetic field strengths for which the atoms can be trapped. This is the first gas for which the occurrence of a Feshbach resonance in the interesting field regime is predicted with large certainty. Also, the probability that the scattering length in a ^{39}K gas changes sign in the interesting field regime is almost 100%.

By illuminating a cloud of cold atoms with a laser, collisions can be influenced drastically. It turns out, for instance, that such “optical” collisions in general take place at much larger interatomic distances (20 to 5000 a_0) than collisions without a laser field (20 to 200 a_0). Furthermore, the collision dynamics is strongly influenced if the time scale of a collision becomes comparable to the spontaneous-emission lifetime of an atom excited by the laser during the collision. These collisions play a role in (magneto-)optical traps because they induce exothermal transitions between trapped and untrapped states and thus give rise to heating and particle loss from the trapped atom cloud. In chapter 8 an introduction to these optical collisions is given and the quantum-mechanical optical-Bloch equations are derived.

In chapter 9 we present the first fully quantum-mechanical study of optical collisions. In these calculations we restrict ourselves to loss rates in first order in the laser intensity. This is justified by experimental evidence that the loss rates vary linearly with laser intensity over a large intensity range. Our fully quantum-mechanical calculations show that the loss rates at low temperatures are suppressed relative to loss rates that were calculated previously along semi-classical lines. This low-temperature suppression has also experimentally been observed. In the final chapter a simple analytical model is presented to describe optical collisions. This model reproduces the quantum-mechanical decay rates very well and offers

the great advantage of a transparent and explicit interpretation of cold optical collisions.

Samenvatting

Snelle ontwikkelingen op het gebied van het koelen en ruimtelijk opsluiten van atomaire gassen met behulp van laserbundels hebben geculmineerd in de realisatie van een zeer nauwkeurige atoomklok in 1989, gebaseerd op een fontein van lasergekoelde cesium atomen, en van Bose-Einstein condensatie (BEC), een macroscopisch quantumverschijnsel, eerst in een koud ^{87}Rb gas (JILA, Boulder, juni 1995) en snel daarna in koude ^7Li (Rice University, Houston, juli 1995) en ^{23}Na (MIT, Cambridge, oktober 1995) gassen. De waarnemingen van BEC zijn een belangrijke stap naar een meer fundamenteel begrip van superfluiditeit en supergeleiding in sterk wisselwerkende systemen.

In beide toepassingen spelen botsingen tussen deeltjes in het koude gas een cruciale rol. Zo blijkt dat de nauwkeurigheid van de cesium atoomklok beperkt wordt door een frequentieverschuiving, veroorzaakt door botsingen, die principieel niet verdwijnt bij verder afkoelen. In de BEC experimenten spelen botsingen in diverse opzichten een belangrijke rol. Om te beginnen kan het gedrag van het condensaat volledig beschreven worden door een parameter, de verstrooiingslengte, die bepaald wordt door het botsingsgedrag van de atomen bij zeer lage energieën. Zo blijkt het teken van de verstrooiingslengte de (in)stabiliteit van een homogeen condensaat te bepalen. Ook is een grote verstrooiingslengte noodzakelijk voor efficiënte afdampkoeling, de laatste koelingsfase in het gehele koelingsproces van kamertemperatuur (300 K) naar BEC-temperaturen (orde nK- μK). Tenslotte bepalen exotherme inelastische botsingen de levensduur van het condensaat.

In hoofdstuk 2 van dit proefschrift worden de basisprincipes van het photoassociatieproces uitgelegd. Dit proces hebben wij gebruikt om botsingseigenschappen van koude ^{85}Rb en ^{87}Rb atomen te bepalen. In hoofdstuk 3 worden de resultaten gepresenteerd, afgeleid uit een ^{85}Rb photoassociatie experiment. In dit experiment zijn de atomen dubbel spin gepolariseerd, zodat ze alleen kunnen botsen via een triplet potentiaal. Verder kan de laser zodanig afgestemd worden dat een specifieke elektronentoestand wordt aangeslagen. De 0_g^- toestand die we gebruikten heeft het grote voordeel dat de complicaties van de hyperfijn "spaghetti" geen rol spelen: de hyperfijnverschuivingen zijn verwaarloosbaar en de kernspins zijn in zeer goede benadering ontkoppeld. Het dubbel spin polariseren en de keuze van de 0_g^- aangeslagen toestand hebben er toe geleid dat de theoretische analyse van de photoassociatie spectra mogelijk was. Op basis van deze spectra hebben we geconcludeerd dat het teken van de verstrooiingslengte voor een ^{85}Rb gas negatief is en, gebruikmakend van een massaschalingswet, dat dit teken voor een ^{87}Rb gas positief is. Een positief teken duidt op een stabiel en een negatief teken op een instabiel homogeen condensaat. Kort na de publicatie van deze resultaten is inderdaad BEC waargenomen in een ^{87}Rb gas in Boulder.

In hoofdstukken 4 en 5 wordt melding gemaakt van vormresonanties in de d -golf verstrooiing van ^{87}Rb atomen en in de g -golf verstrooiing van ^{85}Rb atomen. De waarnemingen

van deze vormresonanties hebben het mogelijk gemaakt zeer nauwkeurige waarden van beide bovengenoemde verstrooiingslengten te bepalen en ook een experimentele waarde voor de C_6 van der Waals dispersie coëfficiënt. De g -golf vormresonantie blijkt zo lang te leven dat het mogelijk is gebleken de tijdafhankelijkheid van het tunnelproces, dat de vormresonantie opbouwt, waar te nemen. Verder heeft de analyse van de g -golf vormresonantie geleid tot een bovengrens voor de vervalsnelheid van een mogelijk vervalsmechanisme van het condensaat, de zogenaamde tweede orde spin-baan interactie, een interactie tussen de valentie-elektronen van de wisselwerkende atomen. Hiervoor was tot nu toe nog geen experimentele waarde bekend.

In hoofdstuk 6 worden de vervalsnelheden van de ^{87}Rb en ^{23}Na condensaten ten gevolge van de magnetische dipolaire interactie theoretisch bepaald. In het ^{23}Na experiment lijkt de belangrijkste beperking van de levensduur van het condensaat niet dit mechanisme maar een 3-deeltjes proces te zijn. Volgens zeer recente experimentele gegevens blijkt de vervalsnelheid van het ^{87}Rb condensaat ruwweg overeen te komen met de berekende magnetische dipool vervalsnelheid. Voor de volledigheid wordt in dit hoofdstuk ook de vervalsnelheid voor een ^{85}Rb gas gegeven.

Naast de eerder genoemde dubbel spin gepolariseerde toestand is er nog een andere hyperfijn toestand die geschikt is voor BEC experimenten in een magnetische valkuil. Een interessant aspect van atomen, geprepareerd in deze toestand, is de mogelijkheid om de verstrooiingslengte van teken te veranderen door het magnetisch veld te variëren als een Feshbach resonantie optreedt in het botsingsproces. Hierdoor kunnen de eigenschappen van het condensaat door een externe "knop" drastisch gewijzigd worden. In hoofdstuk 7 wordt een analyse van ^{39}K gebonden toestanden gepresenteerd waarbij gebruik wordt gemaakt van een nieuwe meer-kanaals inverse storing aanpak. Aan de hand van deze aanpak hebben we de eigenschappen bepaald van de botsing van twee ^{39}K en de botsing van twee ^{41}K atomen in de voor de BEC experimenten relevante hyperfijn toestanden. Het blijkt nu dat, ondanks de zeer zwakke hyperfijninteractie, in een ^{41}K gas van $f = 1, m_f = -1$ atomen een Feshbach resonantie optreedt voor magnetische velden waarvoor de atomen opgesloten kunnen worden. Dit is het eerste gas waarvoor we met grote zekerheid het optreden van een Feshbach resonantie in het interessante veld gebied voorspellen. Ook voor een ^{39}K gas is de kans dat de verstrooiingslengte van teken wisselt in het interessante veld gebied bijna 100%.

Door een gaswolk van koude atomen te beschijnen met een laser kunnen botsingen drastisch beïnvloed worden. Zo blijken deze zogenaamde "optische" botsingen in het algemeen plaats te vinden bij veel grotere interatomaire afstanden (20 tot 5000 a_0) dan botsingen zonder laserveld (20 tot 200 a_0). Bovendien wordt de botsingsdynamica sterk beïnvloed als de tijdschaal waarop een botsing plaatsvindt vergelijkbaar wordt met de spontane emissie levensduur van een atoom geëxciteerd door de laser tijdens de botsing. Deze botsingen spelen een rol in (magneto-)optische valkuilen omdat ze exotherme overgangen induceren tussen opgesloten en niet-opgesloten toestanden en zodoende tot opwarming van en deeltjesverlies uit de gaswolk leiden. In hoofdstuk 8 wordt een inleiding gegeven tot deze optische botsingen

en worden de quantummechanische optische Bloch vergelijkingen afgeleid.

In hoofdstuk 9 presenteren we de eerste volledig quantummechanische studie van optische botsingen. In deze berekeningen beperken we ons tot verliessnelheden in eerste orde in de laser intensiteit over een groot intensiteitsbereik. Dit wordt gerechtvaardigd door experimentele evidentie dat de verliessnelheden lineair variëren met de laser intensiteit. Onze volledig quantummechanische berekeningen laten zien dat de vervalssnelheden bij lage temperaturen onderdrukt worden ten opzichte van tot dan toe berekende semiklassieke vervalssnelheden. Deze lage-temperatuur onderdrukking is ook experimenteel waargenomen. In het laatste hoofdstuk wordt een eenvoudig analytisch model gegeven om optische botsingen te beschrijven. Dit model reproduceert de quantummechanische vervalssnelheden zeer goed en biedt het grote voordeel van een transparante en expliciete interpretatie van koude optische botsingen.

Dankwoord

Aan de totstandkoming van dit proefschrift hebben verscheidene mensen een bijdrage geleverd. Enkelen van hen wil ik hier nog in het bijzonder noemen. Om te beginnen wil ik Boudewijn Verhaar bedanken voor zijn niet aflatend enthousiasme en zijn zeer stimulerende begeleiding. Verder mijn collega Ard-Jan Moerdijk voor de talrijke discussies en zijn ondersteuning op computertechnisch gebied.

Aan een aantal hoofdstukken van dit proefschrift is een significante bijdrage geleverd door diverse stagiairs en afstudeerders. In volgorde van opkomst waren dit Ronald van den Oetelaar, Ton van Heel, Reg Das, Frank van Abeelen, Antoine Moonen, Sjef Tempelaars en Johnny Vogels. Bedankt voor jullie inzet en bijdragen aan dit proefschrift.

I am also very thankful to Dan Heinzen, Chin Chun Tsai, Jeff Gardner, John Miller, and Robert Cline for the pioneering photoassociation experiments they have carried out and their contribution to the chapters on photoassociation in this thesis.

Voor het kritisch doorlezen van enkele hoofdstukken van dit proefschrift ben ik dank verschuldigd aan Petra en Frank. Tenslotte wil ik mijn ouders bedanken voor hun steun achter de schermen.

Curriculum Vitae

29 Augustus 1970	Geboren te Melick
Sep. 1982 - Mei 1988	Gymnasium β aan het Bishoppelijk College Schöndeln te Roermond
Sep. 1988 - Okt. 1992	Studie Technische Natuurkunde aan de Technische Universiteit Eindhoven
Nov. 1992 - Okt. 1996	Promotie onderzoek aan de Technische Universiteit Eindhoven in de vakgroep Theoretische Natuurkunde van de faculteit Technische Natuurkunde

STELLINGEN

behorende bij het proefschrift

COLD COLLISIONS OF ALKALI ATOMS IN A LASER FIELD

van

Hugo Boesten

Eindhoven, 28 oktober 1996

1

De bewering: “No practical examples of Hund’s case (e) have as yet been observed”¹ is achterhaald².

1. G. Herzberg, *Molecular spectra and molecular structure, I. Spectra of diatomic molecules* (Princeton, New Jersey, 1950).
2. Dit proefschrift, hoofdstuk 2.

2

De voordelen, die edelgassen lijken te hebben in vergelijking met alkaligassen bij de bepaling van (complexe) verstrooiingslengten uit fotoassociatie-experimenten, worden teniet gedaan door de complexiteit van een richtingsafhankelijke C_6 -dispersiecoëfficiënt ten gevolge van de open binnenschil.

M.R. Doery, E.J.D. Vredenburg, H.M.J.M. Boesten, K.A.H. van Leeuwen, H.C.W. Beijerinck en B.J. Verhaar, in *Conference proceedings International Conference on Atomic Physics XV* (1996).

3

In tegenstelling tot de opvatting van sommige atoomfysici^{1,2,3} is kennis van alleen de triplet- en singlet-verstrooiingslengte niet voldoende om botsingsgrootheden voor een gas van atomen in een niet-dubbelspingepolariseerde hyperfijn-toestand te bepalen.

1. R. Côté, A. Dalgarno, and R.G. Hulet, *Phys. Rev. Lett.* **74**, 3581 (1995).
2. E.R.I. Abraham, W.I. McAlexander, C.A. Sackett, and R.G. Hulet, *Phys. Rev. Lett.* **74**, 1315 (1995).
3. E.R.I. Abraham, W.I. McAlexander, J.M. Gerton, R.G. Hulet, R. Côté, and A. Dalgarno, *Phys. Rev. A* **53**, R3713 (1996).

4

Hoge-resolutiespectroscopie van langlevende vormresonanties is een geschikte techniek om informatie over elastische en inelastische interacties direct te meten.

Dit proefschrift, hoofdstuk 2 en 5.

5

Ondanks de zeer zwakke hyperfijninteractie blijkt voor een gas van ^{41}K -atomen in de $f = 1, m_f = -1$ hyperfijn-toestand een Feshbach-resonantie op te treden bij magneetvelden waarvoor deze atomen opgesloten kunnen worden.

Dit proefschrift, hoofdstuk 7.

6

Het oplossen van de tijdsonafhankelijke quantummechanische Optische Bloch Vergelijking (OBV) biedt vele voordelen in vergelijking tot het oplossen van de tijdsafhankelijke quantummechanische OBV.

F.A. van Abeelen, Afstudeerverslag, Technische Universiteit Eindhoven (1996).

7

Een fascinerend aspect van de recente stormachtige ontwikkelingen in de fysica van “koude atomen” is de afwezigheid van een duidelijke ondergrens voor de temperaturen die zijn te bereiken met geforceerde afdampkoeling.

8

Met het oog op de exponentiële groei van de wetenschappelijke literatuur moeten auteurs, editors en referees op een meer systematische manier gebruik maken van informatietechnologieën bij het opstellen en controleren van literatuurverwijzingen.

9

De gebruikte waarnemingstechniek voor het toekennen van (doel-)punten in sportwedstrijden dient gecorreleerd te worden aan het (financiële) belang van de sporters bij een overwinning/verlies.

10

De slogan “Roken, dat lossen we samen wel op” getuigt van een eenzijdige blik op de problematiek van mensen met ademhalingsmoeilijkheden.

11

Gezien de snelle ontwikkelingen op het gebied van de informatietechnologie dienen we te waken voor “informatie-analfabetisme”.

12

Het is zinloos om in een weersvoorspelling een regen- en zonnkans te geven als de gehanteerde definitie van die kans niet algemeen bekend is.

13

Gezien het grote aantal fatale verkeersongelukken waarbij auto's betrokken zijn, dient de auto beschouwd te worden als een belangrijk potentieel moordwapen. Bij de afgifte van rijbewijzen dient men dan ook even zorgvuldig te werk te gaan als bij de afgifte van wapenvergunningen.

14

De slordige manier waarop met name door niet-Limburgers de begrippen “vlaai” en “taart” gehanteerd worden, maakt een nauwkeurigere omschrijving in de “Dikke van Dale” noodzakelijk.